AFRL-AFOSR-UK-TR-2017-0026

Osculating Keplerian Elements for Highly Non-Keplerian Orbits

Colin McInnes
THE UNIVERSITY OF GLASGOW

03/27/2017
Final Report

Air Force Research Laboratory
AF Office Of Scientific Research (AFOSR)/ IOE
Arlington, Virginia 22203
Air Force Materiel Command

REPORT DOCUMENTATION PAGE

Form Approved
OMB No. 0704-0188

PLEASE DO NOT RETURN YOUR FORM TO THE ABOVE ORGANIZATION.

1. REPORT DATE *(DD-MM-YYYY)*	2. REPORT TYPE	3. DATES COVERED *(From - To)*
15-12-2016	Final Technical	01 Jul - 31 Dec 2016

4. TITLE AND SUBTITLE
Osculating Keplerian Elements for Highly Non-Keplerian Orbits

5a. CONTRACT NUMBER

5b. GRANT NUMBER
FA9550-16-1-0219

5c. PROGRAM ELEMENT NUMBER

6. AUTHOR(S)
Peloni, Alessandro
McInnes, Colin, R.
Ceriotti, Matteo

5d. PROJECT NUMBER

5e. TASK NUMBER

5f. WORK UNIT NUMBER

7. PERFORMING ORGANIZATION NAME(S) AND ADDRESS(ES)
School of Engineering, University of Glasgow
Glasgow G12 8GG
Scotland, United Kingdom

8. PERFORMING ORGANIZATION REPORT NUMBER

9. SPONSORING/MONITORING AGENCY NAME(S) AND ADDRESS(ES)
European Office of Aerospace Research and Development
86 Blenheim Crescent
Ruislip Middlesex HA47HB
United Kingdom

10. SPONSOR/MONITOR'S ACRONYM(S)
EOARD

11. SPONSOR/MONITOR'S REPORT NUMBER(S)

12. DISTRIBUTION/AVAILABILITY STATEMENT
Distribution A - Approved for Public Release

13. SUPPLEMENTARY NOTES

14. ABSTRACT

This report presents a mapping between the elements of highly non-Keplerian orbits and classical orbital elements. Three sets of elements are discussed and mappings are derived in closed, analytical form for both the direct and inverse problem. Advantages and drawbacks of the use of each set of elements are discussed. A sensitivity analysis is performed on all mappings presented. The spacecraft thrust-induced acceleration used to generate families of highly non-Keplerian orbits is extracted from the inverse mapping from the osculating orbital elements. The key signatures of highly non-Keplerian orbits in Keplerian elements tracking data are determined through a set of representative test cases.

15. SUBJECT TERMS
Non-Keplerian Orbit, Osculating Orbital Elements, Mappings, Key Signatures of Non-Keplerian Orbits, Impact of Noise

16. SECURITY CLASSIFICATION OF:			17. LIMITATION OF ABSTRACT	18. NUMBER OF PAGES	19a. NAME OF RESPONSIBLE PERSON
a. REPORT	b. ABSTRACT	c. THIS PAGE			Colin R. McInnes
U	U	U	UU	97	19b. TELEPHONE NUMBER *(Include area code)* (+44) 141 3308511

Reset

UNIVERSITY OF GLASGOW

SCHOOL OF ENGINEERING

Osculating Keplerian Elements for Highly Non-Keplerian Orbits

FINAL TECHNICAL REPORT

Authors:

Alessandro Peloni, Colin R. McInnes, Matteo Ceriotti

Colin.McInnes@glasgow.ac.uk

Project Officer:

Kent Miller

Kent.Miller.2@us.af.mil

Project dates:
1st July – 31st December 2016

AIR FORCE OFFICE OF SCIENTIFIC RESEARCH
GRANT NUMBER FA9550-16-1-0219

Abstract

New families of highly non-Keplerian orbits can be generated using continuous low-thrust propulsion. These include orbits displaced above/below the orbit plane of a conventional Keplerian orbit using out-of-plane thrust, or inside/outside a Keplerian orbit using radial thrust. For a given non-Keplerian orbit radius, displacement distance, and orbit period the required thrust magnitude and direction can be determined analytically, along with the orbit stability properties.

A key open issue in the analysis of the families of non-Keplerian orbits is the generation of a mapping from the non-Keplerian orbit radius, displacement distance and orbit period to a corresponding set of osculating Keplerian orbital elements. This is of importance both to support the future operational use of non-Keplerian orbits and to understand the signature of a non-Keplerian orbit as seen in spacecraft tracking data. Since families of non-Keplerian orbits are generated using a strong, continuous perturbation, their osculating Keplerian orbital elements will be time varying, although still periodic. Similarly, the inverse problem is also of importance to deduce the non-Keplerian orbit radius, displacement distance, and orbit period from observations of Keplerian elements. Once these elements are known, the thrust-induced acceleration magnitude and direction required for the non-Keplerian orbit can also be determined.

In order to pursue these questions, the key objectives of this work are, therefore, to: (1) map the properties of families of highly non-Keplerian orbits onto the classical Keplerian elements, (2) generate an inverse mapping from Keplerian elements to the properties of the non-Keplerian orbit, and (3) determine the key signatures of non-Keplerian orbits in Keplerian element tracking data. These objectives represent a largely unexplored aspect of the dynamics of families of non-Keplerian orbits and offer a route towards their future operational use.

This report presents a mapping between the elements of highly non-Keplerian orbits and classical orbital elements. Three sets of elements are discussed and mappings are derived in closed, analytical form for both the direct and inverse problem. Advantages and drawbacks of the use of each set of elements are discussed. A sensitivity analysis is performed on all mappings presented. The spacecraft thrust-induced acceleration used to generate families of non-Keplerian orbits is extracted from the inverse mapping from the osculating orbital elements. The key signatures of highly non-Keplerian orbits in Keplerian element tracking data are determined through a set of representative test cases.

Table of Contents

List of Figures

List of Tables

1. Highly Non-Keplerian Orbits: Introduction

In classical Keplerian mechanics, an object of negligible mass orbits around an attractor due to the gravitational interaction existing between the two bodies. Celestial mechanics traditionally deals with Keplerian orbits, treating any non-Keplerian effect (e.g. solar radiation pressure, atmospheric drag, gravitational asymmetries due to the Earth's oblateness, third-body interaction) as a perturbation to the classical Keplerian orbit. However, a non-Keplerian orbit is defined as an orbit in which a perturbative or propulsive acceleration acts in addition to the gravitational attraction of the primary body. Following the definition given in McKay et al.,[1] a highly non-Keplerian orbit is characterized by the magnitude of the average propulsive acceleration over one orbit $\|\boldsymbol{a}_{av}\|$ equal or greater than the sum of gravitational and centripetal force experienced by the orbiting body $\|\nabla U\|$. That is, introducing a parameter λ to represent this ratio, a highly non-Keplerian orbit is characterized by $\lambda = \|\boldsymbol{a}_{av}\| / \|\nabla U\| \approx 1$. For the sake of conciseness, and because only Keplerian and highly non-Keplerian orbits are considered in this paper, all the highly non-Keplerian orbits will be simply referred to as non-Keplerian orbits (NKOs) in this report.

New families of NKOs can be generated using continuous low-thrust propulsion.[1-4] These include orbits displaced above/below the orbit plane of a conventional Keplerian orbit using out-of-plane thrust, or inside/outside a Keplerian orbit using radial thrust. For a given NKO radius, displacement distance and orbit period the required thrust magnitude and direction can be determined analytically.[2] In addition, the linear stability properties of the families of non-Keplerian orbits can be determined and it can be shown that while unstable families of orbits exist (saddle x center eigenvalue spectrum) they are in principle controllable (full rank controllability matrix) using feedback to the thrust direction and/or modulation of the thrust magnitude.[3] Moreover, the nonlinear stability properties of NKOs have also been investigated, and the sufficient and necessary conditions for stability of the motion near the equilibria have been obtained.[5]

In addition, by terminating the low-thrust perturbation, a Keplerian orbit will result allowing Keplerian and non-Keplerian orbits to be patched together to generate rich and complex families of composite orbits that have yet to be fully explored.[6] Potential applications of NKOs include orbits displaced above/below the geostationary ring to increase the number of available slots for communications platforms[4] and on-orbit inspection by formation-flying above/below or inside/outside the orbit of a target spacecraft.[7, 8] For example, a displacement distance of 35 km north/south of the geostationary ring allows a platform on a displaced highly non-Keplerian orbit to sit above/below the standard 70 km station-keeping box of a conventional geostationary platform. Such an orbit would require a thrust of 200 mN for a 1000 kg spacecraft, which is achievable with a single QinetiQ T6+ thruster.[4]

To date, several works have been carried out to study non-Keplerian orbits. As well shown in the survey presented by McKay et al.,[1] the problem has been considered from several aspects by taking into account different propulsion technologies (e.g. impulsive thrust,[6] solar electric propulsion,[9] solar sail,[10, 11] and hybrid SEP/sail[4, 12]) and different dynamical models (e.g. two-body,[2, 3] circular restricted three-body,[13] elliptical restricted three-body,[14] and restricted four-body[15]). Different mission applications are also outlined for non-Keplerian orbits, such as telecommunication,[7] Earth observation,[16] planetary science,[17] and geoengineering.[18] More recently, Wang et al.[19, 20] analyzed the relative motion between heliocentric displaced NKOs. Describing the motion by means of classical Keplerian elements and modified equinoctial elements,[21] they provided an analytical solution to the relative-motion problem.

As discussed above, all prior studies on non-Keplerian orbits have focused on orbit and mission-design. A key open issue in the analysis of the families of non-Keplerian orbits is the generation of a mapping from the NKO geometry to a corresponding set of osculating orbital elements. This is of importance both to support the future operational use of non-Keplerian orbits and to understand the signature of a non-Keplerian orbit as seen in spacecraft tracking data. Since families of NKOs are generated using a strong, continuous perturbation, their osculating orbital elements will be time varying, although still periodic. Similarly, the inverse problem is also of importance to deduce the NKO

geometry from observations of orbital elements. Once these elements are known, the thrust-induced acceleration magnitude and direction required for the non-Keplerian orbit can also be determined.

In order to pursue these questions, the key objectives of this study are, therefore, to:

1. Map the properties of families of highly non-Keplerian orbits onto the classical orbital elements
2. Generate an inverse mapping from orbital elements to the properties of the non-Keplerian orbit
3. Determine the key signatures of non-Keplerian orbits in orbital element tracking data

These objectives represent a largely unexplored aspect of the dynamics of families of non-Keplerian orbits and offer a route towards their future operational use.

The report is divided into two main Sections. Section 2 describes the case of a simplified model, in which the NKO orbital plane is always parallel to the equatorial plane. On the other hand, a generalized model with no assumptions on the NKO orbital plane is described in Section 3. In the case of the simplified model, the forward mappings from NKO geometry to osculating orbital elements are discussed in Section 2.1. The description of the mappings and their sensitivity analyses are analytically investigated in Sections 2.1.1 and 2.1.2, respectively, whereas Section 2.1.3 shows the numerical test cases taken into account for the study of the mappings. In Section 2.2, the inverse mappings from osculating orbital elements to non-Keplerian orbits are discussed together with their sensitivity analyses. The thrust-induced acceleration needed to maintain the chosen non-Keplerian orbits is discussed in Section 2.3. In the case of the generalized model, the analytical description of the forward mappings is investigated in Section 3.1. Sections 3.1.1 and 3.1.2 provide the analytical derivation of the forward maps by using the classical Keplerian elements and the modified equinoctial elements, respectively. Numerical test cases are shown and discussed in Section 3.1.3, whereas a summary of the signatures of a spacecraft being forced on a NKO is provided in Section 3.1.4. A study on the generalized inverse mapping is given in Section 3.2 which provides an analytical description of all families of NKOs that share the same Cartesian state. Lastly, the impact of noise is discussed in Section 3.3. Conclusions and final remarks are drawn in Section 4.

2. Simplified Model: Orbital Plane Parallel to Equatorial Plane

Non-Keplerian orbits can be obtained by considering the dynamics of a low-thrust propelled spacecraft in a rotating reference frame.[2] The angular velocity of rotation of the reference frame ϖ, together with the out-of-plane displacement z and the radius of the orbit ρ, are used as free parameters of the problem. Stationary solutions of the equations of motion in this rotating reference frame correspond to periodic, displaced, circular orbits with the orbital plane parallel to the $\hat{\boldsymbol{X}}-\hat{\boldsymbol{Y}}$ plane when viewed from an inertial reference frame. In this paper, the Earth-Centered Inertial frame $\left\{\hat{\boldsymbol{X}},\hat{\boldsymbol{Y}},\hat{\boldsymbol{Z}}\right\}$ is considered. The acceleration needed to generate such stationary solutions can be derived in a closed, analytical form.[2] The required thrust vector lies in the plane spanned by the radius vector and the axis of symmetry, as shown in Figure 1. Therefore, the propulsive acceleration vector can be described, as a function of the NKO elements $\boldsymbol{x}_{NKO}=\left[z,\rho,\varpi\right]^T$, by its magnitude $\|\boldsymbol{a}\|$ and pitch angle α, as follows.

$$\begin{cases} \left\|\boldsymbol{a}\left(z,\rho,\varpi\right)\right\| = \sqrt{\rho^2\left(\varpi^2-\varpi_*^2\right)^2+z^2\varpi_*^4} \\ \tan\alpha\left(z,\rho,\varpi\right) = \dfrac{\rho}{z}\left[1-\left(\dfrac{\varpi}{\varpi_*}\right)^2\right] \end{cases} \tag{2.1}$$

The term $\varpi_*=\sqrt{\mu/r^3}$ in Eq. (2.1) is the orbital angular velocity of a Keplerian orbit of radius $r=\sqrt{\rho^2+z^2}$. Viewed from an inertial reference frame, the orbits generated by the acceleration described in Eq. (2.1) correspond to circular orbits displaced above the central body. The angular velocity of the rotation of the reference frame ϖ corresponds to the angular velocity of the circular orbit viewed from an inertial reference frame.

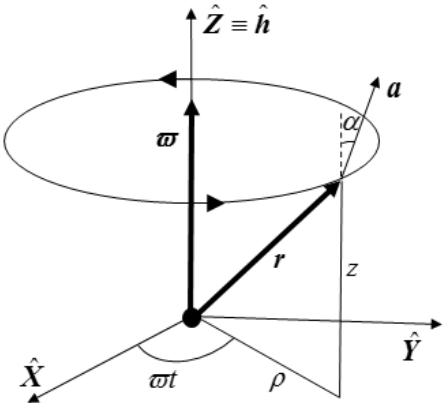

Figure 1. Displaced orbit with thrust-induced acceleration for the simplified model.

The acceleration defined in Eq. (2.1) is that required to generate stationary solutions in the rotating reference frame (i.e. $\|\boldsymbol{a}\|=\|\nabla U\|$). Therefore, such solutions are characterized by $\lambda=1$ and so are defined as highly non-Keplerian orbits.

Three families of NKOs can be defined based on the value of the angular velocity of the rotating reference frame.[2] Type 1 NKOs are defined as those orbits with the minimum required acceleration. From Eq. (2.1), the requirement of minimum acceleration leads to an angular velocity of the rotating reference frame for Type 1 NKOs defined as shown in Eq. (2.2). A second family of NKOs is characterized by orbits synchronous with a body on a circular Keplerian orbit in the $z=0$ plane with the same orbit radius. Lastly, a third family of NKOs is defined by setting the orbital

period to a fixed value. The angular velocities that characterize the aforementioned three families of NKOs are shown in Eq. (2.2).

$$\varpi_{\text{Type 1}} = \sqrt{\mu/r^3}, \quad \varpi_{\text{Type 2}} = \sqrt{\mu/\rho^3}, \quad \varpi_{\text{Type 3}} = \varpi_0 \tag{2.2}$$

In this Section, the mappings between NKO elements and the osculating orbit are derived in closed, analytical form for both the direct and inverse problem. Therefore, the formulation of the spacecraft thrust-induced acceleration given in Eq. (2.1) is derived as a function of the osculating orbital elements.

2.1. Forward Map: Non-Keplerian Orbit to Osculating Orbital Elements

Three sets of elements are chosen to describe the osculating Keplerian orbits:

$$\begin{aligned} &\boldsymbol{x}_{KEP} = \left[a, e, i, \Omega, \omega, \vartheta\right]^T && \text{Classical Keplerian elements (KEP)} \\ &\boldsymbol{x}_{MEE} = \left[p, f, g, h, k, L\right]^T && \text{Modified equinoctial elements (MEE)} \\ &\boldsymbol{x}_{AIoM} = \left[\boldsymbol{h}^T, \boldsymbol{e}^T, L\right]^T && \text{Augmented integrals of motion (AIoM)} \end{aligned} \tag{2.3}$$

From McInnes,[2] the three families of NKO are fully described by the following three elements in an Earth-centered cylindrical reference frame.

$$\begin{cases} \rho & \text{Radius of the orbit} \\ z & \text{Out-of-plane displacement} \\ \varpi & \text{Angular velocity of the spacecraft} \end{cases} \tag{2.4}$$

Therefore, the Cartesian position vector $\boldsymbol{r}$ is simply given by

$$\boldsymbol{r} = \begin{bmatrix} \rho\cos(\varpi t) \\ \rho\sin(\varpi t) \\ z \end{bmatrix} \tag{2.5}$$

and the Cartesian velocity vector $\boldsymbol{v}$ is

$$\boldsymbol{v} = \begin{bmatrix} -\varpi\rho\sin(\varpi t) \\ \varpi\rho\cos(\varpi t) \\ 0 \end{bmatrix} \tag{2.6}$$

Because the NKOs considered are circular, it is worth noting that the radial component of the velocity is always zero, as it can be easily verified by computing $v_r = \boldsymbol{v}\cdot\boldsymbol{r} = 0$.

The orbital angular momentum $\boldsymbol{h}$ can be computed by using the aforementioned expressions of position and velocity as

$$\boldsymbol{h} = \boldsymbol{r}\times\boldsymbol{v} = \begin{bmatrix} -\varpi\rho z\cos(\varpi t) \\ -\varpi\rho z\sin(\varpi t) \\ \varpi\rho^2 \end{bmatrix} \tag{2.7}$$

The analytical formulation of the three mappings is detailed in Section 2.1.1, whereas the sensitivity analysis performed on the mappings is described in Section 2.1.2. Section 2.1.3 provides numerical test cases. Lastly, the three mappings are compared through their advantages and drawbacks in Section 2.1.4.

2.1.1. Mappings

In the following sub-sections, the forward mappings from non-Keplerian orbit to osculating orbital elements are derived for the three sets of elements considered.

2.1.1.1. Classical Keplerian Elements

Starting from the Cartesian state vector (Eqs. (2.5) – (2.6)), the mapping from NKO elements $\left[z,\rho,\varpi\right]^T$ to osculating classical Keplerian elements is obtained, as described in Algorithm 4.2 from Reference 22.

1. *Inclination (i)*

$$i = \arccos\left(\hat{\boldsymbol{h}}\cdot\hat{\boldsymbol{Z}}\right) = \arccos\left(\frac{\rho}{\sqrt{\rho^2+z^2}}\right) \tag{2.8}$$

2. *Right Ascension of the Ascending Node (Ω)*

The line of the nodes shall be defined in order to find the expression for the right ascension of the ascending node (RAAN). The line of the nodes is defined as

$$\hat{\boldsymbol{N}} = \frac{\hat{\boldsymbol{Z}}\times\hat{\boldsymbol{h}}}{\left\|\hat{\boldsymbol{Z}}\times\hat{\boldsymbol{h}}\right\|} = \begin{bmatrix}\sin(\varpi t)\,\mathrm{sgn}(z)\\ -\cos(\varpi t)\,\mathrm{sgn}(z)\\ 0\end{bmatrix} \tag{2.9}$$

It is important to note that the line of the nodes is not defined in case of an in-plane orbit (i.e. $z=0$) because $\mathrm{sgn}(0)=0$. Therefore, the line of the nodes, in this case, is arbitrarily chosen to point in the $\hat{\boldsymbol{X}}$ direction. Therefore, the general formulation of the line of the node is

$$\hat{\boldsymbol{N}} = \begin{bmatrix}\cos(\Omega)\\ \sin(\Omega)\\ 0\end{bmatrix} = \begin{cases}\begin{bmatrix}1\\0\\0\end{bmatrix} & \text{if } z=0 \wedge \mu = \varpi^2\rho^3\\ \begin{bmatrix}\sin(\varpi t)\,\mathrm{sgn}(z)\\ -\cos(\varpi t)\,\mathrm{sgn}(z)\\ 0\end{bmatrix} & \text{otherwise}\end{cases} \tag{2.10}$$

Defining the four-quadrant inverse tangent as* $\arctan(X,Y) = \tan^{-1}(Y/X) + (\pi/2)\,\mathrm{sgn}(Y)\left(1-\mathrm{sgn}(X)\right)$, the right ascension of the ascending node is simply given by Eq. (2.11), in which $\Omega^* = \arccos\left(\sin(\varpi t)\,\mathrm{sgn}(z)\right)$.

$$\Omega = \arctan\left(\hat{\boldsymbol{N}}\cdot\hat{\boldsymbol{X}}, \hat{\boldsymbol{N}}\cdot\hat{\boldsymbol{Y}}\right) = \begin{cases}0 & \text{if } z=0\\ \Omega^* & \text{if } \left(\cos(\varpi t)\le 0 \wedge z>0\right)\vee\left(\cos(\varpi t)\ge 0\wedge z<0\right)\\ 2\pi-\Omega^* & \text{otherwise}\end{cases} \tag{2.11}$$

* Definition from MATLAB User's Guide, Ver. R2014b, *atan2 – Symbolic four-quadrant inverse tangent*.

3. Eccentricity (e)

The eccentricity vector is given by

$$\boldsymbol{e} = -\hat{\boldsymbol{r}} + \frac{\boldsymbol{v}\times\boldsymbol{h}}{\mu} \tag{2.12}$$

Using the vector triple product rule and remembering that $v_r = 0$, the expression for the eccentricity vector in Eq. (2.12) can be rewritten as

$$\boldsymbol{e} = \left(\frac{v^2}{\mu} - \frac{1}{r}\right)\boldsymbol{r} = \left(\frac{\varpi^2\rho^2}{\mu} - \frac{1}{\sqrt{\rho^2+z^2}}\right)\begin{bmatrix}\rho\cos(\varpi t)\\ \rho\sin(\varpi t)\\ z\end{bmatrix} \tag{2.13}$$

The value of the eccentricity is, therefore, given by the norm of the eccentricity vector, as

$$e = \frac{\left|\mu - \varpi^2\rho^2\sqrt{\rho^2+z^2}\right|}{\mu} \tag{2.14}$$

Note that a circular planar Keplerian orbit is characterized by $\mu = \varpi^2\rho^3$, which satisfies the zero-eccentricity condition. However, the eccentricity vector is not defined in this case and this is an issue in the following computation of the true anomaly. Therefore, the eccentricity unit vector, in this case, is arbitrarily chosen to point in the $\hat{\boldsymbol{X}}$ direction. Therefore, the general formulation of the eccentricity vector is

$$\boldsymbol{e} = \begin{cases} \begin{bmatrix}1\\0\\0\end{bmatrix} & \text{if } z = 0 \wedge \mu = \varpi^2\rho^3 \\ \left(\dfrac{\varpi^2\rho^2}{\mu} - \dfrac{1}{\sqrt{\rho^2+z^2}}\right)\begin{bmatrix}\rho\cos(\varpi t)\\ \rho\sin(\varpi t)\\ z\end{bmatrix} & \text{otherwise} \end{cases} \tag{2.15}$$

4. Semi-major axis (a)

The semi-major axis is given by

$$a = \frac{\|\boldsymbol{h}\|^2}{\mu\left(1-e^2\right)} = \frac{\mu\sqrt{\rho^2+z^2}}{2\mu - \varpi^2\rho^2\sqrt{\rho^2+z^2}} \tag{2.16}$$

5. Argument of perigee (ω)

The argument of perigee is given by

$$\omega = \arccos\left(\hat{\boldsymbol{N}}\cdot\hat{\boldsymbol{e}}\right) \tag{2.17}$$

After some mathematical manipulations and arbitrarily choosing $\omega = 0$ in the case of planar circular Keplerian orbit, the general expression for the argument of perigee is

$$\omega = \begin{cases} 0 & \text{if } z = 0 \wedge \mu = \varpi^2 \rho^3 \\ \varpi t & \text{if } z = 0 \wedge \mu < \varpi^2 \rho^3 \\ \pi + \varpi t & \text{if } z = 0 \wedge \mu > \varpi^2 \rho^3 \\ \pi/2 & \text{if } \left(z > 0 \wedge \mu < \varpi^2 \rho^2 \sqrt{\rho^2 + z^2} \right) \vee \left(z < 0 \wedge \mu > \varpi^2 \rho^2 \sqrt{\rho^2 + z^2} \right) \\ 3\pi/2 & \text{if } \left(z > 0 \wedge \mu > \varpi^2 \rho^2 \sqrt{\rho^2 + z^2} \right) \vee \left(z < 0 \wedge \mu < \varpi^2 \rho^2 \sqrt{\rho^2 + z^2} \right) \end{cases} \tag{2.18}$$

6. True anomaly (ϑ)

The true anomaly is given by

$$\cos(\vartheta) = \hat{\boldsymbol{e}} \cdot \hat{\boldsymbol{r}} \tag{2.19}$$

In the case of a circular planar Keplerian orbit, Eq. (2.19) becomes Eq. (2.20), because of the choice of the eccentricity vector shown in Eq. (2.15).

$$\cos(\vartheta) = \cos(\varpi t) \quad \Rightarrow \quad \vartheta = \varpi t \tag{2.20}$$

On the other hand, a NKO is characterized by the expression of the true anomaly given, after some mathematical manipulations, as

$$\vartheta = \begin{cases} 0 & \text{if } \mu < \varpi^2 \rho^2 \sqrt{\rho^2 + z^2} \\ \pi & \text{if } \mu > \varpi^2 \rho^2 \sqrt{\rho^2 + z^2} \end{cases} \tag{2.21}$$

Therefore, the general expression for the true anomaly is found by unifying Eqs. (2.20)-(2.21), as follows.

$$\vartheta = \begin{cases} \varpi t & \text{if } z = 0 \wedge \mu = \varpi^2 \rho^3 \\ 0 & \text{if } \mu < \varpi^2 \rho^2 \sqrt{\rho^2 + z^2} \\ \pi & \text{if } \mu > \varpi^2 \rho^2 \sqrt{\rho^2 + z^2} \end{cases} \tag{2.22}$$

Note that the case $\left(z \neq 0 \wedge \mu = \varpi^2 \rho^2 \sqrt{\rho^2 + z^2} \right)$ is not taken into account inside Eq. (2.22). However, this case corresponds to an osculating circular orbit and this is not possible for the types of NKOs taken into account within this study.

Summary

The forward map from NKOs to osculating classical Keplerian elements described in Section 2.1.1.1 is summarized as:

$$
\begin{aligned}
a &= \frac{\mu\sqrt{\rho^2+z^2}}{2\mu-\varpi^2\rho^2\sqrt{\rho^2+z^2}} \\
e &= \frac{\left|\mu-\varpi^2\rho^2\sqrt{\rho^2+z^2}\right|}{\mu} \\
i &= \arccos\left(\frac{\rho}{\sqrt{\rho^2+z^2}}\right) \\
\Omega &= \begin{cases} 0 & \text{if } z=0 \\ \arccos\left(\sin\left(\varpi t\right)\operatorname{sgn}\left(z\right)\right) & \text{if } \left(\cos\left(\varpi t\right)\le 0 \wedge z>0\right)\vee\left(\cos\left(\varpi t\right)\ge 0 \wedge z<0\right) \\ 2\pi-\arccos\left(\sin\left(\varpi t\right)\operatorname{sgn}\left(z\right)\right) & \text{otherwise} \end{cases} \\
\omega &= \begin{cases} 0 & \text{if } z=0\wedge\mu=\varpi^2\rho^3 \\ \varpi t & \text{if } z=0\wedge\mu<\varpi^2\rho^3 \\ \pi+\varpi t & \text{if } z=0\wedge\mu>\varpi^2\rho^3 \\ \pi/2 & \text{if } \left(z>0\wedge\mu<\varpi^2\rho^2\sqrt{\rho^2+z^2}\right)\vee\left(z<0\wedge\mu>\varpi^2\rho^2\sqrt{\rho^2+z^2}\right) \\ 3\pi/2 & \text{if } \left(z>0\wedge\mu>\varpi^2\rho^2\sqrt{\rho^2+z^2}\right)\vee\left(z<0\wedge\mu<\varpi^2\rho^2\sqrt{\rho^2+z^2}\right) \end{cases} \\
\vartheta &= \begin{cases} \varpi t & \text{if } z=0\wedge\mu=\varpi^2\rho^3 \\ 0 & \text{if } \mu<\varpi^2\rho^2\sqrt{\rho^2+z^2} \\ \pi & \text{if } \mu>\varpi^2\rho^2\sqrt{\rho^2+z^2} \end{cases}
\end{aligned}
\tag{2.23}
$$

2.1.1.2. Modified Equinoctial Elements

In order to have a mapping with no singularities, a map from Cartesian position and velocity to Modified Equinoctial Elements (MEE) is derived. MEE have been introduced to avoid singularities occurring in Keplerian orbits in the case of planar and/or circular orbits and are defined as follows:[21]

$$\begin{cases} p = a\left(1-e^2\right) \\ f = e\cos\left(\omega+\Omega\right) \\ g = e\sin\left(\omega+\Omega\right) \\ h = \tan\left(i/2\right)\cos\left(\Omega\right) \\ k = \tan\left(i/2\right)\sin\left(\Omega\right) \\ L = \omega+\Omega+\vartheta \end{cases} \tag{2.24}$$

Starting from the expressions of the Cartesian position and velocity vectors (Eqs. (2.5) – (2.6)) and the analytical mapping of the osculating classical Keplerian elements described in Section 2.1.1.1 (Eq. (2.23)), the mapping from NKO elements $\left[z,\rho,\varpi\right]^T$ to osculating modified equinoctial elements is derived in the following sub-sections.

1. *Semi-latus rectum (p)*

$$p = \frac{\|\boldsymbol{h}\|^2}{\mu} = \frac{\varpi^2\rho^2\left(\rho^2+z^2\right)}{\mu} \tag{2.25}$$

2. *In-plane element (f)*

In order to derive the general formulation for the in-plane element f, let us first consider the case of zero-displacement orbits (i.e. $z=0$).

From Eq. (2.11), the value of the right ascension of the ascending node for a zero-displacement orbit is simply

$$\Omega\big|_{z=0} = 0 \tag{2.26}$$

From Eq. (2.18), the value of the argument of perigee for a zero-displacement orbit is

$$\omega = \begin{cases} 0 & \text{if } z=0 \wedge \mu = \varpi^2\rho^3 \\ \varpi t & \text{if } z=0 \wedge \mu < \varpi^2\rho^3 \\ \pi+\varpi t & \text{if } z=0 \wedge \mu > \varpi^2\rho^3 \end{cases} \tag{2.27}$$

From Eqs. (2.26)-(2.27), the value of the longitude of perigee $\omega+\Omega$ is

$$\omega+\Omega = \begin{cases} 0 & \text{if } z=0 \wedge \mu = \varpi^2\rho^3 \\ \varpi t & \text{if } z=0 \wedge \mu < \varpi^2\rho^3 \\ \pi+\varpi t & \text{if } z=0 \wedge \mu > \varpi^2\rho^3 \end{cases} \Rightarrow \tag{2.28}$$

$$\Rightarrow \quad \cos\left(\omega+\Omega\right) = \begin{cases} 1 & \text{if } z=0 \wedge \mu = \varpi^2\rho^3 \\ \cos\left(\varpi t\right) & \text{if } z=0 \wedge \mu < \varpi^2\rho^3 \\ -\cos\left(\varpi t\right) & \text{if } z=0 \wedge \mu > \varpi^2\rho^3 \end{cases} \tag{2.29}$$

From Eq. (2.29), and remembering the expression of the eccentricity provided in Eq. (2.14), the expression of the in-plane element f for a zero-displacement orbit is

$$f\big|_{z=0} = e\cos(\omega+\Omega) = \frac{\varpi^2\rho^3-\mu}{\mu}\cos(\varpi t) \tag{2.30}$$

Considering now a displaced orbit, Eq. (2.11) gives the expression of the RAAN as

$$\Omega\big|_{z\neq 0} = \begin{cases} \Omega^* & \text{if } A \\ 2\pi-\Omega^* & \text{if } \sim A \end{cases} \tag{2.31}$$

in which the condition

$$A = \left(\cos(\varpi t)\le 0 \wedge z>0\right)\vee\left(\cos(\varpi t)\ge 0\wedge z<0\right) \tag{2.32}$$

The expression of the argument of perigee, given by Eq. (2.18), is

$$\omega = \begin{cases} \pi/2 & \text{if } B \\ 3\pi/2 & \text{if } C \end{cases} \tag{2.33}$$

in which the two conditions above are

$$\begin{cases} B = \left(z>0\wedge\mu<\varpi^2\rho^2\sqrt{\rho^2+z^2}\right)\vee\left(z<0\wedge\mu>\varpi^2\rho^2\sqrt{\rho^2+z^2}\right) \\ C = \left(z>0\wedge\mu>\varpi^2\rho^2\sqrt{\rho^2+z^2}\right)\vee\left(z<0\wedge\mu<\varpi^2\rho^2\sqrt{\rho^2+z^2}\right) \end{cases} \tag{2.34}$$

From Eqs. (2.31)-(2.33), the cosine of the longitude of perigee is

$$\cos(\omega+\Omega) = \begin{cases} \cos(\pi/2+\Omega^*) = -\sin(\Omega^*) & \text{if } A\wedge B \\ \cos(3\pi/2+\Omega^*) = \sin(\Omega^*) & \text{if } A\wedge C \\ \cos(5\pi/2-\Omega^*) = \sin(\Omega^*) & \text{if } \sim A\wedge B \\ \cos(7\pi/2-\Omega^*) = -\sin(\Omega^*) & \text{if } \sim A\wedge C \end{cases} \Rightarrow \tag{2.35}$$

$$\Rightarrow \quad f\big|_{z\neq 0} = e\cos(\omega+\Omega) = \begin{cases} e\sin(\Omega^*) & \text{if } (A\wedge C)\vee(\sim A\wedge B) \\ -e\sin(\Omega^*) & \text{if } (A\wedge B)\vee(\sim A\wedge C) \end{cases} \tag{2.36}$$

After some mathematical manipulations, Eq. (2.36) becomes

$$f\big|_{z\neq 0} = e\cos(\omega+\Omega) = \begin{cases} e\cos(\varpi t)\,\mathrm{sgn}(z) & \text{if } B \\ -e\cos(\varpi t)\,\mathrm{sgn}(z) & \text{if } C \end{cases} \tag{2.37}$$

Recalling the expression of the eccentricity given in Eq. (2.14) and the conditions shown in Eq. (2.34), it is possible to demonstrate that the expression of the in-plane element f for out-of-plane orbits shown in Eq. (2.37) becomes

$$f\big|_{z\neq 0} = \frac{\varpi^2\rho^2\sqrt{\rho^2+z^2}-\mu}{\mu}\cos(\varpi t) \tag{2.38}$$

Note that the expression for the in-plane element f in case of zero-displacement orbits shown in Eq. (2.30) is a particular case of Eq. (2.38). Therefore, the general expression for the in-plane element f is given by Eq. (2.39).

$$f = \frac{\varpi^2\rho^2\sqrt{\rho^2+z^2}-\mu}{\mu}\cos(\varpi t) \tag{2.39}$$

3. In-plane element (g)

As for the case of the in-plane element f, let us divide the derivation of the general mapping for the in-plane element g considering the in-plane and out-of-plane orbits separately at first. Starting by considering a zero-displacement orbit and remembering the value of the longitude of perigee shown in Eq. (2.28), the value of the sine of the longitude of perigee is given by

$$\sin(\omega+\Omega)=\begin{cases}0 & \text{if } z=0 \wedge \mu=\varpi^2\rho^3 \\ \sin(\varpi t) & \text{if } z=0 \wedge \mu<\varpi^2\rho^3 \\ -\sin(\varpi t) & \text{if } z=0 \wedge \mu>\varpi^2\rho^3\end{cases} \tag{2.40}$$

From Eq. (2.40), and remembering the expression of the eccentricity shown in Eq. (2.14), the expression of the in-plane element g for a zero-displacement orbit is

$$g\big|_{z=0}=e\sin(\omega+\Omega)=\frac{\varpi^2\rho^3-\mu}{\mu}\sin(\varpi t) \tag{2.41}$$

Following the same arguments as those for the derivation of Eq. (2.35), the sine of the longitude of perigee is

$$\sin(\omega+\Omega)=\begin{cases}\sin(\pi/2+\Omega^*)=\cos(\Omega^*) & \text{if } A\wedge B \\ \sin(3\pi/2+\Omega^*)=-\cos(\Omega^*) & \text{if } A\wedge C \\ \sin(5\pi/2-\Omega^*)=\cos(\Omega^*) & \text{if } \sim A\wedge B \\ \sin(7\pi/2-\Omega^*)=-\cos(\Omega^*) & \text{if } \sim A\wedge C\end{cases} \Rightarrow \tag{2.42}$$

$$\Rightarrow \quad g\big|_{z\neq 0}=e\sin(\omega+\Omega)=\begin{cases}e\cos(\Omega^*) & \text{if } (A\wedge B)\vee(\sim A\wedge B) \\ -e\cos(\Omega^*) & \text{if } (A\wedge C)\vee(\sim A\wedge C)\end{cases} \tag{2.43}$$

Note that both the conditions in Eq. (2.43) do not depend on the condition A, so that Eq. (2.43) can be rewritten as

$$g\big|_{z\neq 0}=e\sin(\omega+\Omega)=\begin{cases}e\cos(\Omega^*) & \text{if } B \\ -e\cos(\Omega^*) & \text{if } C\end{cases} \tag{2.44}$$

Recalling the definition of the angle $\Omega^*=\arccos(\sin(\varpi t)\operatorname{sgn}(z))$, Eq. (2.44) can be further simplified and re-written as

$$g\big|_{z\neq 0}=e\sin(\omega+\Omega)=\begin{cases}e\sin(\varpi t)\operatorname{sgn}(z) & \text{if } B \\ -e\sin(\varpi t)\operatorname{sgn}(z) & \text{if } C\end{cases} \tag{2.45}$$

As for the in-plane element f, recalling the expression of the eccentricity given in Eq. (2.14) and the conditions shown in Eq. (2.34), it is possible to demonstrate that the expression for the in-plane element g for out-of-plane orbits shown in Eq. (2.45) becomes

$$g\big|_{z\neq 0}=\frac{\varpi^2\rho^2\sqrt{\rho^2+z^2}-\mu}{\mu}\sin(\varpi t) \tag{2.46}$$

Note that the expression for the in-plane element g in case of the zero-displacement orbit shown in Eq. (2.41) is a particular case of Eq. (2.46). Therefore, the general expression for the in-plane element g is given by Eq. (2.47).

$$g = \frac{\varpi^2 \rho^2 \sqrt{\rho^2 + z^2} - \mu}{\mu} \sin(\varpi t) \tag{2.47}$$

4. Out-of-plane element (h)

Before deriving the expression for the out-of-plane element h, let us recall the following identity.

$$\tan\left(\frac{x}{2}\right) = \frac{1 - \cos(x)}{\sin(x)} \tag{2.48}$$

Recalling the formulation of the inclination shown in Eq. (2.8) as $i = \arccos\left(\frac{\rho}{\sqrt{\rho^2 + z^2}}\right)$, the expression of $\tan(i/2)$ is, therefore, given by

$$\tan\left(\frac{i}{2}\right) = \frac{1 - \frac{\rho}{\sqrt{\rho^2 + z^2}}}{\sin\left(\arccos\left(\frac{\rho}{\sqrt{\rho^2 + z^2}}\right)\right)} = \left(1 - \frac{\rho}{\sqrt{\rho^2 + z^2}}\right)\sqrt{\frac{\rho^2 + z^2}{z^2}} \quad \Rightarrow \tag{2.49}$$

$$\Rightarrow \quad \tan\left(\frac{i}{2}\right) = -\frac{\rho - \sqrt{\rho^2 + z^2}}{|z|} \tag{2.50}$$

From Eq. (2.50), and recalling the value of $\cos(\Omega) = \sin(\varpi t)\,\mathrm{sgn}(z)$ introduced in Eq. (2.11), the expression of the out-of-plane element h is

$$h = -\frac{\sin(\varpi t)\left(\rho - \sqrt{\rho^2 + z^2}\right)}{z} \tag{2.51}$$

Note that there are no singularities in Eq. (2.51) in the case of zero-displacement orbits. It can be seen, in fact, that

$$\lim_{z \to 0} h = 0 \tag{2.52}$$

5. Out-of-plane element (k)

For the expression of the out-of-plane element k, the formulation of $\sin(\Omega)$ is needed. From Eq. (2.11), it is

$$\sin(\Omega) = \begin{cases} \sin(\Omega^*) = \sqrt{1 - \sin^2(\varpi t)\,\mathrm{sgn}^2(z)} & \text{if } z = 0 \vee \left(\cos(\varpi t) \le 0 \wedge z > 0\right) \vee \left(\cos(\varpi t) \ge 0 \wedge z < 0\right) \\ \sin(2\pi - \Omega^*) = -\sqrt{1 - \sin^2(\varpi t)\,\mathrm{sgn}^2(z)} & \text{otherwise} \end{cases} \tag{2.53}$$

Defining the auxiliary variable $w := \sqrt{1-\sin^2(\varpi t)\,\mathrm{sgn}^2(z)}$, the formulation of the out-of-plane element k is

$$k = \tan\left(\frac{i}{2}\right)\sin(\Omega) = \begin{cases} -\dfrac{\rho-\sqrt{\rho^2+z^2}}{|z|}\,w & \text{if } z=0 \vee \left(\cos(\varpi t)\le 0 \wedge z>0\right) \vee \left(\cos(\varpi t)\ge 0 \wedge z<0\right) \\ \dfrac{\rho-\sqrt{\rho^2+z^2}}{|z|}\,w & \text{otherwise} \end{cases} \tag{2.54}$$

Let us study the two branches of the solution separately starting from the first one. If the first condition in Eq. (2.54) is verified, there is

$$k = -\frac{\rho-\sqrt{\rho^2+z^2}}{|z|}\sqrt{1-\sin^2(\varpi t)\,\mathrm{sgn}^2(z)} = \begin{cases} 0 & \text{if } z=0 \\ -\dfrac{|\cos(\varpi t)|\left(\rho-\sqrt{\rho^2+z^2}\right)}{z} & \text{if } z>0 \\ \dfrac{|\cos(\varpi t)|\left(\rho-\sqrt{\rho^2+z^2}\right)}{z} & \text{if } z<0 \end{cases} \Rightarrow \tag{2.55}$$

$$\Rightarrow \quad k = \begin{cases} 0 & \text{if } z=0 \\ \dfrac{\cos(\varpi t)\left(\rho-\sqrt{\rho^2+z^2}\right)}{z} & \text{otherwise} \end{cases} \tag{2.56}$$

On the contrary, if the second condition of Eq. (2.54) is verified then

$$k = \frac{\rho-\sqrt{\rho^2+z^2}}{|z|}\sqrt{1-\sin^2(\varpi t)\,\mathrm{sgn}^2(z)} = \begin{cases} \dfrac{|\cos(\varpi t)|\left(\rho-\sqrt{\rho^2+z^2}\right)}{z} & \text{if } z>0 \\ -\dfrac{|\cos(\varpi t)|\left(\rho-\sqrt{\rho^2+z^2}\right)}{z} & \text{if } z<0 \end{cases} \Rightarrow \tag{2.57}$$

$$k = \frac{\cos(\varpi t)\left(\rho-\sqrt{\rho^2+z^2}\right)}{z} \tag{2.58}$$

Therefore, Eq. (2.54) can be rewritten, by unifying Eq. (2.56) and Eq. (2.58), as

$$k = \begin{cases} 0 & \text{if } z=0 \\ \dfrac{\cos(\varpi t)\left(\rho-\sqrt{\rho^2+z^2}\right)}{z} & \text{otherwise} \end{cases} \tag{2.59}$$

However, it can be demonstrated that

$$\lim_{z\to 0}\left[\frac{\cos(\varpi t)\left(\rho-\sqrt{\rho^2+z^2}\right)}{z}\right]=0 \tag{2.60}$$

Therefore, the first condition in Eq. (2.59) is actually redundant and unnecessary. The general expression for the out-of-plane element k is therefore given by

$$k=\frac{\cos(\varpi t)\left(\rho-\sqrt{\rho^2+z^2}\right)}{z} \tag{2.61}$$

6. True longitude (L)

In order to derive the general formulation for the true longitude L, let us consider three cases $z=0$, $z>0$, and $z<0$, respectively.

In the case of zero-displacement orbits (i.e. $z=0$), the expression of the true longitude is simply given by the formulations of RAAN, argument of perigee, and true anomaly given in Eq. (2.23), as

$$L\big|_{z=0}=\varpi t \tag{2.62}$$

In the case of positive out-of-plane displacement (i.e. $z>0$), the formulations of the angles Ω, ω, and ϑ are the following.

$$\Omega\big|_{z>0}=\begin{cases}\Omega^* & \text{if } \cos(\varpi t)\le 0\\ 2\pi-\Omega^* & \text{otherwise}\end{cases} \tag{2.63}$$

$$\omega\big|_{z>0}=\begin{cases}\pi/2 & \text{if } \mu<\varpi^2\rho^2\sqrt{\rho^2+z^2}\\ 3\pi/2 & \text{if } \mu>\varpi^2\rho^2\sqrt{\rho^2+z^2}\end{cases} \tag{2.64}$$

$$\vartheta\big|_{z>0}=\begin{cases}0 & \text{if } \mu<\varpi^2\rho^2\sqrt{\rho^2+z^2}\\ \pi & \text{if } \mu>\varpi^2\rho^2\sqrt{\rho^2+z^2}\end{cases} \tag{2.65}$$

From Eqs. (2.64)-(2.65) and considering the angles lying in the interval $[0,2\pi)$ then

$$\left[\omega+\vartheta\right]_{z>0}=\frac{\pi}{2} \tag{2.66}$$

Therefore, the expression of the true longitude for positive out-of-plane displacement is

$$L\big|_{z>0}=\frac{\pi}{2}+\Omega\big|_{z>0}=\begin{cases}\dfrac{\pi}{2}+\Omega^* & \text{if } \cos(\varpi t)\le 0\\ \dfrac{5}{2}\pi-\Omega^* & \text{otherwise}\end{cases} \tag{2.67}$$

In the case of negative out-of-plane displacement (i.e. $z<0$), the formulations of the angles Ω, ω, and ϑ are the following.

$$\Omega\big|_{z<0} = \begin{cases} \Omega^* & \text{if } \cos(\varpi t) \geq 0 \\ 2\pi - \Omega^* & \text{otherwise} \end{cases} \tag{2.68}$$

$$\omega\big|_{z<0} = \begin{cases} \pi/2 & \text{if } \mu > \varpi^2 \rho^2 \sqrt{\rho^2 + z^2} \\ 3\pi/2 & \text{if } \mu < \varpi^2 \rho^2 \sqrt{\rho^2 + z^2} \end{cases} \tag{2.69}$$

$$\vartheta\big|_{z<0} = \begin{cases} 0 & \text{if } \mu < \varpi^2 \rho^2 \sqrt{\rho^2 + z^2} \\ \pi & \text{if } \mu > \varpi^2 \rho^2 \sqrt{\rho^2 + z^2} \end{cases} \tag{2.70}$$

From Eqs. (2.69)-(2.71) and considering the angles lying in the interval $[0, 2\pi)$ then

$$[\omega + \vartheta]_{z<0} = \frac{3}{2}\pi \tag{2.71}$$

Therefore, the expression of the true longitude for negative out-of-plane displacement is

$$L\big|_{z<0} = \frac{3}{2}\pi + \Omega\big|_{z<0} = \begin{cases} \dfrac{3}{2}\pi + \Omega^* & \text{if } \cos(\varpi t) \geq 0 \\ \dfrac{7}{2}\pi - \Omega^* & \text{otherwise} \end{cases} \tag{2.72}$$

The general expression for the true longitude L is given by unifying Eq. (2.62), Eq. (2.67), and Eq. (2.72) as

$$L = \begin{cases} \varpi t & \text{if } z = 0 \\ \dfrac{\pi}{2} + \Omega^* & \text{if } z > 0 \wedge \cos(\varpi t) \leq 0 \\ \dfrac{5}{2}\pi - \Omega^* & \text{if } z > 0 \wedge \cos(\varpi t) > 0 \\ \dfrac{3}{2}\pi + \Omega^* & \text{if } z < 0 \wedge \cos(\varpi t) \geq 0 \\ \dfrac{7}{2}\pi - \Omega^* & \text{if } z < 0 \wedge \cos(\varpi t) < 0 \end{cases} \tag{2.73}$$

A further simplification of the general formulation of the true longitude shown in Eq. (2.73) can be carried out by studying the variation of the angle Ω^*. In order to further simplify the expression of the true longitude, let us start recalling the formulation of the angle $\Omega^* = \arccos\left(\sin(\varpi t)\,\mathrm{sgn}(z)\right)$. A study on the characteristics of this function can be done by plotting the value of Ω^* against the angle $x = \varpi t$. From Eq. (2.73) it is evident that there is no interest in studying the value $\Omega^*\big|_{z=0}$. Therefore, two separate plots are shown in Figure 2, considering the case of positive and negative vertical displacement, respectively.

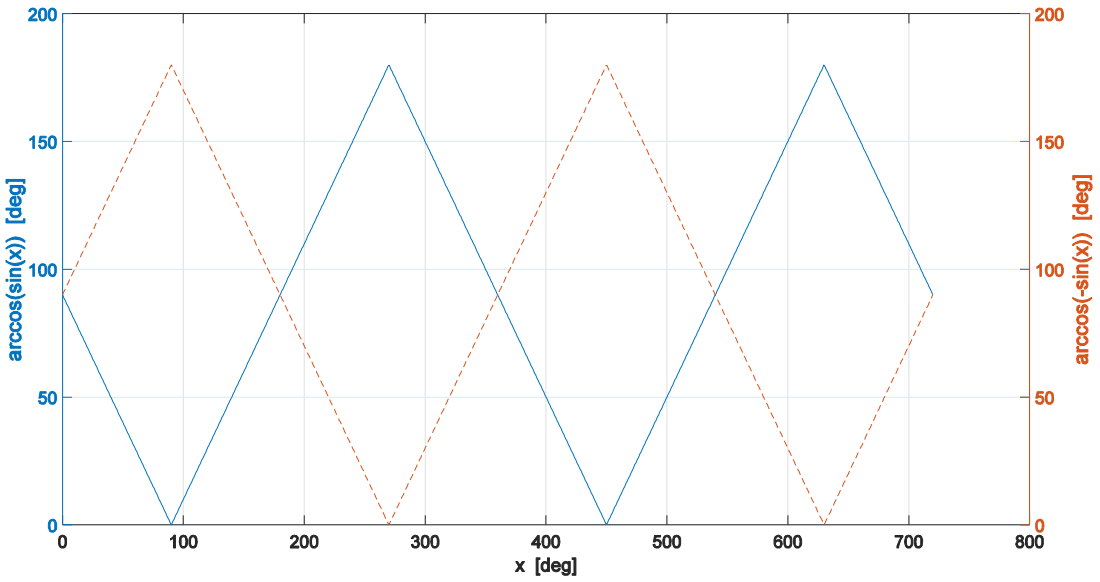

Figure 2. Plot of arccos(sin(x)sgn(z)).

From the plots shown in Figure 2, it can be verified that the expression of Ω^* in Eq. (2.74) is true.

$$\Omega^* = \begin{cases} -\pi/2 + \varpi t & \text{if } z > 0 \wedge \cos(\varpi t) \le 0 \\ 5\pi/2 - \varpi t & \text{if } z > 0 \wedge \cos(\varpi t) > 0 \\ 3\pi/2 - \varpi t & \text{if } z < 0 \wedge \cos(\varpi t) < 0 \\ -3\pi/2 + \varpi t & \text{if } z < 0 \wedge \cos(\varpi t) \ge 0 \end{cases} \tag{2.74}$$

Therefore, Eq. (2.73) can be rewritten in a simpler form as

$$L = \varpi t \tag{2.75}$$

Summary

The forward map from NKOs to osculating modified equinoctial elements described in Section 2.1.1.2 is summarized as:

$$\begin{aligned} p &= \frac{\varpi^2 \rho^2 \left(\rho^2 + z^2\right)}{\mu} & h &= -\frac{\sin(\varpi t)\left(\rho - \sqrt{\rho^2 + z^2}\right)}{z} \\ f &= \frac{\varpi^2 \rho^2 \sqrt{\rho^2 + z^2} - \mu}{\mu} \cos(\varpi t) & k &= \frac{\cos(\varpi t)\left(\rho - \sqrt{\rho^2 + z^2}\right)}{z} \\ g &= \frac{\varpi^2 \rho^2 \sqrt{\rho^2 + z^2} - \mu}{\mu} \sin(\varpi t) & L &= \varpi t \end{aligned} \tag{2.76}$$

2.1.1.3. Augmented Integrals of Motion

The augmented integrals of motion are defined as

$$\begin{cases} \boldsymbol{h} & \text{Orbital angular momentum vector} \\ \boldsymbol{e} & \text{Eccentricity vector} \\ L & \text{True longitude} \end{cases} \tag{2.77}$$

Note that there exists a relationship between the two integrals of motion (i.e. $\boldsymbol{h}\cdot\boldsymbol{e}=0$), which reduces the number of independent elements for the orbit description from 7 to 6.

Starting from the expressions of the Cartesian position and velocity vectors (Eqs. (2.5)-(2.6)), the mapping from NKO elements $\left[z,\rho,\varpi\right]^T$ to osculating augmented integrals of motion is shown in Eq. (2.78). The formulations of angular momentum vector, eccentricity vector, and true longitude are given from Eqs. (2.7), (2.15), and (2.75), respectively.

$$\begin{aligned} \boldsymbol{h} &= \begin{bmatrix} -\varpi\rho z\cos\left(\varpi t\right) \\ -\varpi\rho z\sin\left(\varpi t\right) \\ \varpi\rho^2 \end{bmatrix} \\ \boldsymbol{e} &= \left(\frac{\varpi^2\rho^2}{\mu}-\frac{1}{\sqrt{\rho^2+z^2}}\right)\begin{bmatrix} \rho\cos\left(\varpi t\right) \\ \rho\sin\left(\varpi t\right) \\ z \end{bmatrix} \\ L &= \varpi t \end{aligned} \tag{2.78}$$

2.1.2. Sensitivity Analysis

A sensitivity analysis has been performed in order to study the behavior of the mappings in the presence of errors in the NKO elements $\left[z,\rho,\varpi\right]^T$. Both analytical and numerical sensitivity analyses have been carried out to confirm the results found.

The analytical sensitivity analysis is centered on the computation of the Jacobian $\mathbf{J}$ of the mapping. Defining the non-Keplerian orbit to osculating orbital elements map as $\boldsymbol{\Phi}$ and the set of NKO elements $\boldsymbol{y}=\left[z,\rho,\varpi\right]^T$, the analytical sensitivity analysis is performed by means of the Jacobian of the system such that

$$\mathbf{J}=\frac{\partial\boldsymbol{\Phi}}{\partial\boldsymbol{y}} \tag{2.79}$$

In the following sub-sections, the definition of the parameters used for the sensitivity analysis and a definition of the structure of the Jacobian are given for each set of osculating orbital elements.

2.1.2.1. Classical Keplerian Elements

The mapping $\mathbf{\Phi}$ from non-Keplerian orbit to osculating classical Keplerian elements is shown in Eq. (2.23). The Jacobian of this mapping is

$$\mathbf{J}_{KEP} = \begin{bmatrix} \frac{\partial a}{\partial z} & \frac{\partial e}{\partial z} & \frac{\partial i}{\partial z} & \frac{\partial \Omega}{\partial z} & \frac{\partial \omega}{\partial z} & \frac{\partial \vartheta}{\partial z} \\ \frac{\partial a}{\partial \rho} & \frac{\partial e}{\partial \rho} & \frac{\partial i}{\partial \rho} & \frac{\partial \Omega}{\partial \rho} & \frac{\partial \omega}{\partial \rho} & \frac{\partial \vartheta}{\partial \rho} \\ \frac{\partial a}{\partial \varpi} & \frac{\partial e}{\partial \varpi} & \frac{\partial i}{\partial \varpi} & \frac{\partial \Omega}{\partial \varpi} & \frac{\partial \omega}{\partial \varpi} & \frac{\partial \vartheta}{\partial \varpi} \end{bmatrix}^T \tag{2.80}$$

The elements of the Jacobian are not shown here for the sake of conciseness.

It is important to note that some of the formulations found for the NKO to osculating classical Keplerian elements map are expressed through a piecewise law, which creates difficulties in dealing with analytical sensitivity analysis. It is not possible, for instance, to analytically differentiate the expression of right ascension of the ascending node, argument of perigee, and true anomaly. Therefore, for what concerns these elements, only a study based on numerical sensitivity analysis has been carried out.

The parameters used to test the sensitivity of the mapping to uncertainties in the NKO parameter y_i are as follows.

- Relative error of the semi-major axis due to uncertainties in the NKO elements.

$$\varepsilon_{a,y_i} := \frac{|a-\tilde{a}|}{a} = \frac{|a-(a+\delta a)|}{a} = \frac{|\delta a|}{a} = \frac{\left|J_{a,y_i}\cdot \delta y_i\right|}{a} \tag{2.81}$$

- Absolute error of the eccentricity due to uncertainties in the NKO elements.

$$\varepsilon_{e,y_i} := |e-\tilde{e}| = |e-(e+\delta e)| = |\delta e| = \left|J_{e,y_i}\cdot \delta y_i\right| \tag{2.82}$$

- Normalized error of the angles $\xi = \{i, \Omega, \omega, \vartheta\}$ due to uncertainties in the NKO elements.

$$\varepsilon_{\xi,y_i} := \frac{\delta \xi}{\pi} = \frac{\left|J_{\xi,y_i}\cdot \delta y_i\right|_{\pi}}{\pi} \tag{2.83}$$

2.1.2.2. Modified Equinoctial Elements

The mapping $\mathbf{\Phi}$ from non-Keplerian orbit to osculating modified equinoctial elements is shown in Eq. (2.76). The Jacobian of this mapping is

$$\mathbf{J}_{MEE} = \begin{bmatrix} \frac{\partial p}{\partial z} & \frac{\partial f}{\partial z} & \frac{\partial g}{\partial z} & \frac{\partial h}{\partial z} & \frac{\partial k}{\partial z} & \frac{\partial L}{\partial z} \\ \frac{\partial p}{\partial \rho} & \frac{\partial f}{\partial \rho} & \frac{\partial g}{\partial \rho} & \frac{\partial h}{\partial \rho} & \frac{\partial k}{\partial \rho} & \frac{\partial L}{\partial \rho} \\ \frac{\partial p}{\partial \varpi} & \frac{\partial f}{\partial \varpi} & \frac{\partial g}{\partial \varpi} & \frac{\partial h}{\partial \varpi} & \frac{\partial k}{\partial \varpi} & \frac{\partial L}{\partial \varpi} \end{bmatrix}^T \tag{2.84}$$

Again, the elements of the Jacobian are not shown here for the sake of conciseness.

The parameters used to test the sensitivity of the mapping to uncertainties in the NKO parameter y_i are as follows.

- Relative error of the semi-latus rectum due to uncertainties in the NKO elements.

$$\varepsilon_{p,y_i} := \frac{|p-\tilde{p}|}{p} = \frac{|p-(p+\delta p)|}{p} = \frac{|\delta p|}{p} = \frac{|J_{p,y_i}\cdot\delta y_i|}{p} \tag{2.85}$$

- Absolute error of the elements $x=\{f,g,h,k\}$ due to uncertainties in the NKO elements.

$$\varepsilon_{x,y_i} := |x-\tilde{x}| = |x-(x+\delta x)| = |\delta x| = |J_{x,y_i}\cdot\delta y_i| \tag{2.86}$$

- Normalized error of the true longitude L due to uncertainties in the NKO elements.

$$\varepsilon_{L,y_i} := \frac{\delta L}{\pi} = \frac{|J_{L,y_i}\cdot\delta y_i|_\pi}{\pi} \tag{2.87}$$

2.1.2.3. Augmented Integrals of Motion

The mapping $\boldsymbol{\Phi}$ from non-Keplerian orbit to osculating augmented integrals of motion is shown in Eq. (2.78). The Jacobian of this mapping is

$$\mathbf{J}_{AIoM} = \begin{bmatrix} \frac{\partial h_x}{\partial z} & \frac{\partial h_y}{\partial z} & \frac{\partial h_z}{\partial z} & \frac{\partial e_x}{\partial z} & \frac{\partial e_y}{\partial z} & \frac{\partial e_z}{\partial z} & \frac{\partial L}{\partial z} \\ \frac{\partial h_x}{\partial \rho} & \frac{\partial h_y}{\partial \rho} & \frac{\partial h_z}{\partial \rho} & \frac{\partial e_x}{\partial \rho} & \frac{\partial e_y}{\partial \rho} & \frac{\partial e_z}{\partial \rho} & \frac{\partial L}{\partial \rho} \\ \frac{\partial h_x}{\partial \varpi} & \frac{\partial h_y}{\partial \varpi} & \frac{\partial h_z}{\partial \varpi} & \frac{\partial e_x}{\partial \varpi} & \frac{\partial e_y}{\partial \varpi} & \frac{\partial e_z}{\partial \varpi} & \frac{\partial L}{\partial \varpi} \end{bmatrix}^T \tag{2.88}$$

Again, the elements of the Jacobian are not shown here for the sake of conciseness.

The parameters used to test the sensitivity of the mapping to uncertainties in the NKO parameter y_i are as follows.

- Magnitude of the difference vector between the nominal value of the angular momentum and that related to uncertainties in the NKO elements. Relative error.

$$\varepsilon_{\boldsymbol{h},y_i} := \frac{\|\boldsymbol{h}-\tilde{\boldsymbol{h}}\|}{h} = \frac{\|\boldsymbol{h}-(\boldsymbol{h}+\delta\boldsymbol{h})\|}{h} = \frac{\|\delta\boldsymbol{h}\|}{h} = \frac{\|\boldsymbol{J}_{\boldsymbol{h},y_i}\cdot\delta y_i\|}{h} \tag{2.89}$$

- Magnitude of the difference vector between the nominal value of the eccentricity vector and that related to uncertainties in the NKO elements. Absolute error.

$$\varepsilon_{\boldsymbol{e},y_i} := \|\boldsymbol{e}-\tilde{\boldsymbol{e}}\| = \|\boldsymbol{e}-(\boldsymbol{e}+\delta\boldsymbol{e})\| = \|\delta\boldsymbol{e}\| = \|\boldsymbol{J}_{\boldsymbol{e},y_i}\cdot\delta y_i\| \tag{2.90}$$

- Normalized error of the true longitude L due to uncertainties in the NKO elements.

$$\varepsilon_{L,y_i} := \frac{\delta L}{\pi} = \frac{|J_{L,y_i}\cdot\delta y_i|_\pi}{\pi} \tag{2.91}$$

2.1.3. Numerical Test Cases

Two different sets of test cases have been considered. The first set has been chosen to validate the forward mappings and to study the behavior of the osculating elements. The parameters have been selected for ease of illustration. Therefore, the acceleration required to generate the NKOs considered is not constrained and so can be well above the technical limitations of the current low-thrust technology. The second set has been chosen to study the impact of uncertainties in the non-Keplerian orbit properties on the classical orbital elements. These two sets are described in Section 2.1.3.1 and Section 2.1.3.2, respectively.

2.1.3.1. Mappings

15 different scenarios have been tested in order to both verify the validity of the mappings derived in the previous sections and to study the behavior of the osculating elements, as detailed below. All results of the test cases have been numerically verified by means of MATLAB.

In the following sub-section, all test cases are described. Figure 3 shows the orbits of all these test cases used in this study.

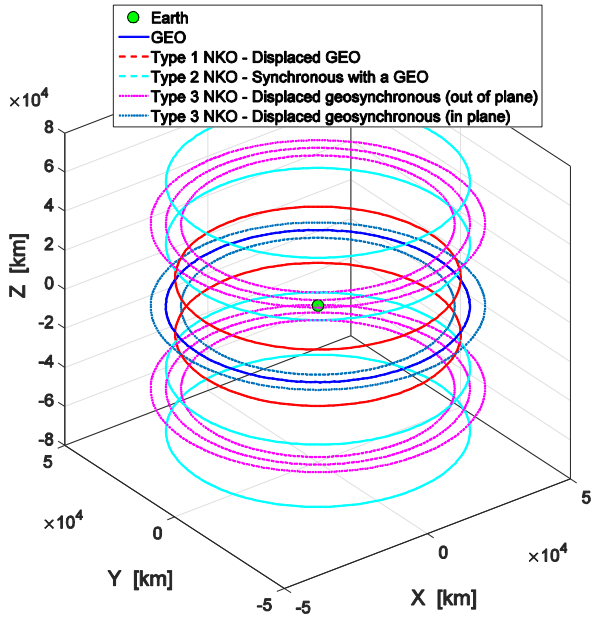

Figure 3. Earth-centered view of the orbits of all test cases used.

Test cases

1. *GEO*

The first test case is a conventional Geostationary Earth Orbit (GEO) described by

$$\text{GEO}: \begin{cases} z_{GEO} = 0 \\ \rho_{GEO} = r_{GEO} = 42{,}164 \text{ km} \\ \varpi_{GEO} = \sqrt{\mu / r_{GEO}^3} \end{cases} \tag{2.92}$$

2. *Type 1 NKO*

Two test cases are considered for the Type 1 NKO.

$$\text{Type 1 NKO}: \begin{cases} z_1 = r_{GEO} \sin(\Delta\lambda) \\ \rho_1 = r_{GEO} \cos(\Delta\lambda) \\ \varpi_1 = \sqrt{\mu / r_{GEO}^3} \end{cases} \tag{2.93}$$

The term $\Delta\lambda$ is the angle between the position vector $\boldsymbol{r}$ and the $\hat{\boldsymbol{X}} - \hat{\boldsymbol{Y}}$ plane. In this case, two values are considered so that both positive and negative out-of-plane displaced NKOs are taken into account.

$$\Delta\lambda = \pm 20 \text{ deg} \Rightarrow \begin{cases} z_1 = \pm 0.34 r_{GEO} \cong \pm 14{,}000 \text{ km} \\ \rho_1 = 0.94 r_{GEO} \cong 39{,}600 \text{ km} \end{cases} \tag{2.94}$$

3. *Type 2 NKO*

Four test cases are considered for the Type 2 NKO.

$$\text{Type 2 NKO}: \begin{cases} z_2 = \{\pm 5 \cdot R_\oplus, \pm 10 \cdot R_\oplus\} \\ \rho_2 = r_{GEO} \\ \varpi_2 = \sqrt{\mu / r_{GEO}^3} \end{cases} \tag{2.95}$$

4. *Type 3 NKO*

Eight test cases are considered for the Type 3 NKO. Six of them are characterized by an out-of-plane displacement while the other two are in-plane displaced NKOs.

$$\begin{matrix} \text{Type 3 NKO} \\ \text{(out-of-plane displacement)} \end{matrix}: \begin{cases} z_{3op} = \pm r_{GEO} \\ \rho_{3op} = \{0.9,\ 1,\ 1.1\} \cdot r_{GEO} \\ \varpi_{3op} = \sqrt{\mu / r_{GEO}^3} \end{cases} \tag{2.96}$$

$$\begin{matrix} \text{Type 3 NKO} \\ \text{(in-plane displacement)} \end{matrix}: \begin{cases} z_{3ip} = 0 \\ \rho_{3ip} = \{0.9,\ 1.1\} \cdot r_{GEO} \\ \varpi_{3ip} = \sqrt{\mu / r_{GEO}^3} \end{cases} \tag{2.97}$$

Results and discussion

Figure 4 shows the Type 1 NKO with $z_1 > 0$ described by Eq.(2.93), together with its osculating Keplerian orbits, corresponding to the instantaneous orbital elements of the spacecraft if the thrust is nulled. In this case, it is shown how the semi-major axis and eccentricity of the osculating orbits do not change, but the osculating orbit plane rotates around the vertical axis. The spacecraft, being always at the apogee of the osculating Keplerian orbits, describes the desired NKO. Therefore, the envelope resulting from the osculating Keplerian orbits after an entire orbit is well approximated by a truncated cone, characterized by height H and radii of the bases r_1, r_2, as follows.

$$\begin{cases} r_1 = a(1-e)\cos i \\ r_2 = \rho \\ H = |z| + |a(1-e)\sin i| \end{cases} \tag{2.98}$$

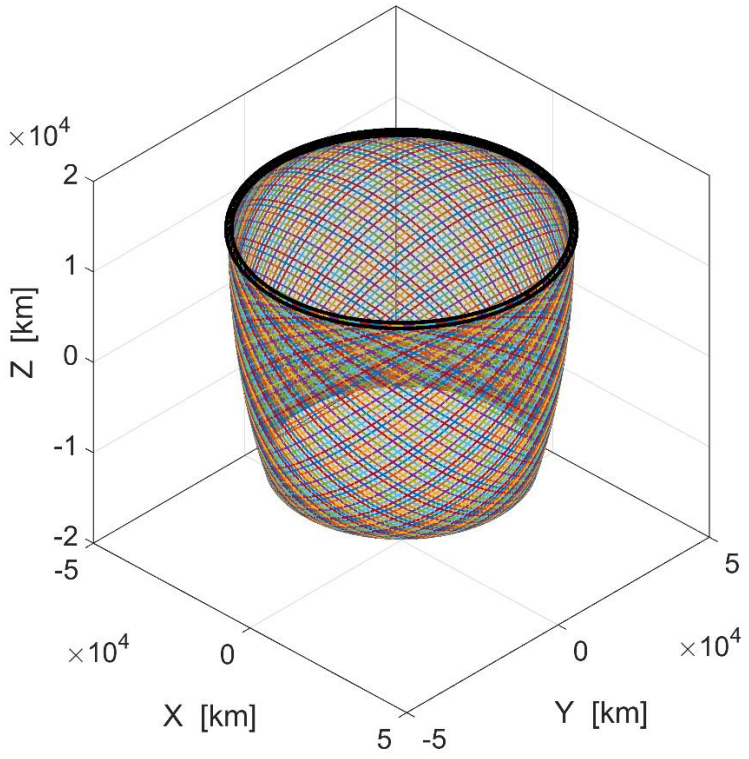

Figure 4. Type 1 out-of-plane displaced GEO (solid black line) and osculating Keplerian orbits. In gray is shown the truncated cone envelope resulting from the osculating Keplerian orbits after an entire orbit.

In the following sub-sections, the results of the mappings using each set of osculating elements are shown and discussed.

1. Classical Keplerian elements

Table 1 shows the summary of the results of the non-Keplerian orbit to classical Keplerian elements map for all the test cases taken into account.

Table 1. Summary of the results of the non-Keplerian orbit to classical Keplerian elements map.*

	GEO	**Type 1 NKO**	**Type 2 NKO**	**Type 3 NKO (out of plane)**	**Type 3 NKO (in plane)**
$a\ [r_{GEO}]$	1	0.9	$\sim 10 \quad (z_2 = \pm 10 R_\oplus)$ $\sim 1.7 \quad (z_2 = \pm 5 R_\oplus)$	$\sim 1.5 \quad (\rho_{3op} = 0.9 r_{GEO})$ $\sim 2.4 \quad (\rho_{3op} = r_{GEO})$ $\sim 7.4 \quad (\rho_{3op} = 1.1 r_{GEO})$	$0.7 \quad (\rho_{3ip} = 0.9 r_{GEO})$ $1.6 \quad (\rho_{3ip} = 1.1 r_{GEO})$
e	0	0.12	$0.8 \quad (z_2 = \pm 10 R_\oplus)$ $0.25 \quad (z_2 = \pm 5 R_\oplus)$	$0.09 \quad (\rho_{3op} = 0.9 r_{GEO})$ $0.4 \quad (\rho_{3op} = r_{GEO})$ $0.8 \quad (\rho_{3op} = 1.1 r_{GEO})$	$0.27 \quad (\rho_{3ip} = 0.9 r_{GEO})$ $0.33 \quad (\rho_{3ip} = 1.1 r_{GEO})$
$i\ [\text{deg}]$	0	20	$56 \quad (z_2 = \pm 10 R_\oplus)$ $37 \quad (z_2 = \pm 5 R_\oplus)$	$48 \quad (\rho_{3op} = 0.9 r_{GEO})$ $45 \quad (\rho_{3op} = r_{GEO})$ $42 \quad (\rho_{3op} = 1.1 r_{GEO})$	0
$\Omega\ [\text{deg}]$	0	$90 \nearrow \quad (z_1 < 0)$ $270 \nearrow \quad (z_1 > 0)$	$90 \nearrow \quad (z_2 < 0)$ $270 \nearrow \quad (z_2 > 0)$	$90 \nearrow \quad (z_{3op} < 0)$ $270 \nearrow \quad (z_{3op} > 0)$	0
$\omega\ [\text{deg}]$	0	$90 \quad (z_1 < 0)$ $270 \quad (z_1 > 0)$	$270 \quad (z_2 < 0)$ $90 \quad (z_2 > 0)$	$270 \quad (z_{3op} < 0)$ $90 \quad (z_{3op} > 0)$	$180 \nearrow \quad (\rho_{3ip} < r_{GEO})$ $0 \nearrow \quad (\rho_{3ip} > r_{GEO})$
$\vartheta\ [\text{deg}]$	$0 \nearrow$	180	0	$0 \quad (\rho_{3op} \geq r_{GEO})$ $180 \quad (\rho_{3op} < r_{GEO})$	$180 \quad (\rho_{3ip} < r_{GEO})$ $0 \quad (\rho_{3ip} > r_{GEO})$

*The symbol $\nearrow$ is used with the meaning "linearly increasing with slope ϖ". The entry $\tau_0 \nearrow$, for instance, means that the value of the generic angle τ in time is $\tau(t) = \tau_0 + \varpi t$.

2. Modified equinoctial elements

Table 2 shows the summary of the results of the non-Keplerian orbit to modified equinoctial elements map for all the test cases taken into account.

Table 2. Summary of the results of the non-Keplerian orbit to modified equinoctial elements map.*

	GEO	Type 1 NKO	Type 2 NKO	Type 3 NKO (out of plane)	Type 3 NKO (in plane)
p $[r_{GEO}]$	1	0.88	$\sim 3.3 \ (z_2 = \pm 10 R_\oplus)$ $\sim 1.6 \ (z_2 = \pm 5 R_\oplus)$	$\sim 1.5 \ (\rho_{3op} = 0.9 r_{GEO})$ $\sim 2 \ \ (\rho_{3op} = r_{GEO})$ $\sim 2.7 \ (\rho_{3op} = 1.1 r_{GEO})$	$0.7 \ \ (\rho_{3ip} = 0.9 r_{GEO})$ $1.5 \ \ (\rho_{3ip} = 1.1 r_{GEO})$
f	0	$f = f_0 \cos(\varpi t)$ with $f_0 < 0$	$f = f_0 \cos(\varpi t)$ with $f_0 > 0$		$f = f_0 \cos(\varpi t)$ with $\begin{cases} f_0 < 0 & (\rho_{3ip} < r_{GEO}) \\ f_0 > 0 & (\rho_{3ip} > r_{GEO}) \end{cases}$
g	0	$g = g_0 \sin(\varpi t)$ with $g\left(t < \frac{T_{orb}}{2}\right) \le 0$	$g = g_0 \sin(\varpi t)$ with $g\left(t < \frac{T_{orb}}{2}\right) > 0$		$g = g_0 \sin(\varpi t)$ with $\begin{cases} g\left(t < \frac{T_{orb}}{2}\right) \le 0 & (\rho_{3ip} < r_{GEO}) \\ g\left(t < \frac{T_{orb}}{2}\right) > 0 & (\rho_{3ip} > r_{GEO}) \end{cases}$
h	0	$h = h_0 \sin(\varpi t)$ with $\begin{cases} h\left(t < \frac{T_{orb}}{2}\right) \le 0 & (z < 0) \\ h\left(t < \frac{T_{orb}}{2}\right) > 0 & (z > 0) \end{cases}$			0
k	0	$k = k_0 \cos(\varpi t)$ with $\begin{cases} k_0 > 0 & (z < 0) \\ k_0 < 0 & (z > 0) \end{cases}$			0
L [deg]	$0 \nearrow$	$0 \nearrow$	$0 \nearrow$	$0 \nearrow$	$0 \nearrow$

* The symbol $\nearrow$ is used with the meaning "linearly increasing with slope ϖ". The entry $\tau_0 \nearrow$, for instance, means that the value of the generic angle τ in time is $\tau(t) = \tau_0 + \varpi t$.

Figures 5-6 show the evolution over one orbit of the in-plane modified equinoctial element f and the out-of-plane modified equinoctial element h, respectively. It can be seen that the amplitudes of the oscillations depend respectively on the eccentricity and inclination of the osculating orbits, as defined in Eq. (2.24).

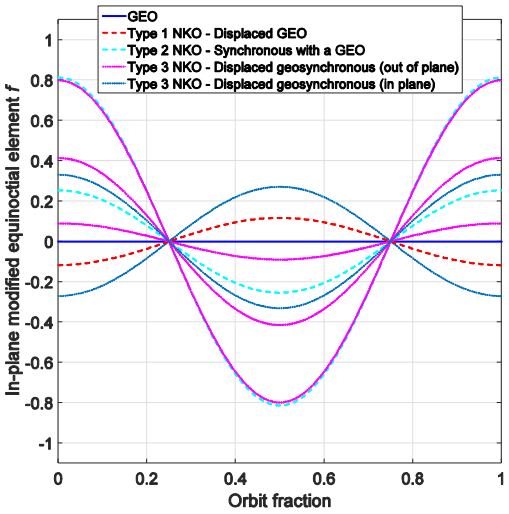

Figure 5. Evolution of the osculating in-plane modified equinoctial element *f* over one orbit.

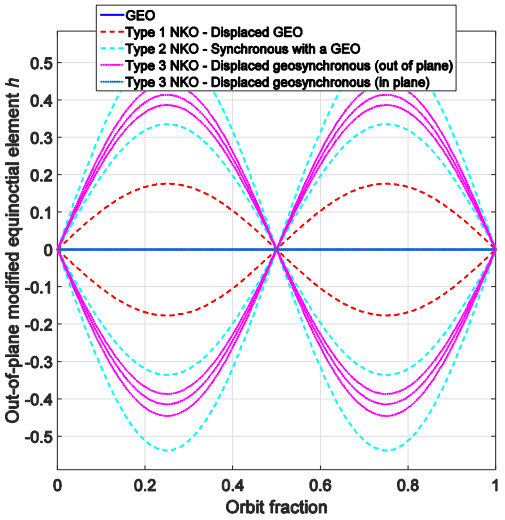

Figure 6. Evolution of the osculating out-of-plane modified equinoctial element *h* over one orbit.

3. Augmented integrals of motion

Figure 7 shows the cone created by the osculating angular momenta due to the rotation of the osculating Keplerian orbits. The height of the cone and its base radius depend on both vertical displacement z and radius of the orbit ρ. For example, the two Type 2 NKOs with the largest vertical displacement are those with the largest base radius. On the other hand, the two Type 2 NKOs with $|z_2| = 5 \cdot R_\oplus$ have a smaller base radius than the out-of-plane Type 3 NKOs, which have $|z_{3op}| = r_{GEO}$. Among the Type 3 NKOs, the orbits with the lowest radius ρ_{3op} have the largest base radius, followed by the orbits with the largest radius and, last, those orbits with $\rho_{3op} \equiv z_{3op}$. The osculating angular momenta for the in-plane Type 3 NKOs is parallel to the angular momentum of GEO and therefore not clearly distinguishable in the plot.

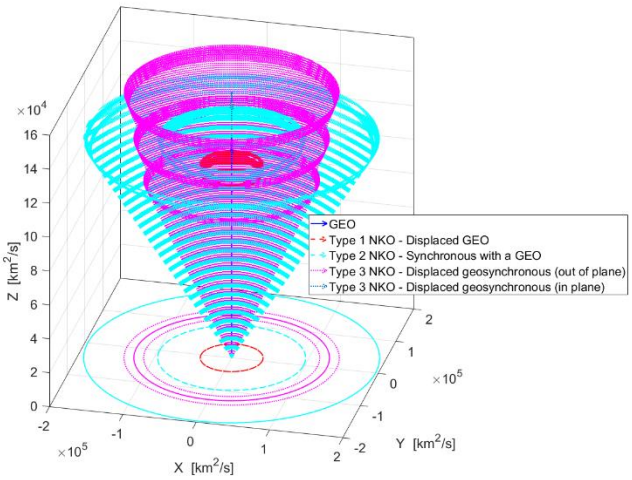

Figure 7. Time evolution of the osculating angular momentum vector. All the test cases studied are shown.

Figure 8 shows the double cone created by the osculating eccentricity vectors due to the rotation of the osculating Keplerian orbits. The height of the cone and its base radius depend on both the vertical displacement z and the radius of the orbit ρ. The osculating eccentricity vector depend on the sign of the vertical displacement, whereas the osculating angular momentum does not. Moreover, in this case, the behavior is different with respect to the angular momentum, as can be better seen from Figure 9. For example, the two Type 2 NKOs with the largest vertical displacement are not those with the largest base radius, but are those with the largest value of eccentricity. On the other hand, the two Type 3 NKOs with $\rho_{3op} = 1.1 \cdot r_{GEO}$ have the largest base radius. The osculating eccentricity vectors for the in-plane Type 3 NKOs lie on the $\hat{\boldsymbol{X}} - \hat{\boldsymbol{Y}}$ plane, while the eccentricity vector in the GEO case is arbitrarily set to $\boldsymbol{e}_{GEO} = \begin{bmatrix} 1 & 0 & 0 \end{bmatrix}^T$.

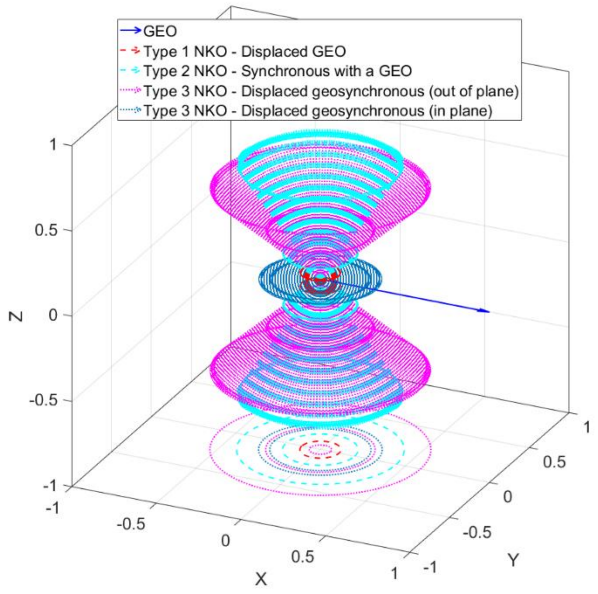

Figure 8. Time evolution of the osculating eccentricity vector. All test cases studied are shown.

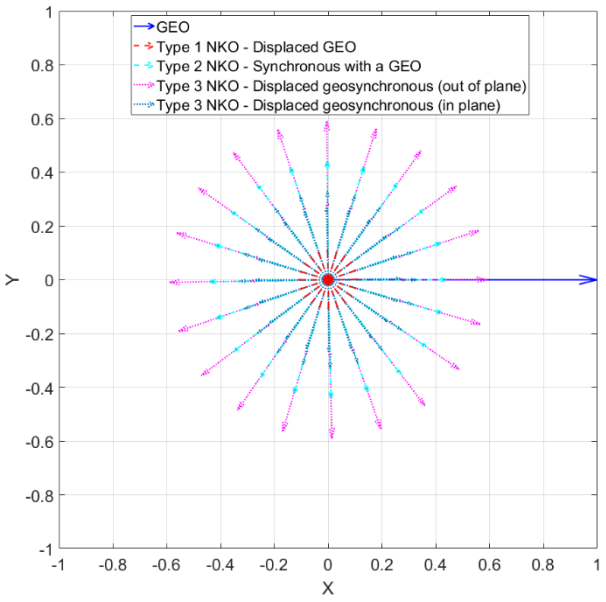

Figure 9. Time evolution of the osculating eccentricity vector. X-Y view.

2.1.3.2. Sensitivity Analysis

Three test cases have been used to investigate the sensitivity of the mappings to a change in the NKO elements $\left[z, \rho, \varpi\right]^T$. All the test cases are chosen as feasible mission scenarios, with reasonable required low-thrust acceleration, and are all displaced GEO.

The first test case is an out-of-plane displaced GEO Type 1 NKO, defined as in Eq. (2.93). The displacement angle $\Delta\lambda$ has been chosen such that the spacecraft hovers above GEO at a vertical displacement equal to twice the station-keeping box. Station-keeping regulations currently require a station-keeping box height of $\Delta\lambda \in \left[0.05,\ 0.1\right]\text{deg}$.[4] The worst-case scenario is taken into account here so that Eq. (2.93) becomes

$$\text{Out-of-plane displaced GEO (Type 1 NKO)}: \begin{cases} z_1 = r_{GEO} \sin\left(0.2\,\text{deg}\right) = 147 \text{ km} \\ \rho_1 = r_{GEO} \cos\left(0.2\,\text{deg}\right) \approx r_{GEO} \\ \varpi_1 = \sqrt{\mu / r_{GEO}^3} \end{cases} \tag{2.99}$$

The second test case is an in-plane displaced GEO Type 3 NKO. A positive in-plane displacement of $\Delta\rho_3 = 147$ km is considered. This value has been chosen to be the same as the out-of-plane displacement, as in Heiligers at al.[4]

$$\text{In-plane displaced GEO (Type 3 NKO)}: \begin{cases} z_3 = 0 \\ \rho_3 = r_{GEO} + 147 \text{ km} \\ \varpi_3 = \sqrt{\mu / r_{GEO}^3} \end{cases} \tag{2.100}$$

The last test case has been chosen in order to verify the behavior of the map in case of very small vertical displacements, such that a small error in the out-of-plane displacement $z_{1(2)}$ causes the orbit to cross the $z = 0$ plane. Such a test case has been chosen as a feasible mission scenario for a displaced GEO Type 1 NKO with a small vertical displacement, defined in Eq. (2.93). The displacement angle $\Delta\lambda$ has been chosen so that the actual out-of-plane displacement is $z_{1(2)} \sim 10^{-1}$ km. Therefore, Eq. (2.93) becomes

$$\text{Out-of-plane displaced GEO (Type 1 NKO)}: \begin{cases} z_{1(2)} = r_{GEO} \sin\left(-10^{-4} \text{ deg}\right) = -0.08 \text{ km} \\ \rho_{1(2)} = r_{GEO} \cos\left(-10^{-4} \text{ deg}\right) \approx r_{GEO} \\ \varpi_{1(2)} = \sqrt{\mu / r_{GEO}^3} \end{cases} \tag{2.101}$$

The relative error of the NKO elements is considered fixed and constant, as follows.

$$\begin{cases} \varepsilon_z = \begin{cases} 10^{-3} & (0.1\%) \quad \text{First two test cases} \\ 2 & (200\%) \quad \text{Third test case} \end{cases} \\ \varepsilon_\rho = \varepsilon_\varpi = 10^{-3} \quad (0.1\%) \end{cases} \tag{2.102}$$

Note that the relative error related to the out-of-plane displacement $z_{1(2)}$ for the third test case is much larger than that considered for the other two. This has been done in order to have a crossing of the $z = 0$ plane. In fact, a 200% error on $z_{1(2)}$ for the third test case corresponds to the same displacement as the original but with a different sign, as shown in Eq. (2.105).

The values of the absolute errors in the three test cases are as follows.

$$\text{Out-of-plane displaced GEO (Type 1 NKO)}: \begin{cases} \delta z_1 = \varepsilon_z z_1 \approx 0.15 \text{ km} \\ \delta\rho_1 = \varepsilon_\rho \rho_1 \approx 42.2 \text{ km} \\ \delta\varpi_1 = \varepsilon_\varpi \varpi_1 \approx 0.36 \text{ deg/day} \end{cases} \tag{2.103}$$

$$\text{In-plane displaced GEO (Type 3 NKO)}: \begin{cases} \delta z_3 = \varepsilon_z z_1 \approx 0.15 \text{ km} \\ \delta\rho_3 = \varepsilon_\rho \rho_3 \approx 42.3 \text{ km} \\ \delta\varpi_3 = \varepsilon_\varpi \varpi_3 \approx 0.36 \text{ deg/day} \end{cases} \tag{2.104}$$

$$\text{Out-of-plane small-displacement GEO (Type 1 NKO)}: \begin{cases} \delta z_{1(2)} = \varepsilon_z \left| z_{1(2)} \right| \approx 0.16 \text{ km} \\ \delta\rho_{1(2)} = \varepsilon_\rho \rho_{1(2)} \approx 42.2 \text{ km} \\ \delta\varpi_{1(2)} = \varepsilon_\varpi \varpi_{1(2)} \approx 0.36 \text{ deg/day} \end{cases} \tag{2.105}$$

Note that the term δz_3 in Eq. (2.104) depends on the displacement z_1 of the out-of-plane displaced GEO. This is made on purpose in order to have a non-zero error for the out-of-plane displacement.

The analytical sensitivity analysis has been described in Section 2.1.2. The numerical sensitivity analysis has been performed by computing the values of the osculating elements from the perturbed NKO elements and then computing the errors as described for the analytical case.

Results and discussion

1. Classical Keplerian elements

The sensitivity analysis study demonstrates that the mapping that uses the classical Keplerian elements is extremely sensitive to uncertainties in the NKO elements. This is mainly due to the piecewise formulation of the map itself. A small error on either ρ or ϖ, for example, can cause the value of the argument of perigee ω to jump from one branch to another (see Eq. (2.23)). Moreover, only a numerical sensitivity analysis can be carried out on half of the classical Keplerian elements.

For the sake of conciseness, only the most interesting plots of the sensitivity analysis study are shown here. Table 3 shows a summary of the results of the sensitivity analysis study in the case of classical Keplerian elements.

Table 3. Summary of the results of the sensitivity analysis study in case of classical Keplerian elements.*

Errors due to uncertainties	**Test case**	δz	$\delta\rho$	$\delta\varpi$
ε_a	all	$<10^{-6}$%	0.4%	0.2%
ε_e	all	$<10^{-8}$	3×10^{-3}	2×10^{-3}
ε_i	1	10^{-4}%	10^{-4}%	0
	2		~ 0	
	3	0	0	
ε_Ω	1	0	0	linearly increasing up to 0.2%
	2	up to 100%		0
	3	100%		linearly increasing up to 0.2%
ε_ω	1	0	100%	100%
	2	up to 100%	0	linearly increasing up to 0.2%
	3	100%	100%	100%
ε_ϑ	1-3	0	100%	100%
	2		0	0

* Note that sometimes ~0 is used against 0. This is done to stress the difference between a null value and a very small (numerical) value.

Figure 10 shows the evolution of the osculating RAAN Ω over one orbit. The test case for the small displacement GEO (test case 3) is shown. The nominal value and the values due to the uncertainties on the NKO elements are considered. It is shown that an error in the out-plane displacement causes the RAAN to have a constant 180-deg error due to the piecewise formulation of the map (Eq. (2.23)). Figure 11 shows a zoom on the $\hat{\boldsymbol{Y}}$ axis of the normalized error of the RAAN for the same test case. It is shown how an error on the orbital angular velocity causes the RAAN (and, therefore, the orbit plane) to rotate at a different velocity. The first test case shows the same behavior. Similarly, the argument of perigee shows the same behavior in case of planar orbit (i.e. test case 2).

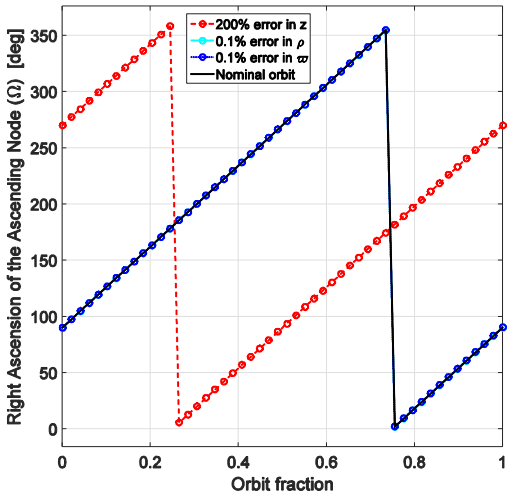

Figure 10. Evolution of the osculating RAAN over one orbit. Very small displacement GEO (test case 3).

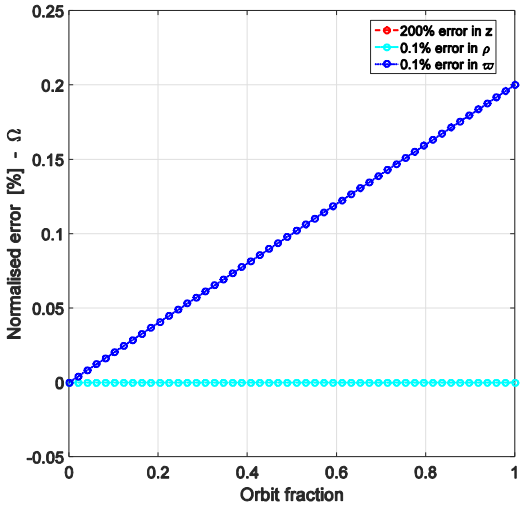

Figure 11. Normalized error of the RAAN for the case of very small displacement GEO (test case 3). Zoom on Y axis.

2. Modified equinoctial elements

For what concerns the modified equinoctial elements, the sensitivity analysis study demonstrates that the mapping that uses these elements is very robust to uncertainties in the NKO elements.

For the sake of conciseness, only the most interesting plots of the sensitivity analysis study are shown here. Table 4 shows a summary of the results of the sensitivity analysis study in the case of modified equinoctial elements.

Table 4. Summary of the results of the sensitivity analysis study in case of modified equinoctial elements.*

Errors due to uncertainties	**Test case**	δz	$\delta\rho$	$\delta\varpi$
ε_p	all	~ 0	0.4%	0.2%
ε_f	all	~ 0	$< 3\times10^{-3}$	$< 2\times10^{-3}$
ε_g	all	~ 0	$< 3\times10^{-3}$	$< 2\times10^{-3}$
ε_h	1	$< 2\times10^{-6}$	$< 2\times10^{-6}$	$< 10^{-5}$
	2		0	0
	3		$< 10^{-9}$	$< 6\times10^{-9}$
ε_k	1	$< 2\times10^{-6}$	$< 2\times10^{-6}$	$< 9\times10^{-6}$
	2		0	0
	3		$< 10^{-9}$	$< 5\times10^{-9}$
ε_L	all	0	0	linearly increasing up to 0.2%

* Note that sometimes ~0 is used against 0. This is done to stress the difference between a null value and a very small (numerical) value.

Figure 12 shows the evolution over one orbit of the in-plane modified equinoctial element f. The test case for the out-of-plane displaced GEO (test case 1) is shown. The nominal value and the values due to errors in the NKO elements are shown. It can be seen that the error on the in-plane element f due to uncertainties in the NKO elements is of the same order of magnitude as the uncertainties themselves. The same behavior is noted for the other in-plane modified equinoctial element g. On the other hand, Figure 13 shows the evolution over one orbit of the out-of-plane modified equinoctial element h. The nominal value and the values due to errors in the NKO elements are shown. Figure 13 shows that the error on the out-of-plane element h due to uncertainties in the NKO elements is orders of magnitude smaller than the value of the uncertainties. The same behavior is noted in the other out-of-plane modified equinoctial element k. Here, the semi-latus rectum shows a constant error due to uncertainties in the NKO elements of the same order of magnitude as the uncertainties themselves. Lastly, the true longitude exhibits a linearly increasing error due to a 0.1% uncertainty on the orbit angular velocity, as shown in Figure 11 for the RAAN case. After one orbit, the absolute error on the true longitude is $\delta L = 0.36$ deg.

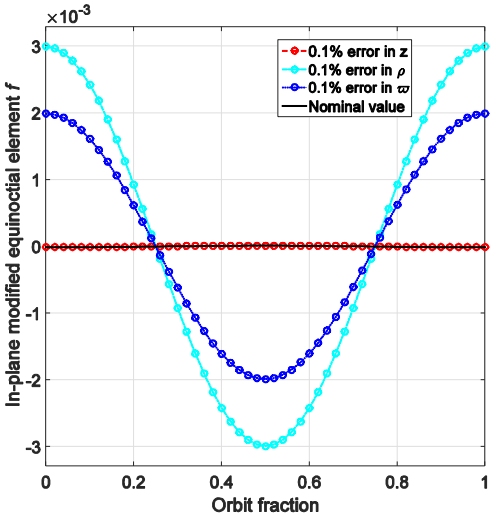

Figure 12. Evolution of the osculating in-plane modified equinoctial element *f* over one orbit. Out-of-plane displaced GEO (test case 1).

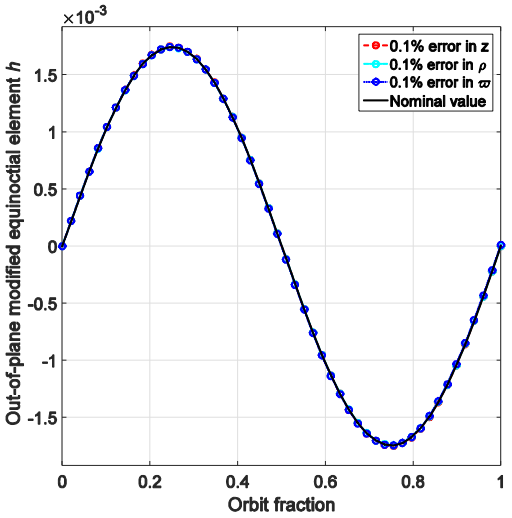

Figure 13. Evolution of the osculating out-of-plane modified equinoctial element *h* over one orbit. Out-of-plane displaced GEO (test case 1).

3. Augmented integrals of motion

For the augmented integrals of motion, the sensitivity analysis study demonstrates that the mapping that uses these elements is robust to uncertainties in the NKO elements.

For the sake of conciseness, and because all the errors are constant, the plots of the sensitivity analysis study are not shown here. Table 5 shows a summary of the results of the sensitivity analysis study in the case of augmented integrals of motion.

Table 5. Summary of the results of the sensitivity analysis study in case of augmented integrals of motion.*

Errors due to uncertainties	**Test case**	δz	$\delta\rho$	$\delta\varpi$
ε_h	all	3×10^{-4}%	0.2%	0.1%
ε_e	all	~ 0	3×10^{-3}	2×10^{-3}
ε_L	all	0	0	linearly increasing up to 0.2%

* Note that sometimes ~0 is used against 0. This is done to stress the difference between a null value and a very small (numerical) value.

2.1.4. Non-Keplerian Orbit to Osculating Orbital Elements Map: Summary

A summary of advantages and drawbacks of the three forward mappings investigated in this study is shown in Table 6.

It has been noted that, regardless of the mapping and the test case chosen, a spacecraft on a non-Keplerian orbit is always at either the apogee or perigee of the osculating Keplerian orbit. This can cause sensitivity issues in case of small eccentricity. If the eccentricity of an orbit if small, as in the test cases presented here, even small variations of the NKO elements can cause the eccentricity vector to change sign. As shown in Eq. (2.23), if the term $\mu - \varpi^2 \rho^2 \sqrt{\rho^2 + z^2}$ changes sign due to a variation in one of the NKO elements, the eccentricity vector changes sign. Similarly, both argument of perigee and true anomaly have a 180-deg difference with respect to their previous values. Therefore, the spacecraft appears to instantaneously change its position in the osculating Keplerian orbit from apogee to perigee or vice versa, without changing its physical position in the Cartesian reference frame. The modified equinoctial elements are not affected by this problem. This characteristic, together with their easy formulation and their robustness to uncertainties in the NKO elements, makes the use of modified equinoctial elements the best choice for the non-Keplerian orbit to osculating orbital elements map.

Table 6. NKO to osculating orbital elements map. Summary of advantages and drawbacks of the chosen mappings.

	Classical Keplerian elements	**Modified equinoctial elements**	**Augmented integrals of motion**
Advantages	• Easy to understand • Only one element is time dependent	• Easy formulation (no piecewise elements) • Robust to uncertainties in the NKO elements • Robust to the switch apogee/perigee • No singularities • Only one element (L) is linearly increasing with time if there are uncertainties in ϖ	• Easy formulation • No singularities
Drawbacks	• Piecewise formulation • Very sensitive to uncertainties • Issues around $z = 0$ • Singularity: $\Omega = 0$ if $z = 0$ • Very sensitive to the switch apogee/perigee • Analytical Jacobian undefined for 3 out of 6 elements because of the piecewise formulation • Two elements (Ω, ω) are linearly increasing with time if there are uncertainties in ϖ	• 5 elements are time dependent	• Less intuitive • 7 elements instead of 6 • Very sensitive to the switch apogee/perigee (eccentricity vector changes sign)

2.2. Inverse Map: Osculating Orbital Elements to Non-Keplerian Orbit

After the forward mappings from non-Keplerian orbits families to osculating orbital elements described in Section 2.1, three different inverse mappings from orbital elements to non-Keplerian orbit geometry have been generated. These mappings have been derived in closed, analytical form. A sensitivity analysis has been performed to understand the impact of uncertainties in the classical orbital elements on the NKO properties.

The analytical formulation of the three inverse mappings is shown in Section 2.2.1, whereas the sensitivity analysis performed on the maps is described in Section 2.2.2. Section 2.2.3 shows the numerical test cases taken into account. Lastly, the three mappings are compared through their advantages and drawbacks in Section 2.2.4.

2.2.1. Mappings

In the following sub-sections, the inverse mappings from osculating orbital elements to non-Keplerian orbits are summarized for the three sets of elements considered.

2.2.1.1. Classical Keplerian Elements

The map from osculating Keplerian elements $\boldsymbol{x}_{KEP}$ to Cartesian position and velocity is here derived. Note that the following map does not work in case the osculating Keplerian orbit is a parabola. However, no NKOs in the two-body problem are described by osculating parabolas.

The semi-latus rectum is given by

$$p = a\left(1-e^2\right) \tag{2.106}$$

The radius of the orbit is

$$r = \frac{p}{1+e\cos\vartheta} \tag{2.107}$$

In the orbital reference frame $\left\{\hat{\boldsymbol{r}},\hat{\boldsymbol{\vartheta}},\hat{\boldsymbol{h}}\right\}$, position and velocity vectors are given by

$$\boldsymbol{r}_{orb} = \begin{bmatrix} r\cos\vartheta \\ r\sin\vartheta \\ 0 \end{bmatrix}, \quad \boldsymbol{v}_{orb} = \begin{bmatrix} \dot{r}\cos\vartheta - r\sin\vartheta\dot{\vartheta} \\ \dot{r}\sin\vartheta + r\cos\vartheta\dot{\vartheta} \\ 0 \end{bmatrix} \tag{2.108}$$

in which

$$\begin{cases} \dot{\vartheta} = \dfrac{h}{r^2} = \dfrac{\sqrt{\mu p}}{r^2} \\ \dot{r} = \dfrac{\partial}{\partial t}\left(\dfrac{p}{1+e\cos\vartheta}\right) = \dfrac{ep\sin\vartheta\dot{\vartheta}}{\left(1+e\cos\vartheta\right)^2} = \sqrt{\dfrac{\mu}{p}}e\sin\vartheta \end{cases} \tag{2.109}$$

The rotation matrix $\mathbf{R} = \mathbf{R}_3(-\omega) \to \mathbf{R}_1(-i) \to \mathbf{R}_3(-\Omega)$ from orbital reference frame to Earth-Centered Inertial (ECI) is

$$\mathbf{R} = \begin{bmatrix} \cos\Omega\cos\omega - \cos i\sin\Omega\sin\omega & -\cos\Omega\sin\omega - \cos i\sin\Omega\cos\omega & \sin i\sin\Omega \\ \sin\Omega\cos\omega + \cos i\cos\Omega\sin\omega & -\sin\Omega\sin\omega + \cos i\cos\Omega\cos\omega & -\sin i\cos\Omega \\ \sin i\sin\omega & \sin i\cos\omega & \cos i \end{bmatrix} \tag{2.110}$$

From Eqs. (2.108) and (2.110), the Cartesian position and velocity vectors in ECI reference frame are

$$\begin{cases} \boldsymbol{r} = \mathbf{R}\boldsymbol{r}_{orb} \\ \boldsymbol{v} = \mathbf{R}\boldsymbol{v}_{orb} \end{cases} \tag{2.111}$$

From the osculating Keplerian elements to Cartesian position vector map (Eq. (2.111)) and the definition of the Cartesian position vector given in Eq. (2.5), the NKO elements $\{z, \rho\}$ are derived as follows.

$$z = r_z = \frac{a\left(1-e^2\right)}{1+e\cos\vartheta}\left(\sin i\sin\omega\cos\vartheta + \sin i\cos\omega\sin\vartheta\right) = \frac{a\left(1-e^2\right)}{1+e\cos\vartheta}\sin i\sin\left(\omega+\vartheta\right) \tag{2.112}$$

$$\rho = \sqrt{r_x^2 + r_y^2} = \frac{a\left(1-e^2\right)}{1+e\cos\vartheta}\sqrt{\left(R_{11}\cos\vartheta + R_{12}\sin\vartheta\right)^2 + \left(R_{21}\cos\vartheta + R_{22}\sin\vartheta\right)^2} \tag{2.113}$$

After some algebraic manipulations of Eq. (2.113), the formulation for the orbital radius ρ is

$$\rho = \frac{a\left(1-e^2\right)}{2\left(1+e\cos\vartheta\right)}\sqrt{3+\cos\left(2i\right)+2\cos\left(2\left(\omega+\vartheta\right)\right)\sin^2 i} \tag{2.114}$$

For what concerns the orbital angular velocity ϖ, let us compute first the magnitude of the velocity vector. Because the rotation matrix $\mathbf{R}$ shown in Eq. (2.110) does not change the magnitude of the vector, it is easier to compute the magnitude of the velocity vector in the orbital reference frame (Eq. (2.108)).

$$v = \sqrt{\left(\dot{r}\cos\vartheta - r\sin\vartheta\dot{\vartheta}\right)^2 + \left(\dot{r}\sin\vartheta + r\cos\vartheta\dot{\vartheta}\right)^2} = \ldots = \sqrt{\dot{r}^2 + r^2\dot{\vartheta}^2} \tag{2.115}$$

Using Eq. (2.109) and after some algebraic manipulation, Eq. (2.115) becomes

$$v = \sqrt{\frac{\mu}{p}\left(1+e^2+2e\cos\vartheta\right)} \tag{2.116}$$

Therefore, the formulation of the orbital angular velocity ϖ is given by

$$\varpi = \frac{v}{\rho} = \sqrt{\frac{\mu}{a^3\left(1-e^2\right)^3}}2\left(1+e\cos\vartheta\right)\sqrt{\frac{1+e^2+2e\cos\vartheta}{3+\cos\left(2i\right)+2\cos\left(2\left(\omega+\vartheta\right)\right)\sin^2 i}} \tag{2.117}$$

Summary

The inverse map from osculating classical Keplerian elements to NKOs elements described in Section 2.2.1.1 is summarized as

$$\begin{aligned} z &= \frac{a\left(1-e^2\right)}{1+e\cos\vartheta}\sin i\sin\left(\omega+\vartheta\right) \\ \rho &= \frac{a\left(1-e^2\right)}{2\left(1+e\cos\vartheta\right)}\sqrt{3+\cos\left(2i\right)+2\cos\left(2\left(\omega+\vartheta\right)\right)\sin^2 i} \\ \varpi &= \sqrt{\frac{\mu}{a^3\left(1-e^2\right)^3}}2\left(1+e\cos\vartheta\right)\sqrt{\frac{1+e^2+2e\cos\vartheta}{3+\cos\left(2i\right)+2\cos\left(2\left(\omega+\vartheta\right)\right)\sin^2 i}} \end{aligned} \tag{2.118}$$

2.2.1.2. Modified Equinoctial Elements

The map from osculating modified equinoctial elements $\boldsymbol{x}_{MEE}$ to Cartesian position and velocity is now derived.

First, let us define the following auxiliary variables, which will be useful in the mathematical derivation to shorten the equations.

$$\begin{cases} q = 1+ f\cos L + g\sin L \\ r = p/q \\ s = 1+h^2+k^2 \\ \beta = h^2-k^2 \end{cases} \tag{2.119}$$

From Broucke and Cefola,[23] and after some algebraic manipulation due to the difference in the elements considered, the formulation of the Cartesian position vector is given as from Betts (Eq. 6.42, page 266).[24]

$$\boldsymbol{r} = \frac{r}{s}\begin{bmatrix} \cos L+\beta\cos L+2hk\sin L \\ \sin L-\beta\sin L+2hk\cos L \\ 2\left(h\sin L-k\cos L\right) \end{bmatrix} \tag{2.120}$$

From the formulation of the position vector in Eq. (2.120), the Cartesian velocity vector is given by Eq. (2.121), in which $dL/dt = \sqrt{\mu p}\left(q/p\right)^2$, as from De Pascale and Vasile.[25]

$$\boldsymbol{v} = \frac{\partial \boldsymbol{r}}{\partial L}\frac{dL}{dt} \tag{2.121}$$

Therefore, the formulation of the Cartesian velocity vector given by Eq. (2.121) is the same as from Betts (Eq. 6.43, page 266).[24]

$$\boldsymbol{v} = \frac{1}{s}\sqrt{\frac{\mu}{p}}\begin{bmatrix} -\sin L-\beta\sin L+2hk\cos L-g+2fhk-\beta g \\ \cos L-\beta\cos L-2hk\sin L+f-2ghk-\beta f \\ 2\left(h\cos L+k\sin L+fh+gk\right) \end{bmatrix} \tag{2.122}$$

From the osculating modified equinoctial elements to Cartesian state map (Eqs. (2.120) and (2.122)) and the definition of the Cartesian position vector given in Eq. (2.5), the NKO elements $\{z, \rho\}$ are derived as follows.

$$z = r_z = \frac{2r}{s}\left(h\sin L - k\cos L\right) \tag{2.123}$$

$$\rho = \sqrt{r_x^2 + r_y^2} = \frac{r}{s}\sqrt{\left(\cos L + \beta\cos L + 2hk\sin L\right)^2 + \left(\sin L - \beta\sin L + 2hk\cos L\right)^2} \tag{2.124}$$

After some algebraic manipulations of Eq. (2.124), the formulation for the orbital radius ρ is

$$\rho = \frac{r}{s}\sqrt{1 + \left(h^2 + k^2\right)^2 + 2\beta\cos\left(2L\right) + 4hk\sin\left(2L\right)} \tag{2.125}$$

For the orbital angular velocity ϖ, let us compute first the magnitude of the velocity vector. From Eq. (2.122), the magnitude of the velocity vector is

$$v = \sqrt{\frac{\mu}{p}}\sqrt{1 + f^2 + g^2 + 2f\cos L + 2g\sin L} \tag{2.126}$$

Therefore, the formulation of the orbital angular velocity ϖ is

$$\varpi = \frac{s}{r}\sqrt{\frac{\mu}{p}}\sqrt{\frac{1 + f^2 + g^2 + 2f\cos L + 2g\sin L}{1 + \left(h^2 + k^2\right)^2 + 2\beta\cos\left(2L\right) + 4hk\sin\left(2L\right)}} \tag{2.127}$$

Summary

The inverse map from osculating modified equinoctial elements to NKOs elements described in Section 2.2.1.2 is summarized as

$$\begin{aligned} z &= \frac{2r}{s}\left(h\sin L - k\cos L\right) \\ \rho &= \frac{r}{s}\sqrt{1 + \left(h^2 + k^2\right)^2 + 2\beta\cos\left(2L\right) + 4hk\sin\left(2L\right)} \\ \varpi &= \frac{s}{r}\sqrt{\frac{\mu}{p}}\sqrt{\frac{1 + f^2 + g^2 + 2f\cos L + 2g\sin L}{1 + \left(h^2 + k^2\right)^2 + 2\beta\cos\left(2L\right) + 4hk\sin\left(2L\right)}} \end{aligned} \tag{2.128}$$

in which

$$\begin{cases} r = \dfrac{p}{1 + f\cos L + g\sin L} \\ s = 1 + h^2 + k^2 \\ \beta = h^2 - k^2 \end{cases} \tag{2.129}$$

2.2.1.3. Augmented Integrals of Motion

The map from osculating augmented integrals of motion $\boldsymbol{x}_{AIoM}$ to Cartesian position and velocity is now derived. Let us recall here the following expressions that link the integrals of motion with the Cartesian position and velocity, which will be useful for the mathematical derivation of the inverse mapping.

$$\boldsymbol{h} = \boldsymbol{r} \times \boldsymbol{v} \tag{2.130}$$

$$\boldsymbol{e} = \left(\frac{v^2}{\mu} - \frac{1}{r} \right) \boldsymbol{r} \tag{2.131}$$

The magnitude of the orbital angular momentum is

$$\|\boldsymbol{h}\| = \sqrt{p\mu} = \sqrt{a\left(1-e^2\right)\mu} \tag{2.132}$$

Therefore, the semi-major axis can be retrieved by Eq. (2.132).

$$a = \frac{\|\boldsymbol{h}\|^2}{\mu\left(1-e^2\right)} \tag{2.133}$$

Reminding us that the instantaneous position vector along the NKO corresponds always with either the apogee or the perigee of the osculating Keplerian orbit, the magnitude of the position vector is given by Eq. (2.134), in which the plus/minus sign is referred to the case of apogee/perigee, respectively.

$$r = a\left(1 \pm e\right) = \frac{\|\boldsymbol{h}\|^2}{\mu\left(1-e^2\right)}\left(1 \pm e\right) \tag{2.134}$$

The direction of the position vector is the same as that of the eccentricity, as shown in Eq. (2.131). However, there is an uncertainty on the sign of the position unit vector which is related to $\operatorname{sgn}\left(\frac{v^2}{\mu} - \frac{1}{r} \right)$.

$$\hat{\boldsymbol{r}} = \begin{cases} -\hat{\boldsymbol{e}} & \text{if } \left(\frac{v^2}{\mu} - \frac{1}{r} \right) < 0 \text{ (apogee)} \\ \hat{\boldsymbol{e}} & \text{if } \left(\frac{v^2}{\mu} - \frac{1}{r} \right) > 0 \text{ (perigee)} \end{cases} \tag{2.135}$$

From Eqs. (2.134) – (2.135), the formulation of the Cartesian position vector is given by

$$\boldsymbol{r} = \begin{cases} -\frac{\|\boldsymbol{h}\|^2}{\mu\left(1-e\right)}\hat{\boldsymbol{e}} & \text{(apogee)} \\ \frac{\|\boldsymbol{h}\|^2}{\mu\left(1+e\right)}\hat{\boldsymbol{e}} & \text{(perigee)} \end{cases} \tag{2.136}$$

The ambiguity on the sign in Eq. (2.136) due to the uncertainty on the apogee or perigee position can be solved by using the information given by the true longitude. That is, the difference between the true longitude and the longitude of perigee ($\omega + \Omega$) can be either null (if the spacecraft is at the perigee of the osculating orbit) or 180 deg (if the spacecraft if at the apogee of the osculating orbit). The longitude of perigee is given by the eccentricity unit vector as follows.

$$\omega+\Omega=\arctan\left(\frac{e_x}{e},\frac{e_y}{e}\right)=\arctan\left(e_x,e_y\right) \tag{2.137}$$

Therefore, apogee and perigee are defined as follows.

$$\begin{cases}\text{apogee} & \text{if } \operatorname{mod}\left(\omega+\Omega+\pi,2\pi\right)=L\\ \text{perigee} & \text{if } \omega+\Omega=L\end{cases} \tag{2.138}$$

in which all the angles are considered to lie in the open interval $\left[0,2\pi\right)$.

From the definition in Eq. (2.138), the formulation of the Cartesian position vector in Eq. (2.136) can be rewritten as

$$\boldsymbol{r}=\begin{cases}-\dfrac{\|\boldsymbol{h}\|^2}{\mu\left(1-e\right)}\hat{\boldsymbol{e}} & \text{if } \operatorname{mod}\left(\arctan\left(e_x,e_y\right)+\pi,2\pi\right)=L\\ \dfrac{\|\boldsymbol{h}\|^2}{\mu\left(1+e\right)}\hat{\boldsymbol{e}} & \text{if } \arctan\left(e_x,e_y\right)=L\end{cases} \tag{2.139}$$

From Eq. (2.130), because the radial component of the velocity is always zero for the NKOs considered, the magnitude of the velocity vector is simply given by

$$v=\frac{\|\boldsymbol{h}\|}{r}=\begin{cases}\dfrac{\mu}{\|\boldsymbol{h}\|}\left(1-e\right) & \text{if } \operatorname{mod}\left(\arctan\left(e_x,e_y\right)+\pi,2\pi\right)=L\\ \dfrac{\mu}{\|\boldsymbol{h}\|}\left(1+e\right) & \text{if } \arctan\left(e_x,e_y\right)=L\end{cases} \tag{2.140}$$

The direction of the velocity is

$$\hat{\boldsymbol{v}}=\hat{\boldsymbol{h}}\times\hat{\boldsymbol{r}}=\begin{cases}-\left(\hat{\boldsymbol{h}}\times\hat{\boldsymbol{e}}\right) & \text{if } \operatorname{mod}\left(\arctan\left(e_x,e_y\right)+\pi,2\pi\right)=L\\ \left(\hat{\boldsymbol{h}}\times\hat{\boldsymbol{e}}\right) & \text{if } \arctan\left(e_x,e_y\right)=L\end{cases} \tag{2.141}$$

Therefore, the expression of the velocity vector is given by

$$\boldsymbol{v}=\begin{cases}-\dfrac{\mu}{\|\boldsymbol{h}\|}\left(1-e\right)\left(\hat{\boldsymbol{h}}\times\hat{\boldsymbol{e}}\right) & \text{if } \operatorname{mod}\left(\arctan\left(e_x,e_y\right)+\pi,2\pi\right)=L\\ \dfrac{\mu}{\|\boldsymbol{h}\|}\left(1+e\right)\left(\hat{\boldsymbol{h}}\times\hat{\boldsymbol{e}}\right) & \text{if } \arctan\left(e_x,e_y\right)=L\end{cases} \tag{2.142}$$

From the osculating augmented integrals of motion to Cartesian position vector map (Eq. (2.139)), and the definition of the Cartesian position vector given in Eq. (2.5), the parameters z and ρ are derived as follows.

$$z=r_z=\begin{cases}-\dfrac{\|\boldsymbol{h}\|^2}{\mu\left(1-e\right)}e_z & \text{if } \operatorname{mod}\left(\arctan\left(e_x,e_y\right)+\pi,2\pi\right)=L\\ \dfrac{\|\boldsymbol{h}\|^2}{\mu\left(1+e\right)}e_z & \text{if } \arctan\left(e_x,e_y\right)=L\end{cases} \tag{2.143}$$

$$\rho = \sqrt{r_x^2 + r_y^2} = \begin{cases} \dfrac{\|\boldsymbol{h}\|^2}{\mu(1-e)}\sqrt{(e_x/e)^2 + (e_y/e)^2} & \text{if } \operatorname{mod}\left(\arctan(e_x, e_y) + \pi, 2\pi\right) = L \\ \dfrac{\|\boldsymbol{h}\|^2}{\mu(1+e)}\sqrt{(e_x/e)^2 + (e_y/e)^2} & \text{if } \arctan(e_x, e_y) = L \end{cases} \tag{2.144}$$

From the osculating augmented integrals of motion to Cartesian velocity vector magnitude map (Eq. (2.140)), and the definition of the Cartesian velocity vector given in Eq. (2.6), the parameter ϖ is derived as follows.

$$\varpi = \frac{v}{\rho} = \frac{\|\boldsymbol{h}\|}{r\rho} = \begin{cases} \dfrac{\mu^2(1-e)^2}{\|\boldsymbol{h}\|^3} \cdot \dfrac{1}{\sqrt{(e_x/e)^2 + (e_y/e)^2}} & \text{if } \operatorname{mod}\left(\arctan(e_x, e_y) + \pi, 2\pi\right) = L \\ \dfrac{\mu^2(1+e)^2}{\|\boldsymbol{h}\|^3} \cdot \dfrac{1}{\sqrt{(e_x/e)^2 + (e_y/e)^2}} & \text{if } \arctan(e_x, e_y) = L \end{cases} \tag{2.145}$$

Summary

The inverse map from osculating augmented integrals of motion to NKOs elements described in Section 2.2.1.3 is summarized as

$$z = \begin{cases} -\dfrac{\|\boldsymbol{h}\|^2}{\mu(1-e)} e_z & \text{if } \operatorname{mod}\left(\arctan(e_x, e_y) + \pi, 2\pi\right) = L \\ \dfrac{\|\boldsymbol{h}\|^2}{\mu(1+e)} e_z & \text{if } \arctan(e_x, e_y) = L \end{cases}$$

$$\rho = \begin{cases} \dfrac{\|\boldsymbol{h}\|^2}{\mu(1-e)}\sqrt{(e_x/e)^2 + (e_y/e)^2} & \text{if } \operatorname{mod}\left(\arctan(e_x, e_y) + \pi, 2\pi\right) = L \\ \dfrac{\|\boldsymbol{h}\|^2}{\mu(1+e)}\sqrt{(e_x/e)^2 + (e_y/e)^2} & \text{if } \arctan(e_x, e_y) = L \end{cases} \tag{2.146}$$

$$\varpi = \begin{cases} \dfrac{\mu^2(1-e)^2}{\|\boldsymbol{h}\|^3} \cdot \dfrac{1}{\sqrt{(e_x/e)^2 + (e_y/e)^2}} & \text{if } \operatorname{mod}\left(\arctan(e_x, e_y) + \pi, 2\pi\right) = L \\ \dfrac{\mu^2(1+e)^2}{\|\boldsymbol{h}\|^3} \cdot \dfrac{1}{\sqrt{(e_x/e)^2 + (e_y/e)^2}} & \text{if } \arctan(e_x, e_y) = L \end{cases}$$

2.2.2. Sensitivity Analysis

A sensitivity analysis has been performed in order to study the behavior of the mappings in the presence of errors in the osculating orbital elements. Only a numerical sensitivity analysis has been carried out by computing the values of the osculating elements from the perturbed input elements and then computing the errors with respect to the nominal values.

Denoting with $\boldsymbol{y}$ the set of elements chosen to describe the osculating Keplerian orbit, the parameters used to test the sensitivity of the mapping to uncertainties in the osculating orbital element y_i are as follows.

- Absolute error of the vertical displacement due to uncertainties in the input elements. The absolute error has been chosen against the relative error because all the test cases under study are characterized by small vertical displacements.

$$\varepsilon_{z,y_i} := |z - \tilde{z}| = |z - (z + \delta z)| = |\delta z| \tag{2.147}$$

- Relative error of the orbit radius due to uncertainties in the input elements. The relative error has been chosen against the absolute error because all the test cases under study are characterized by large orbit radii.

$$\varepsilon_{\rho,y_i} := \frac{|\rho - \tilde{\rho}|}{\rho} = \frac{|\rho - (\rho + \delta\rho)|}{\rho} = \frac{|\delta\rho|}{\rho} \tag{2.148}$$

- Relative error of the orbital angular velocity due to uncertainties in the input elements.

$$\varepsilon_{\varpi,y_i} := \frac{|\varpi - \tilde{\varpi}|}{\varpi} = \frac{|\varpi - (\varpi + \delta\varpi)|}{\varpi} = \frac{|\delta\varpi|}{\varpi} \tag{2.149}$$

2.2.3. Numerical Test Cases

The same two sets of test cases described in Section 2.1.3 have been considered. Therefore, the description of such test cases is not repeated. Section 2.2.3.1 shows a validation of the inverse maps, whereas is Section 2.2.3.2 the sensitivity analysis on the inverse maps is discussed.

2.2.3.1. Forward and Inverse Mappings

All the results of the test cases described in Section 2.1.3.1 have been numerically verified against the nominal values. That is, the osculating orbital elements have been obtained through the forward mappings starting from the nominal NKO elements $[z, \rho, \varpi]^T$. Then, the inverse mappings are used to obtain the original NKO elements. The errors between the nominal values of the NKO elements and those obtained after the conversion give an estimate of the accuracy of both forward and inverse mappings.

Figures 14, 15, and 16 show the absolute errors after forward and inverse mappings in out-of-plane displacement, orbit radius, and orbital angular velocity, respectively. It is clear that the errors after the forward and inverse mappings are negligible. This validates both the forward and inverse mappings.

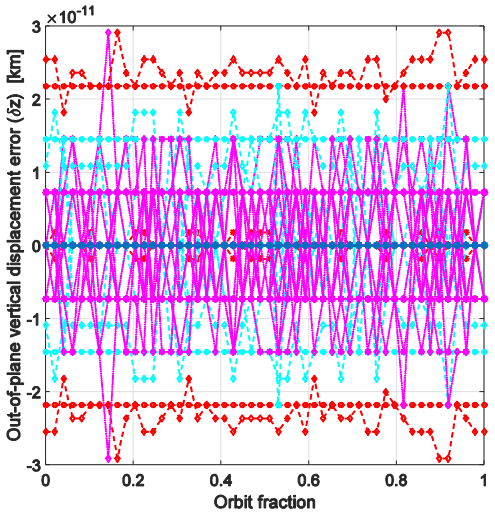

Figure 14. Absolute error in the out-of-plane displacement after forward and inverse mappings.

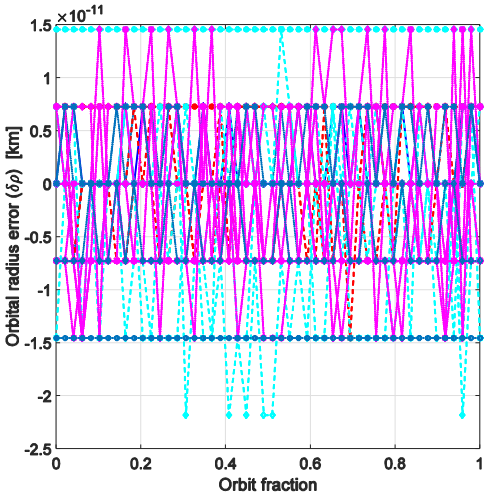

Figure 15. Absolute error in the orbit radius after forward and inverse mappings.

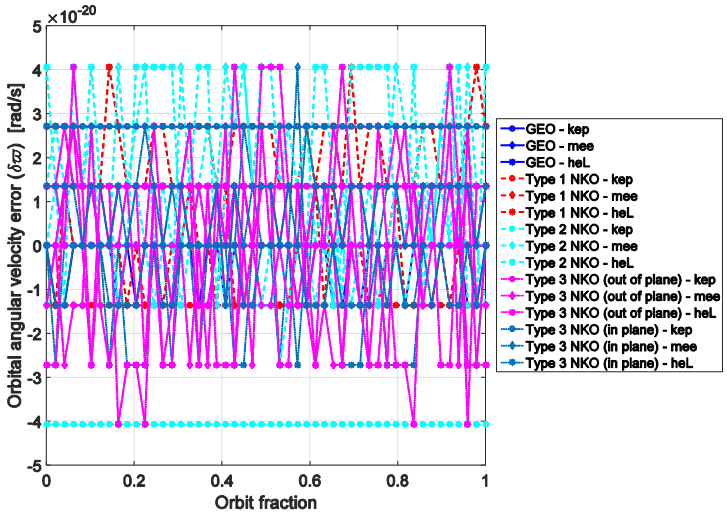

Figure 16. Absolute error in the orbital angular velocity after forward and inverse mappings.

2.2.3.2. Sensitivity Analysis

The same test cases taken into account for the sensitivity analysis of the forward mappings as described in Section 2.1.3.2 have been considered here.

The numerical sensitivity analysis has been performed as described in Section 2.2.2.

The errors of the osculating classical Keplerian elements are considered fixed and constant, as follows.

$$\begin{cases} \varepsilon_a = 10^{-3} & (0.1\%) \\ \varepsilon_e = 10^{-3} & \\ \varepsilon_i = 10^{-3} \cdot \pi & (0.1\% \text{ of the maximum possible error - } 0.18\,\text{deg}) \\ \varepsilon_\Omega = 10^{-3} \cdot \pi & (0.1\% \text{ of the maximum possible error - } 0.18\,\text{deg}) \\ \varepsilon_\omega = 10^{-3} \cdot \pi & (0.1\% \text{ of the maximum possible error - } 0.18\,\text{deg}) \\ \varepsilon_\vartheta = 10^{-3} \cdot \pi & (0.1\% \text{ of the maximum possible error - } 0.18\,\text{deg}) \end{cases} \tag{2.150}$$

The errors of the osculating modified equinoctial elements are considered fixed and constant, as follows.

$$\begin{cases} \varepsilon_p = 10^{-3} & (0.1\%) \\ \varepsilon_f = 10^{-3} & \\ \varepsilon_g = 10^{-3} & \\ \varepsilon_h = 10^{-3} & \\ \varepsilon_k = 10^{-3} & \\ \varepsilon_L = 10^{-3} \cdot \pi & (0.1\% \text{ of the maximum possible error - } 0.18\,\text{deg}) \end{cases} \tag{2.151}$$

No sensitivity analysis has been performed in the case of augmented integrals of motion. This is because, as shown in Eq. (2.146), the augmented integrals of motion to NKO elements map is extremely sensitive to errors in both eccentricity vector and true longitude. The issue is not only the piecewise formulation *per se* but the fact that the formulation takes into account only two points in the orbit, which are the apogee and perigee. If an error in either eccentricity vector or true longitude moves the point from the apogee/perigee, the inverse map fails.

Results and discussion

The sensitivity analysis study demonstrates that the planar elements (i.e. ρ, ϖ) of both mappings are robust to uncertainties in the osculating orbital elements. Both mappings of the out-of-plane displacement z are robust to uncertainties in the in-plane osculating elements. However, the out-of-plane displacement is very sensitive to errors in the out-of-plane osculating elements (i.e. inclination, if KEP are used, or out-of-plane MEE h, k). This is understandable if the Keplerian orbit has a small inclination and a large semi-major axis ($a \sim r_{GEO}$ in this case).

For the sake of conciseness, only the most interesting plots of the sensitivity analysis study are shown here. Table 7 and Table 8 show a summary of the numerical results of the sensitivity analysis study in the case of KEP and MEE, respectively. The three test cases taken into account are those described in Eqs. (2.99) – (2.101).

Table 7. Summary of the results of the sensitivity analysis study in the case of classical Keplerian elements.*

Uncertainty	Test case	ε_z	ε_ρ	ε_{ϖ}
δa	1	~ 150 m (0.1%)	0.1%	0.15%
	2	0		
	3	<0.1 m $(<0.1\%)$		
δe	1	~ 150 m (0.1%)	0.1%	$\sim 0.2\%$ The three test cases are numerically different.
	2	0	0.101%	
	3	<0.1 m $(<0.1\%)$	0.1%	
δi	1	~ 130 km	$1.6\times10^{-3}\%$	$1.6\times10^{-3}\%$
	2	<130 km	$<5\times10^{-4}\%$	$<5\times10^{-4}\%$
	3	~ 130 km	$5\times10^{-4}\%$	$5\times10^{-4}\%$
$\delta\Omega$	1	~ 0	0	0
	2	0	~ 0	~ 0
	3	~ 0 (0.001%)	0	0
$\delta\omega$	1	~ 0.7 m $(5\times10^{-4}\%)$	~ 0 The three test cases are numerically different.	~ 0 The three test cases are numerically different.
	2	0		
	3	$\sim 10^{-3}$ m (0.002%)		
$\delta\vartheta$	1	~ 0.7 m $(5\times10^{-4}\%)$	0	~ 0
	2	0	$5\times10^{-6}\%$	$10^{-5}\%$
	3	$\sim 10^{-3}$ m (0.002%)	0	0

* Note that sometimes ~0 is used against 0. This is done to stress the difference between a null value and a very small (numerical) value.

Figure 17 shows the evolution of the out-of-plane displacement z over one orbit obtained from the classical Keplerian elements. The three test cases are shown. Both the nominal value and a 0.1% error in the inclination are considered. It is shown how a small error in inclination can cause a large error in the out-of-plane displacement. Figure 18 shows the relative error evolution of the orbit radius ρ over one orbit obtained from the classical Keplerian elements. The three test cases are shown. A 0.1% error in the inclination is considered. It is shown how an error in inclination does not affect the orbit radius.

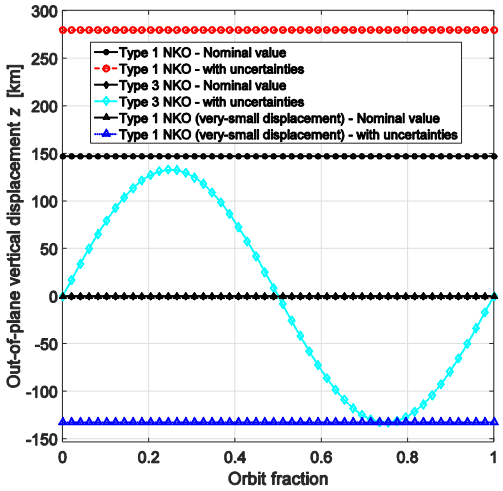

Figure 17. Out-of-plane displacement. Nominal case and 0.1% error in inclination.

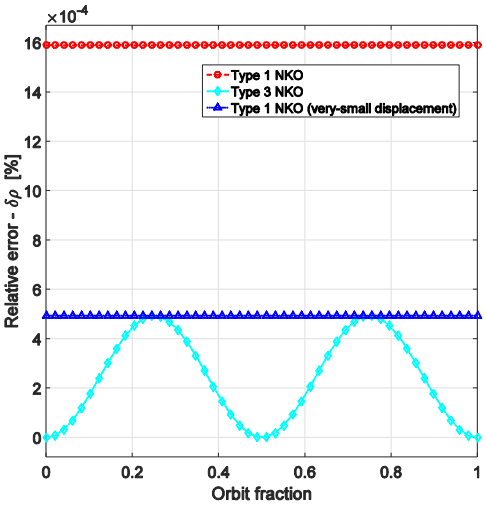

Figure 18. Relative error of the orbit radius in case of 0.1% error in inclination.

Table 8. Summary of the results of the sensitivity analysis study in the case of modified equinoctial elements.*

Uncertainty	Test case	ε_z	ε_ρ	ε_{ϖ}
δp	1	~ 150 m (0.1%)	0.1%	0.15%
	2	0		
	3	<0.1 m $(<0.1\%)$		
δf	1	~ 150 m (0.1%)	$<0.1\%$	$<0.2\%$
	2	0		
	3	<0.1 m $(<0.1\%)$		
δg	1	~ 150 m (0.1%)	$<0.1\%$	$<0.2\%$
	2	0		
	3	<0.1 m $(<0.1\%)$		
δh	1	<85 km	$<10^{-3}\%$	$<10^{-3}\%$
	2 – 3		$<2\times10^{-4}\%$	$<2\times10^{-4}\%$
δk	1	<85 km	$<10^{-3}\%$	$<10^{-3}\%$
	2 – 3		$<2\times10^{-4}\%$	$<2\times10^{-4}\%$
δL	1	~ 0.7 m $(5\times10^{-4}\%)$	~ 0	~ 0
	2	0	$5\times10^{-6}\%$	$10^{-5}\%$
	3	~ 0 $(8\times10^{-5}\%)$	~ 0	~ 0

* Note that sometimes ~0 is used against 0. This is done to stress the difference between a null value and a very small (numerical) value.

Figure 19 shows the relative error evolution of the orbit radius ρ over one orbit obtained from the MEE with a 0.001 error in the in-plane element f. The three test cases are shown. It is shown that the relative error on the orbit radius is at most the same order of magnitude as the initial uncertainty itself. Figure 20 shows the evolution of the out-of-plane displacement z over one orbit obtained from the MEE. The three test cases are shown. Both the nominal value and a 0.001 error in the out-of-plane element h are considered. It is shown how a small error in the out-of-plane element can cause a large error in the out-of-plane displacement.

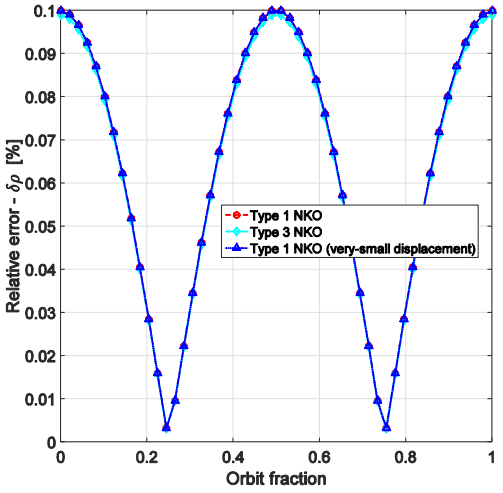

Figure 19. Relative error in orbit radius in case of 0.001 error in the in-plane element *f*.

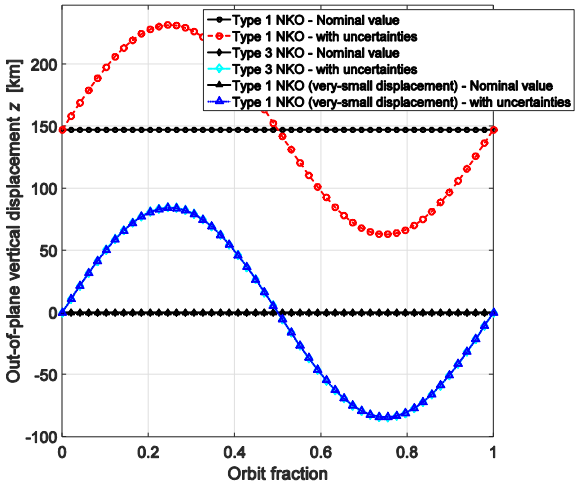

Figure 20. Out-of-plane displacement. Nominal case and 0.001 error in the out-of-plane element *h*.

2.2.4. Osculating Orbital Elements to Non-Keplerian Orbit Map: Summary

A summary of advantages and drawbacks of the inverse mappings investigated in this study is shown in Table 9.

Table 9. Osculating orbital elements to non-Keplerian orbit map. Summary of advantages and drawbacks of the chosen mappings.

	Classical Keplerian elements	Modified equinoctial elements	Augmented integrals of motion
Advantages	• Easy to understand • Easy formulation • Robust to uncertainties	• Easy formulation • Robust to uncertainties on in-plane elements	
Drawbacks	• Out-of-plane displacement very sensitive to uncertainties on inclination	• Out-of-plane displacement very sensitive to uncertainties on out-of-plane elements	• Piecewise formulation • Extremely sensitive to errors in both eccentricity vector and true longitude to the point that the map fails if there is an error in either eccentricity or true longitude

2.3. Determination of Spacecraft Thrust-Induced Acceleration

The magnitude and direction of the spacecraft thrust-induced acceleration used to generate families of non-Keplerian orbits have been extracted from the inverse mapping from the orbital elements discussed in Section 2.2. This has been achieved by using the NKO geometric properties derived from the inverse mapping as inputs to existing analysis of the dynamics of non-Keplerian orbits.[2] This analysis links the thrust-induced acceleration to the non-Keplerian orbit geometry.

The following sub-sections show the analytical expressions obtained for the thrust-induced acceleration if either the classical Keplerian elements or the modified equinoctial elements are used to describe the osculating Keplerian orbit. Because of the very poor robustness of the augmented integrals of motion shown in Section 2.2.1.3 for the inverse mapping, these elements have not been considered in the study of the thrust-induced acceleration.

2.3.1. Classical Keplerian elements

From Eq. (2.1) and using the mappings shown in Eq. (2.118), the thrust-induced acceleration and the thrust pitch angle are obtained as

$$\left\|\boldsymbol{a}\left(\boldsymbol{x}_{KEP}\right)\right\| = \frac{\mu\left(1+e\cos\vartheta\right)}{2a^2\left(1-e^2\right)^2}\sqrt{A+B} \tag{2.152}$$

$$\tan\alpha\left(\boldsymbol{x}_{KEP}\right) = \frac{\sqrt{\sigma_1}}{2\sin i\sin\left(\omega+\vartheta\right)}\left[1-\frac{4\left(1+e^2+2e\cos\vartheta\right)}{\sigma_1\left(1+e\cos\vartheta\right)}\right] \tag{2.153}$$

in which

$$\begin{cases} A = 4\left(1+e\cos\vartheta\right)^2\sin^2 i\sin^2\left(\omega+\vartheta\right) \\ B = \sigma_1\left(1+e\cos\vartheta-4\left(1+e^2+2e\cos\vartheta\right)/\sigma_1\right)^2 \\ \sigma_1 = 3+\cos\left(2i\right)+2\cos\left(2\left(\omega+\vartheta\right)\right)\sin^2 i \end{cases} \tag{2.154}$$

2.3.2. Modified equinoctial elements

From Eq. (2.1) and using the map shown in Eq. (2.128), the thrust-induced acceleration and the thrust pitch angle are obtained as

$$\left\|\boldsymbol{a}\left(\boldsymbol{x}_{MEE}\right)\right\| = \frac{\mu q}{sp^2}\sqrt{4q^2\left(k\cos L-h\sin L\right)^2+\sigma_2\left[q-\frac{s^2\left(1+f^2+g^2+2f\cos L+2g\sin L\right)}{\sigma_2}\right]^2} \tag{2.155}$$

$$\tan\alpha\left(\boldsymbol{x}_{MEE}\right) = \frac{\sqrt{\sigma_2}}{2\left(h\sin L-k\cos L\right)}\left[1-\frac{s^2\left(1+f^2+g^2+2f\cos L+2g\sin L\right)}{q\cdot\sigma_2}\right] \tag{2.156}$$

in which q, s, and β are defined in Eq. (2.119), whereas σ_2 is

$$\sigma_2 = 1+\left(h^2+k^2\right)^2+2\beta\cos\left(2L\right)+4hk\sin\left(2L\right) \tag{2.157}$$

2.3.3. Numerical Test Cases

The same two sets of test cases described in Section 2.1.3 have been considered here. Therefore, the description of such test cases is not repeated.

As noted earlier, the NKOs generated by the thrust-induced acceleration shown in Eq. (2.1) correspond to circular orbits displaced above the central body, viewed from an inertial frame of reference. Therefore, a displacement below the central body is not explicitly taken into account. This is because the tangent of the thrust pitch angle, rather than the pitch angle itself, is given. Therefore, there is an ambiguity in the thrust pitch angle. This can be solved algorithmically by checking the sign of the out-of-plane displacement, so that

$$\alpha = \begin{cases} \tan^{-1}\left(\tan\alpha\right) & \text{if } z > 0 \\ \tan^{-1}\left(\tan\alpha\right) + \pi & \text{if } z < 0 \end{cases} \tag{2.158}$$

The acceleration, in terms of magnitude and pitch angle, resulting from both Eqs. (2.152) – (2.153) and Eqs. (2.155) – (2.156), has been validated using two separate checks. In the first check, the values of acceleration magnitude and pitch angle are compared with those given directly by using Eq. (2.1). The values of both acceleration magnitude and the direction of the acceleration have been verified for all test cases considered with both sets of elements. The errors in the magnitude and direction of the acceleration are $\|\delta\boldsymbol{a}\| \le 2\times10^{-9}$ mm/s^2 and $|\delta\alpha| \le 10^{-10}$ rad, respectively. The second check has been carried out by propagating the equations of motion with the propulsive acceleration given by Eqs. (2.152) – (2.153) and Eqs. (2.155) – (2.156), respectively. The relative errors in position vector and velocity vector between the initial state and the state after one orbital period are used to validate the acceleration. A variable order Adam-Bashford-Moulton PECE solver (as implemented in MATLAB *ode113*) with relative and absolute tolerances equal to 10^{-10} and 10^{-12}, respectively, has been used for the propagation of the equations of motion. The errors in the final position and velocity are $\|\delta\boldsymbol{r}\|/\|\boldsymbol{r}\| \le 7\times10^{-8}$ and $\|\delta\boldsymbol{v}\|/\|\boldsymbol{v}\| \le 10^{-7}$, respectively.

Figure 21 shows the Type 1 NKOs described in Eq. (2.93) together with the acceleration vector required. The acceleration is clearly shown to be always directed along the vertical axis. Figure 22 shows the in-plane Type 3 NKOs described in Eq. (2.97) together with the acceleration vector required. In this case, it is clear how the propulsive acceleration is used to balance the gravitational attraction of the primary body. In the case of $\rho < r_{GEO}$, for instance, the NKO is slower than a Keplerian orbit with the same radius. The spacecraft, in this case, must thrust in the radial direction to balance the gravitational force and be able to move at the desired angular velocity.

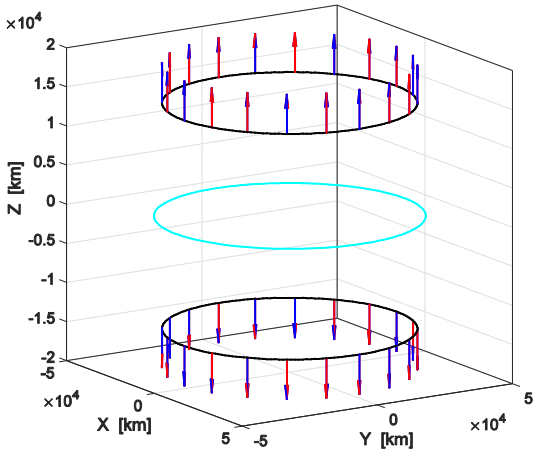

Figure 21. Type 1 NKOs and acceleration (not to scale) needed with GEO shown (dashed cyan line).

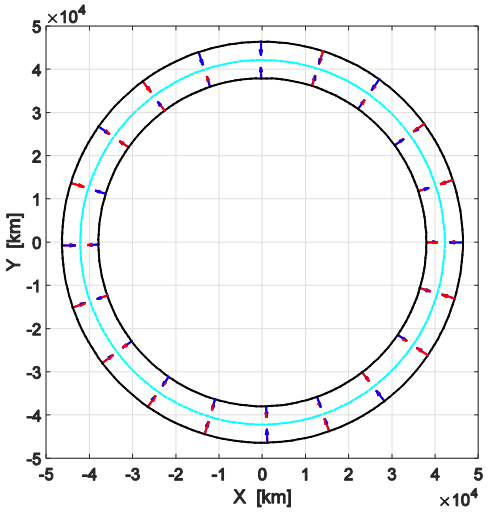

Figure 22. In-plane displaced Type 3 NKOs and acceleration (not to scale) needed with GEO shown (dashed cyan line).

As noted in Section 2.1.3.1 when the test cases used to verify the mappings have been introduced, these cases have been chosen for ease of illustration with the only purpose to verify the validity of the mappings and study the behavior of the osculating elements. That is, such test cases were not meant to be examples of feasible missions. This is evident if the magnitude of acceleration required is considered. The accelerations required for the test cases shown in Section 2.1.3.1 have magnitudes $\|\boldsymbol{a}\| \in [60, 200]$ mm/s^2 , which clearly are too large for a conventional low-thrust spacecraft.

However, the test cases described in Section 2.1.3.2 for the study of the sensitivity analysis have been chosen as feasible mission scenarios. The accelerations required for this second set of test cases have magnitudes $\|\boldsymbol{a}\| \in \left[4\times10^{-4},\ 2.3\right]$ mm/s^2 . Considering a 1000-kg spacecraft, such acceleration can be easily converted into a maximum thrust $T_{max} \in \left[4\times10^{-4},\ 2.3\right]$ N that are feasible accelerations for near-term low-thrust technology.[26]

3. Generalized Model: No Assumptions on Orbital Plane

The mappings derived in Section 2 are related to non-Keplerian orbits whose orbital plane is parallel to the $\hat{\boldsymbol{X}}-\hat{\boldsymbol{Y}}$ plane in a Cartesian reference frame (i.e. the equatorial plane, in this work). A generalized mapping for the direct problem is here investigated, for example where the orbit plane can be rotated relative to the Earth's equatorial plane.

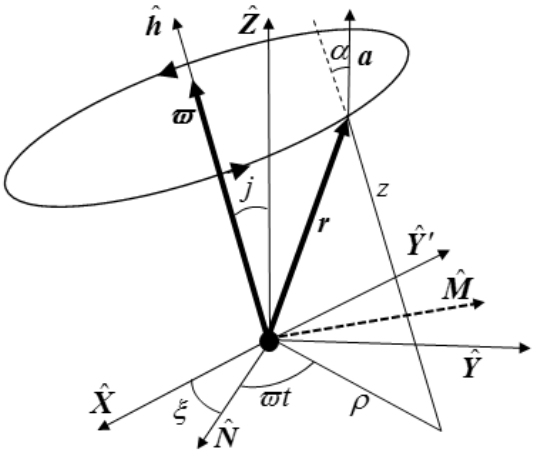

Figure 23. Sketch of a displaced orbit with thrust-induced acceleration. Generalized model.

Two extra elements are introduced for the description of the non-Keplerian orbit in the three-dimensional space, as shown in Figure 23. These are

$$\begin{cases} j & \text{Inclination of the non-Keplerian orbit} \\ \xi & \text{Right ascension of the ascending node of the non-Keplerian orbit} \end{cases} \tag{3.1}$$

Note that the symbols $\{j,\xi\}$ have been used for the description of the NKO elements inclination and right ascension of the ascending node (RAAN) because these elements do not have to be confused with the osculating inclination and RAAN, respectively. Therefore, the set of generalized NKO elements is $\boldsymbol{x}_{NKO}=\left[z,\rho,\varpi,j,\xi\right]^T$.

3.1. Forward Map: Non-Keplerian Orbit to Osculating Orbital Elements

The formulation of the Cartesian position and velocity vectors shown in Eqs. (2.5) – (2.6) can be generalized, considering inclination and RAAN, as

$$\boldsymbol{r}=\begin{bmatrix} \rho\left(\cos\xi\cos\left(\varpi t\right)-\cos j\sin\xi\sin\left(\varpi t\right)\right)+z\sin j\sin\xi \\ \rho\left(\sin\xi\cos\left(\varpi t\right)+\cos j\cos\xi\sin\left(\varpi t\right)\right)-z\sin j\cos\xi \\ \rho\sin j\sin\left(\varpi t\right)+z\cos j \end{bmatrix} \tag{3.2}$$

$$\boldsymbol{v}=\varpi\rho\begin{bmatrix} -\cos\xi\sin\left(\varpi t\right)-\cos j\sin\xi\cos\left(\varpi t\right) \\ -\sin\xi\sin\left(\varpi t\right)+\cos j\cos\xi\cos\left(\varpi t\right) \\ \sin j\cos\left(\varpi t\right) \end{bmatrix} \tag{3.3}$$

The orbital angular momentum $\boldsymbol{h}$ can be computed by using the aforementioned expressions of position and velocity as

$$\boldsymbol{h} = \boldsymbol{r} \times \boldsymbol{v} = \varpi\rho \begin{bmatrix} \rho \sin j \sin\xi - z\cos\xi\cos(\varpi t) + z\cos j \sin\xi \sin(\varpi t) \\ -z\sin\xi\cos(\varpi t) - \rho \sin j \cos\xi - z\cos j \cos\xi \sin(\varpi t) \\ \rho\cos j - z \sin j \sin(\varpi t) \end{bmatrix} \tag{3.4}$$

Following the same procedure used to obtain the mappings in the simplified case, the generalized mappings from NKO elements to osculating orbital elements are obtained. Because of the very poor robustness of the osculating AIoM for the inverse mapping, these elements have not been considered in this study.

In the following sub-sections, the generalized forward mappings from non-Keplerian orbit to osculating orbital elements are derived for the two sets of elements considered.

3.1.1. Classical Keplerian Elements

Starting from the Cartesian state vector (Eqs. (3.2) – (3.3)), the mapping from generalized NKO elements $[z, \rho, \varpi, j, \xi]^T$ to osculating classical Keplerian elements is obtained as described in Algorithm 4.2 from Reference 22.

1. *Inclination (i)*

$$i = \arccos\left(\hat{\boldsymbol{h}} \cdot \hat{\boldsymbol{Z}}\right) = \arccos\left(\frac{\rho\cos j - z\sin j \sin(\varpi t)}{\sqrt{\rho^2 + z^2}}\right) \tag{3.5}$$

Note that, if the NKO orbital plane is parallel to the equator, Eq. (3.5) becomes the following, which is the description already obtained in the simplified case (Eq. (2.23)).

$$i_{\parallel} = \arccos\left(\hat{\boldsymbol{h}}(j=0) \cdot \hat{\boldsymbol{Z}}\right) = \arccos\left(\frac{\rho}{\sqrt{\rho^2 + z^2}}\right) \tag{3.6}$$

2. *Right Ascension of the Ascending Node (Ω)*

The line of the nodes shall be defined in order to find the expression for the right ascension of the ascending node. The line of the nodes is defined as

$$\hat{\boldsymbol{N}} = \frac{\hat{\boldsymbol{Z}} \times \hat{\boldsymbol{h}}}{\left\|\hat{\boldsymbol{Z}} \times \hat{\boldsymbol{h}}\right\|} = \frac{1}{N}\begin{bmatrix} \rho\sin j\cos\xi + z\left(\cos j\cos\xi\sin(\varpi t) + \sin\xi\cos(\varpi t)\right) \\ \rho\sin j\sin\xi + z\left(\cos j\sin\xi\sin(\varpi t) - \cos\xi\cos(\varpi t)\right) \\ 0 \end{bmatrix} \tag{3.7}$$

in which

$$N = \sqrt{z^2\cos^2(\varpi t) + \left(\rho\sin j + z\cos j\sin(\varpi t)\right)^2} \tag{3.8}$$

It is important to note that the line of the nodes is not defined in the case of a planar orbit with the orbital plane parallel to the equatorial plane (i.e. $z = j = 0$). Therefore, the line of the nodes, in this case, is arbitrarily chosen to point in the $\hat{\boldsymbol{X}}$ direction. Therefore, the general formulation of the line of the node is

$$\hat{\boldsymbol{N}} = \begin{bmatrix} \cos(\Omega) \\ \sin(\Omega) \\ 0 \end{bmatrix} = \begin{cases} \begin{bmatrix} 1 \\ 0 \\ 0 \end{bmatrix} & \text{if } z = 0 \wedge j = 0 \\ \frac{1}{N} \begin{bmatrix} \rho \sin j \cos\xi + z\left(\cos j \cos\xi \sin(\varpi t) + \sin\xi \cos(\varpi t)\right) \\ \rho \sin j \sin\xi + z\left(\cos j \sin\xi \sin(\varpi t) - \cos\xi \cos(\varpi t)\right) \\ 0 \end{bmatrix} & \text{otherwise} \end{cases} \tag{3.9}$$

Note that, if the NKO orbital plane is parallel to the equator and $z \neq 0$, Eq. (3.9) becomes the following.

$$\hat{\boldsymbol{N}}(j = 0) = \frac{z}{|z|} \begin{bmatrix} \cos\xi \sin(\varpi t) + \sin\xi \cos(\varpi t) \\ -\cos\xi \cos(\varpi t) + \sin\xi \sin(\varpi t) \\ 0 \end{bmatrix} \tag{3.10}$$

Because the NKO RAAN ξ is not defined for $j = 0$, it can be arbitrarily set to zero and Eq. (3.10) becomes the following, which is the description already obtained in the simplified case (Eq. (2.10)).

$$\hat{\boldsymbol{N}}_{\parallel} = \frac{z}{|z|} \begin{bmatrix} \sin(\varpi t) \\ -\cos(\varpi t) \\ 0 \end{bmatrix} \tag{3.11}$$

The right ascension of the ascending node is simply given by

$$\Omega = \arctan\left(\hat{\boldsymbol{N}} \cdot \hat{\boldsymbol{X}}, \hat{\boldsymbol{N}} \cdot \hat{\boldsymbol{Y}}\right) = \begin{cases} 0 & \text{if } z = 0 \wedge j = 0 \\ \Omega^* & \text{otherwise} \end{cases} \tag{3.12}$$

in which

$$\Omega^* = \arctan\left(\rho \sin j \cos\xi + z\left(\cos j \cos\xi \sin(\varpi t) + \sin\xi \cos(\varpi t)\right), \rho \sin j \sin\xi + z\left(\cos j \sin\xi \sin(\varpi t) - \cos\xi \cos(\varpi t)\right)\right) \tag{3.13}$$

Note that the term $1/N$ has been neglected in Eq. (3.13) because it is always a positive value.

Note that, if $z = 0$ but $j \neq 0$, the osculating RAAN equals that of the NKO:

$$\Omega(z = 0) = \xi \tag{3.14}$$

On the other hand, if the NKO orbital plane is parallel to the equator, Eq. (3.12) becomes Eq. (3.15), which is the description already obtained in the simplified case (Eq. (2.23)).

$$\Omega(j = \xi = 0) = \begin{cases} 0 & \text{if } z = 0 \\ \arctan\left(\sin(\varpi t)\,\mathrm{sgn}(z), -\cos(\varpi t)\,\mathrm{sgn}(z)\right) & \text{otherwise} \end{cases} \tag{3.15}$$

Considering that it is arbitrarily chosen that $\xi = 0$ for a NKO with the orbital plane parallel to the equatorial plane, Eq. (3.12) could simply be rewritten as $\Omega = \Omega^*$, taking into account Eq. (3.14). However, it can be seen that

$$\Omega^*(j = z = 0) = \arctan(0,0) \tag{3.16}$$

Numerically, Eq. (3.16) often assumes the zero value but the expression in Eq. (3.16) is indefinite, if solved analytically. Moreover, if one wants to compute the limits to find the exact analytic value of Eq. (3.16), it can be demonstrated

that the limits are different depending on the order of the limits themselves. If the previous statement is true, the following holds.

$$\lim_{j\to 0}\left(\lim_{z\to 0}\Omega^*\right)\neq\lim_{z\to 0}\left(\lim_{j\to 0}\Omega^*\right) \tag{3.17}$$

If Eq. (3.17) is true, it means that $\Omega^*\left(j=z=0\right)=\arctan\left(0,0\right)$ is indeterminate and, therefore, the general analytical expression for the osculating right ascension of the ascending node is the one given in Eq. (3.12).

The left-hand side of Eq. (3.17) is

$$\lim_{j\to 0}\left(\lim_{z\to 0}\Omega^*\right)=\lim_{j\to 0}\left(\arctan\left(\rho\sin j\cos\xi,\rho\sin j\sin\xi\right)\right)=\xi \tag{3.18}$$

Note that the second limit in Eq. (3.18) has been solved using the L'Hopital's rule. The right-hand side of Eq. (3.17) is

$$\begin{aligned}\lim_{z\to 0^+}\left(\lim_{j\to 0}\Omega^*\right)&=\lim_{z\to 0^+}\left(\arctan\left(z\left(\cos\xi\sin\left(\varpi t\right)+\sin\xi\cos\left(\varpi t\right)\right),z\left(\sin\xi\sin\left(\varpi t\right)-\cos\xi\cos\left(\varpi t\right)\right)\right)\right)=\\&=\arctan\left(\cos\xi\sin\left(\varpi t\right)+\sin\xi\cos\left(\varpi t\right),\sin\xi\sin\left(\varpi t\right)-\cos\xi\cos\left(\varpi t\right)\right)=\\&=\arctan\left(\sin\left(\varpi t+\xi\right),-\cos\left(\varpi t+\xi\right)\right)=\arctan\left(\cos\left(\varpi t+\xi-\pi/2\right),\sin\left(\varpi t+\xi-\pi/2\right)\right)\Rightarrow\end{aligned} \tag{3.19}$$

$$\Rightarrow\quad\lim_{z\to 0^+}\left(\lim_{j\to 0}\Omega^*\right)=\varpi t+\xi-\frac{\pi}{2}\neq\xi=\lim_{j\to 0}\left(\lim_{z\to 0}\Omega^*\right) \tag{3.20}$$

Therefore, Eq. (3.20) demonstrates that the general analytical expression for the osculating right ascension of the ascending node is the one given in Eq. (3.12).

Lastly, the term Ω^* can be rewritten as

$$\Omega^*=\begin{cases}\arccos\left(N_x/N\right) & \text{if } N_y\geq 0\\ 2\pi-\arccos\left(N_x/N\right) & \text{otherwise}\end{cases} \tag{3.21}$$

in which

$$\begin{cases}N=\sqrt{z^2\cos^2\left(\varpi t\right)+\left(\rho\sin j+z\cos j\sin\left(\varpi t\right)\right)^2}\\ N_x=\rho\sin j\cos\xi+z\left(\cos j\cos\xi\sin\left(\varpi t\right)+\sin\xi\cos\left(\varpi t\right)\right)\\ N_y=\rho\sin j\sin\xi+z\left(\cos j\sin\xi\sin\left(\varpi t\right)-\cos\xi\cos\left(\varpi t\right)\right)\end{cases} \tag{3.22}$$

3. Eccentricity (e)

The eccentricity vector is given by

$$\boldsymbol{e}=-\hat{\boldsymbol{r}}+\frac{\boldsymbol{v}\times\boldsymbol{h}}{\mu} \tag{3.23}$$

Using the vector triple product rule and remembering that $v_r=0$, the expression of the eccentricity vector in Eq. (3.23) can be rewritten as

$$\boldsymbol{e}=\left(\frac{v^2}{\mu}-\frac{1}{r}\right)\boldsymbol{r}=\left(\frac{\varpi^2\rho^2}{\mu}-\frac{1}{\sqrt{\rho^2+z^2}}\right)\begin{bmatrix}\rho\left(\cos\xi\cos\left(\varpi t\right)-\cos j\sin\xi\sin\left(\varpi t\right)\right)+z\sin j\sin\xi\\ \rho\left(\sin\xi\cos\left(\varpi t\right)+\cos j\cos\xi\sin\left(\varpi t\right)\right)-z\sin j\cos\xi\\ \rho\sin j\sin\left(\varpi t\right)+z\cos j\end{bmatrix} \tag{3.24}$$

Therefore, the value of the eccentricity is given by the norm of the eccentricity vector, as

$$e=\frac{\left|\mu-\varpi^2\rho^2\sqrt{\rho^2+z^2}\right|}{\mu} \tag{3.25}$$

Note that a circular planar Keplerian orbit is characterized by $\mu=\varpi^2\rho^3$, which satisfies the zero-eccentricity condition. However, the eccentricity vector is not defined in this case and this is an issue in the following computation of the true anomaly. Therefore, the eccentricity unit vector, in this case, is arbitrarily chosen to point in the $\hat{\boldsymbol{X}}$ direction. Therefore, the general formulation of the eccentricity vector is

$$\boldsymbol{e}=\begin{cases}\begin{bmatrix}1\\0\\0\end{bmatrix} & \text{if } z=0\wedge\mu=\varpi^2\rho^3\\ \left(\frac{\varpi^2\rho^2}{\mu}-\frac{1}{\sqrt{\rho^2+z^2}}\right)\begin{bmatrix}\rho\left(\cos\xi\cos\left(\varpi t\right)-\cos j\sin\xi\sin\left(\varpi t\right)\right)+z\sin j\sin\xi\\ \rho\left(\sin\xi\cos\left(\varpi t\right)+\cos j\cos\xi\sin\left(\varpi t\right)\right)-z\sin j\cos\xi\\ \rho\sin j\sin\left(\varpi t\right)+z\cos j\end{bmatrix} & \text{otherwise}\end{cases} \tag{3.26}$$

4. Semi-major axis (a)

The semi-major axis is given by

$$a=\frac{\|\boldsymbol{h}\|^2}{\mu\left(1-e^2\right)}=\frac{\mu\sqrt{\rho^2+z^2}}{2\mu-\varpi^2\rho^2\sqrt{\rho^2+z^2}} \tag{3.27}$$

5. Argument of perigee (ω)

The argument of perigee is given by

$$\omega=\begin{cases}\arccos\left(\hat{\boldsymbol{N}}\cdot\hat{\boldsymbol{e}}\right) & \text{if } e_z\geq 0\\ 2\pi-\arccos\left(\hat{\boldsymbol{N}}\cdot\hat{\boldsymbol{e}}\right) & \text{otherwise}\end{cases} \tag{3.28}$$

After algebraic manipulations and arbitrarily choosing $\omega=0$ in the case of osculating circular orbit, the general expression for the argument of perigee is

$$\omega=\begin{cases}0 & \text{if } \mu=\varpi^2\rho^2\sqrt{\rho^2+z^2}\\ \omega^* & \text{if } \left(\mu-\varpi^2\rho^2\sqrt{\rho^2+z^2}\right)\left(z\cos j+\rho\sin j\sin\left(\varpi t\right)\right)\leq 0\\ 2\pi-\omega^* & \text{otherwise}\end{cases} \tag{3.29}$$

in which

$$\omega^* = \arccos\left(-\frac{\sin j \cos(\varpi t)\sqrt{\rho^2+z^2}}{\sqrt{z^2\cos^2(\varpi t)+\left(\rho\sin j + z\cos j \sin(\varpi t)\right)^2}} \operatorname{sgn}\left(\mu - \varpi^2\rho^2\sqrt{\rho^2+z^2}\right)\right) \tag{3.30}$$

Note that, if the NKO orbital plane is parallel to the equator and $z \neq 0$, Eq. (3.29) becomes the following, which is the description already obtained in the simplified case (Eq. (2.23)).

$$\omega(j=0) = \begin{cases} \pi/2 & \text{if } \left(z>0 \wedge \mu < \varpi^2\rho^2\sqrt{\rho^2+z^2}\right) \vee \left(z<0 \wedge \mu > \varpi^2\rho^2\sqrt{\rho^2+z^2}\right) \\ 3\pi/2 & \text{if } \left(z>0 \wedge \mu > \varpi^2\rho^2\sqrt{\rho^2+z^2}\right) \vee \left(z<0 \wedge \mu < \varpi^2\rho^2\sqrt{\rho^2+z^2}\right) \end{cases} \tag{3.31}$$

If the NKO orbital plane is parallel to the equator and $z = 0$, Eq. (3.29) becomes the following, which is the description already obtained in the simplified case (Eq. (2.23)).

$$\lim_{j\to 0}\left(\lim_{z\to 0}\omega\right) = \begin{cases} 0 & \text{if } \mu = \varpi^2\rho^3 \\ \varpi t & \text{if } \mu < \varpi^2\rho^3 \\ \pi + \varpi t & \text{if } \mu > \varpi^2\rho^3 \end{cases} \tag{3.32}$$

Note that Eq. (3.31) has been obtained by simply substituting $j = 0$ within Eq. (3.29). On the other hand, Eq. (3.32) has been obtained by computing two limits. Therefore, the general complete expression for the argument of perigee is given by unifying Eqs. (3.29) and (3.32), as follows.

$$\omega = \begin{cases} 0 & \text{if } \mu = \varpi^2\rho^2\sqrt{\rho^2+z^2} \\ \varpi t & \text{if } j=0 \wedge z=0 \wedge \mu < \varpi^2\rho^3 \\ \pi + \varpi t & \text{if } j=0 \wedge z=0 \wedge \mu > \varpi^2\rho^3 \\ \omega^* & \text{if } \left(\mu - \varpi^2\rho^2\sqrt{\rho^2+z^2}\right)\left(z\cos j + \rho\sin j \sin(\varpi t)\right) \leq 0 \\ 2\pi - \omega^* & \text{otherwise} \end{cases} \tag{3.33}$$

6. True anomaly (ϑ)

The true anomaly is given by

$$\cos(\vartheta) = \hat{\boldsymbol{e}} \cdot \hat{\boldsymbol{r}} \tag{3.34}$$

In the case of a circular planar Keplerian orbit, Eq. (3.34) becomes the following. This is due to the choice of the eccentricity vector shown in Eq. (3.26).

$$\cos(\vartheta) = \cos(\varpi t) \quad \Rightarrow \quad \vartheta = \varpi t \tag{3.35}$$

On the other hand, a NKO is characterized by the expression of the true anomaly given as

$$\vartheta = \arccos\left(-\operatorname{sgn}\left(\mu - \varpi^2\rho^2\sqrt{\rho^2+z^2}\right)\right) \tag{3.36}$$

Eq. (3.36) becomes

$$\vartheta = \begin{cases} 0 & \text{if } \mu < \varpi^2\rho^2\sqrt{\rho^2+z^2} \\ \pi & \text{if } \mu > \varpi^2\rho^2\sqrt{\rho^2+z^2} \end{cases} \tag{3.37}$$

Note that the case $\left(z \neq 0 \wedge \mu = \varpi^2 \rho^2 \sqrt{\rho^2 + z^2}\right)$ is not taken into account inside Eq. (3.37). From Eq. (3.36), it can be seen that $\vartheta\left(z \neq 0 \wedge \mu = \varpi^2 \rho^2 \sqrt{\rho^2 + z^2}\right) = \pi/2$. However, it does not exist any case for which $\mu = \varpi^2 \rho^2 \sqrt{\rho^2 + z^2}$ if $z \neq 0$, i.e. there are no osculating circular orbits for non-Keplerian orbits. Therefore, the general expression for the true anomaly can be rewritten by unifying Eqs. (3.35) and (3.37) as

$$\vartheta = \begin{cases} \varpi t & \text{if } z = 0 \wedge \mu = \varpi^2 \rho^3 \\ 0 & \text{if } \mu < \varpi^2 \rho^2 \sqrt{\rho^2 + z^2} \\ \pi & \text{if } \mu > \varpi^2 \rho^2 \sqrt{\rho^2 + z^2} \end{cases} \tag{3.38}$$

Summary

The generalized forward map from NKOs to osculating classical Keplerian elements described in Section 3.1.1 is summarized as:

$$
\begin{aligned}
a &= \frac{\mu\sqrt{\rho^2+z^2}}{2\mu-\varpi^2\rho^2\sqrt{\rho^2+z^2}} \\
e &= \frac{\left|\mu-\varpi^2\rho^2\sqrt{\rho^2+z^2}\right|}{\mu} \\
i &= \arccos\left(\frac{\rho\cos j - z\sin j\sin(\varpi t)}{\sqrt{\rho^2+z^2}}\right) \\
\Omega &= \begin{cases} 0 & \text{if } z=0 \wedge j=0 \\ \Omega^* & \text{otherwise} \end{cases} \\
\omega &= \begin{cases} 0 & \text{if } \mu=\varpi^2\rho^2\sqrt{\rho^2+z^2} \\ \varpi t & \text{if } j=0 \wedge z=0 \wedge \mu<\varpi^2\rho^3 \\ \pi+\varpi t & \text{if } j=0 \wedge z=0 \wedge \mu>\varpi^2\rho^3 \\ \omega^* & \text{if } \left(\mu-\varpi^2\rho^2\sqrt{\rho^2+z^2}\right)\left(z\cos j+\rho\sin j\sin(\varpi t)\right)\le 0 \\ 2\pi-\omega^* & \text{otherwise} \end{cases} \\
\vartheta &= \begin{cases} \varpi t & \text{if } z=0 \wedge \mu=\varpi^2\rho^3 \\ 0 & \text{if } \mu<\varpi^2\rho^2\sqrt{\rho^2+z^2} \\ \pi & \text{if } \mu>\varpi^2\rho^2\sqrt{\rho^2+z^2} \end{cases}
\end{aligned}
\tag{3.39}
$$

in which

$$
\begin{cases}
\Omega^* = \begin{cases} \arccos(N_x/N) & \text{if } N_y \ge 0 \\ 2\pi-\arccos(N_x/N) & \text{otherwise} \end{cases} \\
N = \sqrt{z^2\cos^2(\varpi t)+\left(\rho\sin j+z\cos j\sin(\varpi t)\right)^2} \\
N_x = \rho\sin j\cos\xi + z\left(\cos j\cos\xi\sin(\varpi t)+\sin\xi\cos(\varpi t)\right) \\
N_y = \rho\sin j\sin\xi + z\left(\cos j\sin\xi\sin(\varpi t)-\cos\xi\cos(\varpi t)\right) \\
\omega^* = \arccos\left(-\gamma\,\mathrm{sgn}\left(\mu-\varpi^2\rho^2\sqrt{\rho^2+z^2}\right)\right) \\
\gamma = \dfrac{\sin j\cos(\varpi t)\sqrt{\rho^2+z^2}}{\sqrt{z^2\cos^2(\varpi t)+\left(\rho\sin j+z\cos j\sin(\varpi t)\right)^2}}
\end{cases}
\tag{3.40}
$$

3.1.2. Modified Equinoctial Elements

Starting from the expressions of the Cartesian position and velocity vectors (Eqs. (3.2) – (3.3)), the orbital angular momentum (Eq. (3.4)) and the analytical map of the osculating classical Keplerian elements described in Section 3.1.1 (Eq. (3.39)), a map of the osculating MEE from Cartesian position and velocity is derived.

1. *Semi-latus rectum (p)*

$$p = \frac{\|\boldsymbol{h}\|^2}{\mu} = \frac{\varpi^2 \rho^2 \left(\rho^2 + z^2\right)}{\mu} \tag{3.41}$$

2. *In-plane element (f)*

In order to derive the general formulation for the in-plane element f, let us first consider the case of zero-displacement orbits (i.e. $z = 0$).

From the formulation of Ω shown in Eq. (3.39), the value of the right ascension of the ascending node for a zero-displacement orbit is simply

$$\Omega\big|_{z=0} = \xi \tag{3.42}$$

From the formulation of ω shown in Eq. (3.39) and noting that $\rho \sin j \geq 0$ always, the value of the argument of perigee for a zero-displacement orbit is

$$\omega\big|_{z=0} = \begin{cases} \varpi t & \text{if } \mu < \varpi^2 \rho^3 \\ \pi + \varpi t & \text{if } \mu > \varpi^2 \rho^3 \end{cases} \tag{3.43}$$

From Eqs. (3.42) – (3.43), the value of the longitude of perigee $\left[\omega + \Omega\right]_{z=0}$ is

$$\left[\omega + \Omega\right]_{z=0} = \begin{cases} \xi + \varpi t & \text{if } \mu < \varpi^2 \rho^3 \\ \xi + \pi + \varpi t & \text{if } \mu > \varpi^2 \rho^3 \end{cases} \quad \Rightarrow \tag{3.44}$$

$$\Rightarrow \quad \cos\left(\omega + \Omega\right)\big|_{z=0} = \begin{cases} \cos\left(\xi + \varpi t\right) & \text{if } \mu < \varpi^2 \rho^3 \\ -\cos\left(\xi + \varpi t\right) & \text{if } \mu > \varpi^2 \rho^3 \end{cases} \tag{3.45}$$

From Eq. (3.45) and remembering the expression of the eccentricity shown in Eq. (3.39), the expression of the in-plane element f for a zero-displacement orbit is

$$f\big|_{z=0} = \left[e \cos\left(\omega + \Omega\right)\right]_{z=0} = \frac{\varpi^2 \rho^3 - \mu}{\mu} \cos\left(\xi + \varpi t\right) \quad \Rightarrow \tag{3.46}$$

$$f\big|_{z=0} = \frac{\varpi^2 \rho^3 - \mu}{\mu} \left[\cos\xi \cos\left(\varpi t\right) - \sin\xi \sin\left(\varpi t\right)\right] \tag{3.47}$$

If the NKO orbital plane is parallel to the equator (i.e. $j = 0$ but also $\xi = 0$), the same procedure described in Section 2.1.1.2 can be used to obtain

$$f\big|_{j=0} = \frac{\varpi^2 \rho^2 \sqrt{\rho^2 + z^2} - \mu}{\mu} \cos\left(\varpi t\right) \tag{3.48}$$

Note that, if the orbital plane is parallel to the equator and $z = 0$, Eqs. (3.47) and (3.48) are equivalent.

Let us consider now a displaced orbit. From the formulation of Ω shown in Eq. (3.39), the value of the right ascension of the ascending node for a displaced orbit is

$$\Omega\big|_{z\neq 0} = \Omega^* \tag{3.49}$$

From the formulation of ω shown in Eq. (3.39), the value of the argument of perigee for a displaced orbit is

$$\omega\big|_{z\neq 0} = \begin{cases} \arccos(\gamma) & \text{if } \mu - \varpi^2\rho^2\sqrt{\rho^2+z^2} \le 0 \wedge z\cos j + \rho\sin j \sin(\varpi t) \ge 0 \\ \arccos(-\gamma) & \text{if } \mu - \varpi^2\rho^2\sqrt{\rho^2+z^2} \ge 0 \wedge z\cos j + \rho\sin j \sin(\varpi t) < 0 \\ -\arccos(-\gamma) & \text{if } \mu - \varpi^2\rho^2\sqrt{\rho^2+z^2} > 0 \wedge z\cos j + \rho\sin j \sin(\varpi t) \ge 0 \\ -\arccos(\gamma) & \text{if } \mu - \varpi^2\rho^2\sqrt{\rho^2+z^2} < 0 \wedge z\cos j + \rho\sin j \sin(\varpi t) < 0 \end{cases} \tag{3.50}$$

in which γ has been defined in Eq. (3.40).

From Eqs. (3.49) – (3.50) and recalling that $\arccos(-x) = \pi - \arccos(x)$, the value of the cosine of the longitude of perigee $\cos(\omega+\Omega)\big|_{z\neq 0}$ is

$$\cos(\omega+\Omega)\big|_{z\neq 0} = \begin{cases} \cos\left(\Omega^* + \arccos(\gamma)\right) & \text{if } \mu - \varpi^2\rho^2\sqrt{\rho^2+z^2} \le 0 \wedge z\cos j + \rho\sin j \sin(\varpi t) \ge 0 \\ -\cos\left(\Omega^* - \arccos(\gamma)\right) & \text{if } \mu - \varpi^2\rho^2\sqrt{\rho^2+z^2} \ge 0 \wedge z\cos j + \rho\sin j \sin(\varpi t) < 0 \\ -\cos\left(\Omega^* + \arccos(\gamma)\right) & \text{if } \mu - \varpi^2\rho^2\sqrt{\rho^2+z^2} > 0 \wedge z\cos j + \rho\sin j \sin(\varpi t) \ge 0 \\ \cos\left(\Omega^* - \arccos(\gamma)\right) & \text{if } \mu - \varpi^2\rho^2\sqrt{\rho^2+z^2} < 0 \wedge z\cos j + \rho\sin j \sin(\varpi t) < 0 \end{cases} \tag{3.51}$$

From Eq. (3.51) and remembering the expression of the eccentricity shown in Eq. (3.39), the expression of the in-plane element f for a displaced orbit is

$$f\big|_{z\neq 0} = \frac{\varpi^2\rho^2\sqrt{\rho^2+z^2}-\mu}{\mu} \cdot \begin{cases} \cos\left(\Omega^* + \arccos(\gamma)\right) & \text{if } z\cos j + \rho\sin j \sin(\varpi t) \ge 0 \\ \cos\left(\Omega^* - \arccos(\gamma)\right) & \text{if } z\cos j + \rho\sin j \sin(\varpi t) < 0 \end{cases} \tag{3.52}$$

Note that, if $z = 0$, Eq. (3.52) becomes Eq. (3.47). On the other hand, if $j = 0$, Eq. (3.52) becomes Eq. (3.48), which is the expression found in the simplified case (Eq. (2.76)). This can be easily demonstrated as follows.

Let us first consider the $z \neq 0$ case. It can be seen that $\gamma\big|_{j=0} = 0$. That is, Eq. (3.52) becomes

$$f\big|_{j=0} = \frac{\varpi^2\rho^2\sqrt{\rho^2+z^2}-\mu}{\mu} \cdot \begin{cases} \cos\left(\Omega^* + \dfrac{\pi}{2}\right) & \text{if } z > 0 \\ \cos\left(\Omega^* - \dfrac{\pi}{2}\right) & \text{if } z < 0 \end{cases} \tag{3.53}$$

As demonstrated in Eq. (3.19), $\Omega^*\big|_{j=0} = \xi + \varpi t - \pi/2$ if $z > 0$. Following the same procedure, it can be demonstrated that the following holds.

$$\Omega^*\big|_{j=0} = \begin{cases} \xi + \varpi t - \pi/2 & \text{if } z > 0 \\ \xi + \varpi t + \pi/2 & \text{if } z < 0 \end{cases} \tag{3.54}$$

Substituting Eq. (3.54) into Eq. (3.53) and recalling that it is arbitrarily chosen that $\xi = 0$ if $j = 0$, the expression of the in-plane element f becomes the same as that shown in Eq. (3.48).

Let us consider now the $z = 0$ case. It can be seen that $\gamma|_{j=z=0} = \cos(\varpi t)$. Recalling that $\Omega|_{j=z=0} = 0$ (Eq. (3.39)), Eq. (3.52) becomes Eq. (3.48).

Therefore, the general expression for the in-plane element f is

$$f = \frac{\varpi^2 \rho^2 \sqrt{\rho^2 + z^2} - \mu}{\mu} \cdot \begin{cases} \cos(\varpi t) & \text{if } z = 0 \wedge j = 0 \\ \cos\left(\Omega^* + \arccos(\gamma)\right) & \text{if } z\cos j + \rho \sin j \sin(\varpi t) \geq 0 \\ \cos\left(\Omega^* - \arccos(\gamma)\right) & \text{if } z\cos j + \rho \sin j \sin(\varpi t) < 0 \end{cases} \tag{3.55}$$

It is important to note that Eq. (3.55) is a piecewise formulation characterized by nested direct and inverse trigonometric functions. Moreover, Ω^* itself is defined through a piecewise law (Eq. (3.40)). For these reasons, an alternative formulation can be found, after some mathematical manipulations, as follows.

Using the same nomenclature used for Ω^*, γ can be rewritten as $\gamma = \frac{\tilde{\gamma}}{N}$. That is,

$$\tilde{\gamma} = \sin j \cos(\varpi t) \sqrt{\rho^2 + z^2} \tag{3.56}$$

Taking into account the second condition in Eq. (3.55) and the condition $N_y \geq 0$, the expression for the in-plane element f is

$$f = \frac{\varpi^2 \rho^2 \sqrt{\rho^2 + z^2} - \mu}{\mu} \cos\left(\arccos\left(\frac{N_x}{N}\right) + \arccos\left(\frac{\tilde{\gamma}}{N}\right)\right) \tag{3.57}$$

Let us recall some useful relations between trigonometric functions.

$$\arccos(x) = 2\tan^{-1}\left(\frac{\sqrt{1-x^2}}{1+x}\right) \tag{3.58}$$

$$\tan^{-1}(x) \pm \tan^{-1}(y) = \tan^{-1}\left(\frac{x \pm y}{1 \mp xy}\right) \tag{3.59}$$

$$\cos\left(2\tan^{-1}(x)\right) = \frac{2}{x^2+1} - 1 \tag{3.60}$$

Using Eqs. (3.58)-(3.59) and after some algebraic manipulations, the following relation can be obtained.

$$\arccos\left(\frac{N_x}{N}\right) + \arccos\left(\frac{\tilde{\gamma}}{N}\right) = \ldots = 2\tan^{-1}\left(\frac{\sqrt{N^2 - {N_x}^2}\left(N + \tilde{\gamma}\right) + \sqrt{N^2 - \tilde{\gamma}^2}\left(N + N_x\right)}{\left(N + N_x\right)\left(N + \tilde{\gamma}\right) - \sqrt{\left(N^2 - {N_x}^2\right)\left(N^2 - \tilde{\gamma}^2\right)}} \right) \tag{3.61}$$

Applying Eq. (3.60) to Eq. (3.61), the following can be obtained.

$$\cos\left(\arccos\left(\frac{N_x}{N}\right) + \arccos\left(\frac{\tilde{\gamma}}{N}\right)\right) = \ldots = \frac{N_x \tilde{\gamma} - \sqrt{\left(N^2 - {N_x}^2\right)\left(N^2 - \tilde{\gamma}^2\right)}}{N^2} \tag{3.62}$$

Following the same procedure described in Eqs. (3.57) – (3.62), the formulation of the in-plane element f can be rewritten as

$$f = \frac{\varpi^2\rho^2\sqrt{\rho^2+z^2}-\mu}{\mu N^2}\cdot\begin{cases} N^2\cos(\varpi t) & \text{if } z=0 \wedge j=0 \\ N_x\tilde{\gamma}-\sqrt{\left(N^2-N_x^{\,2}\right)\left(N^2-\tilde{\gamma}^2\right)} & \text{if } N_y\cdot\left(z\cos j+\rho\sin j\sin(\varpi t)\right)\geq 0 \\ N_x\tilde{\gamma}+\sqrt{\left(N^2-N_x^{\,2}\right)\left(N^2-\tilde{\gamma}^2\right)} & \text{if } N_y\cdot\left(z\cos j+\rho\sin j\sin(\varpi t)\right)<0 \end{cases} \tag{3.63}$$

The formulation of the in-plane MEE f shown in Eq. (3.63) is free from any nested direct and inverse trigonometric function. Nevertheless, this formulation is not any simpler than the one shown in Eq. (3.55). Moreover, from a numerical point of view, the computation of the latter is faster. For these reasons, Eq. (3.55) is considered as the final formulation of the in-plane MEE f.

3. In-plane element (g)

As for the case of the in-plane element f, let us derive the general mapping for the in-plane element g considering the in-plane and out-of-plane orbits separately at first. In order to derive the general formulation for the in-plane element g, let us first consider the case of zero-displacement orbits (i.e. $z=0$).

From Eq. (3.44), the value of the longitude of perigee $\left[\omega+\Omega\right]_{z=0}$ is

$$\left[\omega+\Omega\right]_{z=0} = \begin{cases} \xi+\varpi t & \text{if } \mu<\varpi^2\rho^3 \\ \xi+\pi+\varpi t & \text{if } \mu>\varpi^2\rho^3 \end{cases} \quad \Rightarrow \tag{3.64}$$

$$\Rightarrow \quad \sin(\omega+\Omega)\big|_{z=0} = \begin{cases} \sin(\xi+\varpi t) & \text{if } \mu<\varpi^2\rho^3 \\ -\sin(\xi+\varpi t) & \text{if } \mu>\varpi^2\rho^3 \end{cases} \tag{3.65}$$

From Eq. (3.65) and remembering the expression of the eccentricity shown in Eq. (3.39), the expression of the in-plane element g for a zero-displacement orbit is

$$g\big|_{z=0} = \left[e\sin(\omega+\Omega)\right]_{z=0} = \frac{\varpi^2\rho^3-\mu}{\mu}\sin(\xi+\varpi t) \quad \Rightarrow \tag{3.66}$$

$$g\big|_{z=0} = \frac{\varpi^2\rho^3-\mu}{\mu}\left[\sin\xi\cos(\varpi t)+\cos\xi\sin(\varpi t)\right] \tag{3.67}$$

If the NKO orbital plane is parallel to the equator (i.e. $j=0$ but also $\xi=0$), the same procedure described in Section 2.1.1.2 can be used to obtain

$$g\big|_{j=0} = \frac{\varpi^2\rho^2\sqrt{\rho^2+z^2}-\mu}{\mu}\sin(\varpi t) \tag{3.68}$$

Note that, if the orbital plane is parallel to the equator and $z=0$, Eqs. (3.67) and (3.68) are equivalent.

Let us consider now a displaced orbit. Following what have been done for the case of the in-plane element f, the value of the sine of the longitude of perigee $\sin(\omega+\Omega)\big|_{z\neq 0}$ is

$$\sin\left(\omega+\Omega\right)\Big|_{z\neq 0}=\begin{cases}\sin\left(\Omega^{*}+\arccos\left(\gamma\right)\right) & \text{if } \mu-\varpi^{2}\rho^{2}\sqrt{\rho^{2}+z^{2}}\le 0\wedge z\cos j+\rho\sin j\sin\left(\varpi t\right)\ge 0\\ -\sin\left(\Omega^{*}-\arccos\left(\gamma\right)\right) & \text{if } \mu-\varpi^{2}\rho^{2}\sqrt{\rho^{2}+z^{2}}\ge 0\wedge z\cos j+\rho\sin j\sin\left(\varpi t\right)<0\\ -\sin\left(\Omega^{*}+\arccos\left(\gamma\right)\right) & \text{if } \mu-\varpi^{2}\rho^{2}\sqrt{\rho^{2}+z^{2}}>0\wedge z\cos j+\rho\sin j\sin\left(\varpi t\right)\ge 0\\ \sin\left(\Omega^{*}-\arccos\left(\gamma\right)\right) & \text{if } \mu-\varpi^{2}\rho^{2}\sqrt{\rho^{2}+z^{2}}<0\wedge z\cos j+\rho\sin j\sin\left(\varpi t\right)<0\end{cases} \tag{3.69}$$

From Eq. (3.69) and remembering the expression of the eccentricity shown in Eq. (3.39), the expression of the in-plane element g for a displaced orbit is

$$g\big|_{z\neq 0}=\frac{\varpi^{2}\rho^{2}\sqrt{\rho^{2}+z^{2}}-\mu}{\mu}\cdot\begin{cases}\sin\left(\Omega^{*}+\arccos\left(\gamma\right)\right) & \text{if } z\cos j+\rho\sin j\sin\left(\varpi t\right)\ge 0\\ \sin\left(\Omega^{*}-\arccos\left(\gamma\right)\right) & \text{if } z\cos j+\rho\sin j\sin\left(\varpi t\right)<0\end{cases} \tag{3.70}$$

Note that, if $z=0$, Eq. (3.70) becomes Eq. (3.67). On the other hand, if $j=0$, Eq. (3.70) becomes Eq. (3.68), which was found in the simplified case (Eq. (2.76)). The demonstration of this follows the same steps shown in the case of the in-plane element f.

Therefore, the general expression for the in-plane element g is

$$g=\frac{\varpi^{2}\rho^{2}\sqrt{\rho^{2}+z^{2}}-\mu}{\mu}\cdot\begin{cases}\sin\left(\varpi t\right) & \text{if } z=0\wedge j=0\\ \sin\left(\Omega^{*}+\arccos\left(\gamma\right)\right) & \text{if } z\cos j+\rho\sin j\sin\left(\varpi t\right)\ge 0\\ \sin\left(\Omega^{*}-\arccos\left(\gamma\right)\right) & \text{if } z\cos j+\rho\sin j\sin\left(\varpi t\right)<0\end{cases} \tag{3.71}$$

As for the in-plane element f, it can be noted that Eq. (3.55) is a piecewise formulation characterized by nested direct and inverse trigonometric functions. Nevertheless, it can be demonstrated that a procedure similar to that for the in-plane element f does not simplify the formulation. Therefore, such a mathematical derivation is not shown here for the sake of conciseness and Eq. (3.71) is considered as the final formulation for the in-plane MEE g.

4. Out-of-plane element (h)

Before deriving the expression for the out-of-plane element h, let us recall the following identity.

$$\tan\left(\frac{x}{2}\right)=\frac{1-\cos\left(x\right)}{\sin\left(x\right)} \tag{3.72}$$

Recalling the formulation of the inclination shown in Eq. (3.39) as $i=\arccos\left(\dfrac{\rho\cos j-z\sin j\sin\left(\varpi t\right)}{\sqrt{\rho^{2}+z^{2}}}\right)$, the expression of $\tan\left(i/2\right)$ is, therefore, given by

$$\tan\left(\frac{i}{2}\right)=\frac{1-\dfrac{\rho\cos j - z\sin j\sin(\varpi t)}{\sqrt{\rho^2+z^2}}}{\sin\left(\arccos\left(\dfrac{\rho\cos j - z\sin j\sin(\varpi t)}{\sqrt{\rho^2+z^2}}\right)\right)}= \tag{3.73}$$

$$=\left(1-\frac{\rho\cos j - z\sin j\sin(\varpi t)}{\sqrt{\rho^2+z^2}}\right)\sqrt{\frac{\rho^2+z^2}{\rho^2+z^2-\left(\rho\cos j - z\sin j\sin(\varpi t)\right)^2}} \quad \Rightarrow$$

$$\Rightarrow \quad \tan\left(\frac{i}{2}\right)=\frac{\sqrt{\rho^2+z^2}-\left(\rho\cos j - z\sin j\sin(\varpi t)\right)}{\sqrt{\rho^2+z^2-\left(\rho\cos j - z\sin j\sin(\varpi t)\right)^2}} \tag{3.74}$$

Noting that the denominator of Eq. (3.74) can be rewritten as $\sqrt{A^2-B^2}=\sqrt{(A+B)\cdot(A-B)}$, Eq. (3.74) can be simplified as

$$\tan\left(\frac{i}{2}\right)=\sqrt{\frac{\sqrt{\rho^2+z^2}-\left(\rho\cos j - z\sin j\sin(\varpi t)\right)}{\sqrt{\rho^2+z^2}+\left(\rho\cos j - z\sin j\sin(\varpi t)\right)}} \tag{3.75}$$

From Eq. (3.75) and recalling the value of

$$\cos(\Omega)=\begin{cases} 1 & \text{if } z=0\wedge j=0 \\ \dfrac{\rho\sin j\cos\xi + z\left(\cos j\cos\xi\sin(\varpi t)+\sin\xi\cos(\varpi t)\right)}{\sqrt{z^2\cos^2(\varpi t)+\left(\rho\sin j + z\cos j\sin(\varpi t)\right)^2}} & \text{otherwise} \end{cases} \tag{3.76}$$

introduced in Eq. (3.9), the expression of the out-of-plane element h is

$$h=\sqrt{\frac{\sqrt{\rho^2+z^2}-\left(\rho\cos j - z\sin j\sin(\varpi t)\right)}{\sqrt{\rho^2+z^2}+\left(\rho\cos j - z\sin j\sin(\varpi t)\right)}}\begin{cases} 1 & \text{if } z=0\wedge j=0 \\ \dfrac{\rho\sin j\cos\xi + z\left(\cos j\cos\xi\sin(\varpi t)+\sin\xi\cos(\varpi t)\right)}{\sqrt{z^2\cos^2(\varpi t)+\left(\rho\sin j + z\cos j\sin(\varpi t)\right)^2}} & \text{otherwise} \end{cases} \tag{3.77}$$

Note that the piecewise formulation in Eq. (3.77) can be removed by performing the two-variable limit, as follows. Let us consider only the second branch of Eq. (3.77) to demonstrate that

$$\lim_{(z,j)\to(0,0)} h=0 \tag{3.78}$$

First, let us rewrite the two variables z, j in polar coordinates as

$$\begin{cases} z=\tilde{r}\cos\tilde{\vartheta} \\ j=\tilde{r}\sin\tilde{\vartheta} \end{cases} \tag{3.79}$$

Using Eq. (3.79), the second branch of Eq. (3.77) becomes

$$\tilde{h} = \sqrt{\frac{\sqrt{\rho^2+\tilde{r}^2\cos\tilde{\vartheta}}-\rho\cos\left(\tilde{r}\sin\tilde{\vartheta}\right)+\tilde{r}\cos\tilde{\vartheta}\sin\left(\tilde{r}\sin\tilde{\vartheta}\right)\sin\left(\varpi t\right)}{\sqrt{\rho^2+\tilde{r}^2\cos^2\tilde{\vartheta}}+\rho\cos\left(\tilde{r}\sin\tilde{\vartheta}\right)-\tilde{r}\cos\tilde{\vartheta}\sin\left(\tilde{r}\sin\tilde{\vartheta}\right)\sin\left(\varpi t\right)}}\cdot \frac{\rho\cos\xi\sin\left(\tilde{r}\sin\tilde{\vartheta}\right)+\tilde{r}\cos\tilde{\vartheta}\left(\cos\xi\cos\left(\tilde{r}\sin\tilde{\vartheta}\right)\sin\left(\varpi t\right)+\sin\xi\cos\left(\varpi t\right)\right)}{\sqrt{\tilde{r}^2\cos^2\tilde{\vartheta}\cos^2\left(\varpi t\right)+\left(\rho\sin\left(\tilde{r}\sin\tilde{\vartheta}\right)+\tilde{r}\cos\tilde{\vartheta}\cos\left(\tilde{r}\sin\tilde{\vartheta}\right)\sin\left(\varpi t\right)\right)^2}} \tag{3.80}$$

The limit shown in Eq. (3.78) can be now re-written, using the transformations in Eq. (3.79), as

$$\lim_{\tilde{r}\to 0^+}\tilde{h}=0 \tag{3.81}$$

It can be easily demonstrated that Eq. (3.81) is verified for any value of $\tilde{\vartheta}$ and, therefore, the two-variable limit shown in Eq. (3.78) is verified as well.

Considering that $\lim_{(z,j)\to(0,0)} h=0$, the expression of the out-of-plane element h is simply

$$h=\sqrt{\frac{\sqrt{\rho^2+z^2}-\left(\rho\cos j-z\sin j\sin\left(\varpi t\right)\right)}{\sqrt{\rho^2+z^2}+\left(\rho\cos j-z\sin j\sin\left(\varpi t\right)\right)}}\cdot\frac{\rho\sin j\cos\xi+z\left(\cos j\cos\xi\sin\left(\varpi t\right)+\sin\xi\cos\left(\varpi t\right)\right)}{\sqrt{z^2\cos^2\left(\varpi t\right)+\left(\rho\sin j+z\cos j\sin\left(\varpi t\right)\right)^2}} \tag{3.82}$$

5. Out-of-plane element (k)

As computed in Eq. (3.75) for the out-of-plane element h, the expression of $\tan\left(i/2\right)$ is

$$\tan\left(\frac{i}{2}\right)=\sqrt{\frac{\sqrt{\rho^2+z^2}-\left(\rho\cos j-z\sin j\sin\left(\varpi t\right)\right)}{\sqrt{\rho^2+z^2}+\left(\rho\cos j-z\sin j\sin\left(\varpi t\right)\right)}} \tag{3.83}$$

From Eq. (3.83) and recalling the value of

$$\sin\left(\Omega\right)=\begin{cases}0 & \text{if } z=0\wedge j=0\\ \dfrac{\rho\sin j\sin\xi+z\left(\cos j\sin\xi\sin\left(\varpi t\right)-\cos\xi\cos\left(\varpi t\right)\right)}{\sqrt{z^2\cos^2\left(\varpi t\right)+\left(\rho\sin j+z\cos j\sin\left(\varpi t\right)\right)^2}} & \text{otherwise}\end{cases} \tag{3.84}$$

introduced in Eq. (3.9), the expression of the out-of-plane element k is

$$k=\sqrt{\frac{\sqrt{\rho^2+z^2}-\left(\rho\cos j-z\sin j\sin\left(\varpi t\right)\right)}{\sqrt{\rho^2+z^2}+\left(\rho\cos j-z\sin j\sin\left(\varpi t\right)\right)}}\begin{cases}0 & \text{if } z=0\wedge j=0\\ \dfrac{\rho\sin j\sin\xi+z\left(\cos j\sin\xi\sin\left(\varpi t\right)-\cos\xi\cos\left(\varpi t\right)\right)}{\sqrt{z^2\cos^2\left(\varpi t\right)+\left(\rho\sin j+z\cos j\sin\left(\varpi t\right)\right)^2}} & \text{otherwise}\end{cases} \tag{3.85}$$

Note that the piecewise formulation in Eq. (3.85) can be removed by performing the two-variable limit, as demonstrated for the out-of-plane element h. Let us consider only the second branch of Eq. (3.85) to demonstrate that

$$\lim_{(z,j)\to(0,0)} k = 0 \tag{3.86}$$

First, let us rewrite the two variables z, j in polar coordinates as

$$\begin{cases} z = \tilde{r}\cos\tilde{\vartheta} \\ j = \tilde{r}\sin\tilde{\vartheta} \end{cases} \tag{3.87}$$

Using Eq. (3.87), the second branch of Eq. (3.85) becomes

$$\tilde{k} = \sqrt{\frac{\sqrt{\rho^2+\tilde{r}^2\cos^2\tilde{\vartheta}} - \rho\cos\left(\tilde{r}\sin\tilde{\vartheta}\right) + \tilde{r}\cos\tilde{\vartheta}\sin\left(\tilde{r}\sin\tilde{\vartheta}\right)\sin\left(\varpi t\right)}{\sqrt{\rho^2+\tilde{r}^2\cos^2\tilde{\vartheta}} + \rho\cos\left(\tilde{r}\sin\tilde{\vartheta}\right) - \tilde{r}\cos\tilde{\vartheta}\sin\left(\tilde{r}\sin\tilde{\vartheta}\right)\sin\left(\varpi t\right)}} \cdot \frac{\rho\sin\xi\sin\left(\tilde{r}\sin\tilde{\vartheta}\right) + \tilde{r}\cos\tilde{\vartheta}\left(\sin\xi\cos\left(\tilde{r}\sin\tilde{\vartheta}\right)\sin\left(\varpi t\right) - \cos\xi\cos\left(\varpi t\right)\right)}{\sqrt{\tilde{r}^2\cos^2\tilde{\vartheta}\cos^2\left(\varpi t\right) + \left(\rho\sin\left(\tilde{r}\sin\tilde{\vartheta}\right) + \tilde{r}\cos\tilde{\vartheta}\cos\left(\tilde{r}\sin\tilde{\vartheta}\right)\sin\left(\varpi t\right)\right)^2}} \tag{3.88}$$

The limit shown in Eq. (3.86) can now be re-written, using the transformations in Eq. (3.87), as

$$\lim_{\tilde{r}\to 0^+} \tilde{k} = 0 \tag{3.89}$$

It can be easily demonstrated that Eq. (3.89) is verified for any value of $\tilde{\vartheta}$ and, therefore, the two-variable limit shown in Eq. (3.86) is verified as well.

Considering that $\lim_{(z,j)\to(0,0)} k = 0$, the expression of the out-of-plane element k is simply

$$k = \sqrt{\frac{\sqrt{\rho^2+z^2} - \left(\rho\cos j - z\sin j\sin\left(\varpi t\right)\right)}{\sqrt{\rho^2+z^2} + \left(\rho\cos j - z\sin j\sin\left(\varpi t\right)\right)}} \cdot \frac{\rho\sin j\sin\xi + z\left(\cos j\sin\xi\sin\left(\varpi t\right) - \cos\xi\cos\left(\varpi t\right)\right)}{\sqrt{z^2\cos^2\left(\varpi t\right) + \left(\rho\sin j + z\cos j\sin\left(\varpi t\right)\right)^2}} \tag{3.90}$$

6. True longitude (L)

In order to derive the general formulation for the true longitude L, let us consider the two cases $z = 0$ and $z \neq 0$, respectively.

From the formulations of Ω and ω shown in Eq. (3.39), the value of the longitude of perigee $\left[\omega+\Omega\right]_{z=0}$ is

$$\left[\omega+\Omega\right]_{z=0} = \begin{cases} \xi & \text{if } \mu = \varpi^2\rho^3 \\ \xi + \varpi t & \text{if } \mu < \varpi^2\rho^3 \\ \xi + \pi + \varpi t & \text{if } \mu > \varpi^2\rho^3 \end{cases} \tag{3.91}$$

Therefore, the value of the true longitude in the case of zero-displacement NKO is obtained from Eqs. (3.39) and (3.91) as

$$L\big|_{z=0} = \xi + \varpi t \tag{3.92}$$

Let us consider now a displaced orbit. From Eqs. (3.49), (3.50), and (3.39) and recalling that $\arccos(-x) = \pi - \arccos(x)$, the value of the true longitude for an out-of-plane displaced orbit is

$$L\big|_{z\neq 0} = \begin{cases} \Omega^* + \arccos(\gamma) & \text{if } z\cos j + \rho \sin j \sin(\varpi t) \geq 0 \\ \Omega^* - \arccos(\gamma) & \text{if } z\cos j + \rho \sin j \sin(\varpi t) < 0 \end{cases} \tag{3.93}$$

It is possible to demonstrate that Eq. (3.93) becomes Eq. (3.92) in the case of zero-displacement orbit. However, the case of zero-displacement NKOs with the orbital plane parallel to the equator must be treated in a different way, as demonstrated in the calculation of the right ascension of the ascending node and shown in Eq. (3.39). Therefore, the general expression for the true longitude is

$$L = \begin{cases} \varpi t & \text{if } z = 0 \wedge j = 0 \\ \Omega^* + \arccos(\gamma) & \text{if } z\cos j + \rho \sin j \sin(\varpi t) \geq 0 \\ \Omega^* - \arccos(\gamma) & \text{if } z\cos j + \rho \sin j \sin(\varpi t) < 0 \end{cases} \tag{3.94}$$

An alternative formulation for the true longitude can be obtained which does not involve inverse trigonometric functions, as described in the case of the in-plane element f. However, as discussed for the in-plane modified equinoctial elements, it can be demonstrated that such a formulation does not further simplify what has already been obtained.

Summary

The generalized forward map from NKOs to osculating modified equinoctial elements described in Section 3.1.2 is summarized as:

$$\begin{aligned}
p &= \frac{\varpi^2 \rho^2 \left(\rho^2 + z^2\right)}{\mu} \\
f &= \frac{\varpi^2 \rho^2 \sqrt{\rho^2 + z^2} - \mu}{\mu} \cdot \begin{cases} \cos(\varpi t) & \text{if } z = 0 \wedge j = 0 \\ \cos\left(\Omega^* + \arccos(\gamma)\right) & \text{if } z\cos j + \rho \sin j \sin(\varpi t) \geq 0 \\ \cos\left(\Omega^* - \arccos(\gamma)\right) & \text{if } z\cos j + \rho \sin j \sin(\varpi t) < 0 \end{cases} \\
g &= \frac{\varpi^2 \rho^2 \sqrt{\rho^2 + z^2} - \mu}{\mu} \cdot \begin{cases} \sin(\varpi t) & \text{if } z = 0 \wedge j = 0 \\ \sin\left(\Omega^* + \arccos(\gamma)\right) & \text{if } z\cos j + \rho \sin j \sin(\varpi t) \geq 0 \\ \sin\left(\Omega^* - \arccos(\gamma)\right) & \text{if } z\cos j + \rho \sin j \sin(\varpi t) < 0 \end{cases} \\
h &= \sqrt{\frac{\sqrt{\rho^2 + z^2} - \left(\rho\cos j - z \sin j \sin(\varpi t)\right)}{\sqrt{\rho^2 + z^2} + \left(\rho\cos j - z \sin j \sin(\varpi t)\right)}} \cdot \frac{\rho \sin j \cos\xi + z\left(\cos j \cos\xi \sin(\varpi t) + \sin\xi \cos(\varpi t)\right)}{\sqrt{z^2\cos^2(\varpi t) + \left(\rho \sin j + z\cos j \sin(\varpi t)\right)^2}} \\
k &= \sqrt{\frac{\sqrt{\rho^2 + z^2} - \left(\rho\cos j - z \sin j \sin(\varpi t)\right)}{\sqrt{\rho^2 + z^2} + \left(\rho\cos j - z \sin j \sin(\varpi t)\right)}} \cdot \frac{\rho \sin j \sin\xi + z\left(\cos j \sin\xi \sin(\varpi t) - \cos\xi \cos(\varpi t)\right)}{\sqrt{z^2\cos^2(\varpi t) + \left(\rho \sin j + z\cos j \sin(\varpi t)\right)^2}} \\
L &= \begin{cases} \varpi t & \text{if } z = 0 \wedge j = 0 \\ \Omega^* + \arccos(\gamma) & \text{if } z\cos j + \rho \sin j \sin(\varpi t) \geq 0 \\ \Omega^* - \arccos(\gamma) & \text{if } z\cos j + \rho \sin j \sin(\varpi t) < 0 \end{cases}
\end{aligned} \tag{3.95}$$

in which Ω^* and γ are defined in Eq. (3.40).

3.1.3. Numerical Test Cases

Three scenarios have been tested in order to both verify the validity of the mappings shown in Sections 3.1.1 – 3.1.2 and study the behavior of the osculating elements. The three test cases have been chosen to be feasible mission scenarios in the near future. For this reason, only small-displacement non-Keplerian orbits are taken into account, which can be generated with current or near-term technology. All results of the test cases have been numerically verified by means of MATLAB functions.

In the following sub-sections, all the test cases taken into account are described and the mappings are shown and analyzed.

3.1.3.1. Test cases

1. *Displaced GEO*

Figure 24 shows the orbits (not to scale) of all the test cases taken into account related to the GEO case. The value of the displacement is set to 35 km for both in-plane and out-of-plane displacements so that the spacecraft hovers above/below or inside/outside the GEO station-keeping box.[12]

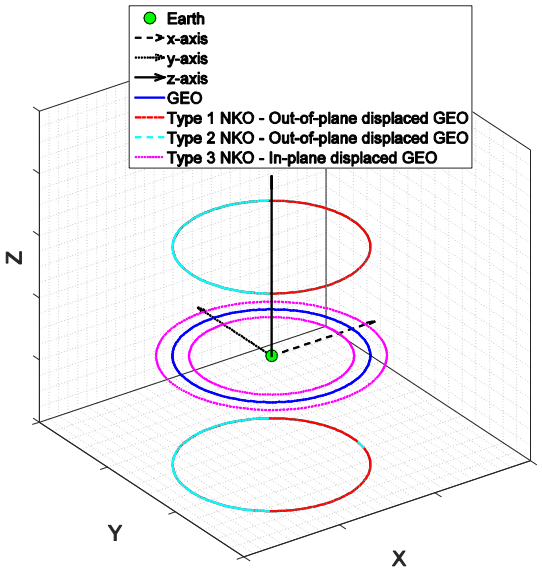

Figure 24. Earth-centered view (not to scale) of the orbits of all the case studies taken into account for the GEO case.

The characteristics of the Keplerian GEO are shown in Eq. (2.92). The characteristics of the Type 1 NKO are as follows.

$$\text{Type 1 NKO}: \begin{cases} z_1 = r_{GEO} \sin(\Delta\lambda) \\ \rho_1 = r_{GEO} \cos(\Delta\lambda) \\ \varpi_1 = \sqrt{\mu / r_{GEO}^3} \\ j_1 = 0 \\ \xi_1 = 0 \end{cases} \tag{3.96}$$

In this case, two values of $\Delta\lambda$ are considered so that both positive and negative out-of-plane displaced NKOs are taken into account. These values are considered such that the spacecraft in the non-Keplerian orbit hovers above the GEO station-keeping box, which is 70-km high.[12]

$$\Delta\lambda = \pm\arcsin\left(\frac{z_1}{r_{GEO}}\right) = \pm\arcsin\left(\frac{35\text{ km}}{r_{GEO}}\right) \Rightarrow \begin{cases} z_1 = \pm 35\text{ km} \\ \rho_1 = 42{,}164.1551\text{ km} \end{cases} \tag{3.97}$$

Two case studies are considered for Type 2 NKOs as well.

$$\text{Type 2 NKO}: \begin{cases} z_2 = \pm 35\text{ km} \\ \rho_2 = r_{GEO} \\ \varpi_2 = \sqrt{\mu / r_{GEO}^3} \\ j_2 = 0 \\ \xi_2 = 0 \end{cases} \tag{3.98}$$

Two case studies are considered for Type 3 NKOs. Only an in-plane displacement is considered in this case.

$$\begin{matrix}\text{Type 3 NKO} \\ \text{(in-plane displacement)}\end{matrix}: \begin{cases} z_3 = 0 \\ \rho_3 = r_{GEO} \pm 35\text{ km} \\ \varpi_3 = \sqrt{\mu / r_{GEO}^3} \\ j_3 = 0 \\ \xi_3 = 0 \end{cases} \tag{3.99}$$

2. Displaced global positioning system (GPS)

Figure 25 shows the orbits (not to scale) of all the test cases taken into account related to the GPS case. The value of the displacement is set to 5 km for both in-plane and out-of-plane displacements so that the spacecraft hovers above/below or inside/outside the GPS spacecraft for visual inspection of the same. Moreover, a distance of 5 km can be considered within the range for proximity operations.[27]

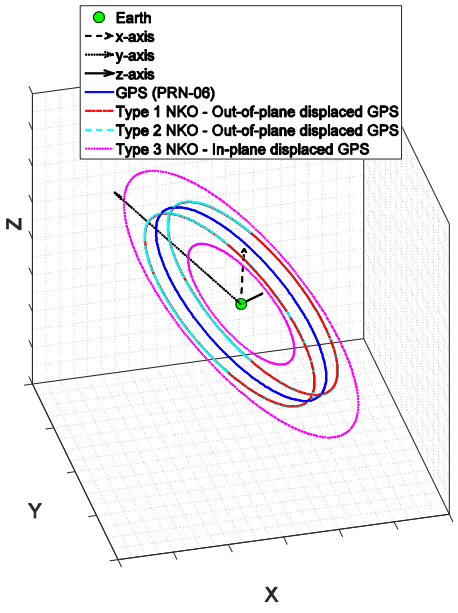

Figure 25. Earth-centered view (not to scale) of the orbits of all the case studies taken into account for the GPS case.

The orbit taken into account for describing the GPS is related to the PRN-06 satellite and its orbital parameters are accurate with respect to the Yuma Almanac 2016* (week 0896, GPS Time of Applicability 405504 s). PRN-06 has been chosen because is the one with the lowest value of eccentricity ($e = 0.22 \times 10^{-3}$) among the ones reported in the Yuma Almanac.

$$\text{GPS (PRN-06)}: \begin{cases} z_{GPS} = 0 \\ \rho_{GPS} = r_{GPS} = 26,560.9478 \text{ km} \\ \varpi_{GPS} = \sqrt{\mu / r_{GPS}^3} \\ j_{GPS} = 55.2885 \text{ deg} \\ \xi_{GPS} = 77.7881 \text{ deg} \end{cases} \tag{3.100}$$

The characteristics of the Type 1 NKO are as follows.

$$\text{Type 1 NKO}: \begin{cases} z_1 = r_{GPS} \sin(\Delta\lambda) \\ \rho_1 = r_{GPS} \cos(\Delta\lambda) \\ \varpi_1 = \sqrt{\mu / r_{GPS}^3} \\ j_1 = 55.2885 \text{ deg} \\ \xi_1 = 77.7881 \text{ deg} \end{cases} \tag{3.101}$$

In this case, two values of $\Delta\lambda$ are considered so that both positive and negative out-of-plane displaced NKOs are taken into account. These values are considered such that the spacecraft in the non-Keplerian orbit hovers 5 km above/below and outside/inside the GPS.

$$\Delta\lambda = \pm \arcsin\left(\frac{z_1}{r_{GPS}}\right) = \pm \arcsin\left(\frac{5 \text{ km}}{r_{GPS}}\right) \Rightarrow \begin{cases} z = \pm 5 \text{ km} \\ \rho = 26,5609.4733 \text{ km} \end{cases} \tag{3.102}$$

Two case studies are considered for Type 2 NKOs.

$$\text{Type 2 NKO}: \begin{cases} z_2 = \pm 5 \text{ km} \\ \rho_2 = r_{GPS} \\ \varpi_2 = \sqrt{\mu / r_{GPS}^3} \\ j_2 = 55.2885 \text{ deg} \\ \xi_2 = 77.7881 \text{ deg} \end{cases} \tag{3.103}$$

Two case studies are considered for Type 3 NKOs. Only the in-plane displacement is considered for Type 3 NKOs.

$$\begin{matrix} \text{Type 3 NKO} \\ \text{(in-plane displacement)} \end{matrix}: \begin{cases} z_3 = 0 \\ \rho_3 = r_{GPS} \pm 5 \text{ km} \\ \varpi_3 = \sqrt{\mu / r_{GPS}^3} \\ j_3 = 55.2885 \text{ deg} \\ \xi_3 = 77.7881 \text{ deg} \end{cases} \tag{3.104}$$

* Data available online at https://celestrak.com/GPS/almanac/Yuma/2016/ [retrieved 25 October 2016].

3. Displaced Sun-synchronous orbit (SSO)

Figure 26 shows the orbits (not to scale) of all the test cases taken into account related to the SSO case. The value of the displacement is set to 1 km for both in-plane and out-of-plane displacements so that the spacecraft hovers above/below or inside/outside the SSO spacecraft for visual inspection of the same. Moreover, a distance of 1 km can be considered within the range for proximity operations.[27]

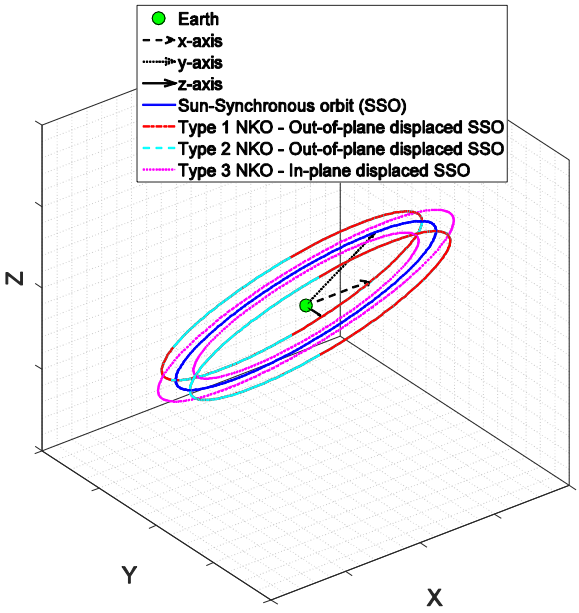

Figure 26. Earth-centered view (not to scale) of the orbits of all the case studies taken into account for the SSO case.

A circular Sun-synchronous orbit with a radius $r_{SSO} = 1{,}000$ km is considered. The value of the inclination can be easily computed considering the effect of J_2 as $j = \arccos\left(-\frac{2\omega_E}{3\sqrt{\mu}J_2R_E^2}r_{SSO}^{7/2}\right)$.

$$\text{SSO}: \begin{cases} z_{SSO} = 0 \\ \rho_{SSO} = r_{SSO} = R_\oplus + 1{,}000 \text{ km} \\ \varpi_{SSO} = \sqrt{\mu/r_{SSO}^3} \\ j_{SSO} = 99.4845 \text{ deg} \\ \xi_{SSO} = 0 \end{cases} \tag{3.105}$$

The characteristics of Type 1 NKOs are as follows.

$$\text{Type 1 NKO}: \begin{cases} z_1 = r_{SSO}\sin(\Delta\lambda) \\ \rho_1 = r_{SSO}\cos(\Delta\lambda) \\ \varpi_1 = \sqrt{\mu/r_{SSO}^3} \\ j_1 = 99.4845 \text{ deg} \\ \xi_1 = 0 \end{cases} \tag{3.106}$$

In this case, two values of $\Delta\lambda$ are considered so that both positive and negative out-of-plane displaced NKOs are taken into account. These values are considered such that the spacecraft in the non-Keplerian orbit hovers 1 km above/below and outside/inside the spacecraft in SSO.

$$\Delta\lambda = \pm\arcsin\left(\frac{z_1}{r_{SSO}}\right) = \pm\arcsin\left(\frac{1\text{ km}}{r_{SSO}}\right) \Rightarrow \begin{cases} z_1 = \pm 1\text{ km} \\ \rho_1 \cong r_{SSO} \end{cases} \tag{3.107}$$

Two case studies are considered for Type 2 NKOs.

$$\text{Type 2 NKO}: \begin{cases} z_2 = \pm 1\text{ km} \\ \rho_2 = r_{SSO} \\ \varpi_2 = \sqrt{\mu / r_{SSO}^3} \\ j_2 = 99.4845\text{ deg} \\ \xi_2 = 0 \end{cases} \tag{3.108}$$

Two case studies are considered for Type 3 NKOs. Only the in-plane displacement is considered for Type 3 NKOs.

$$\begin{matrix}\text{Type 3 NKO} \\ \text{(in-plane displacement)}\end{matrix}: \begin{cases} z_3 = 0 \\ \rho_3 = r_{SSO} \pm 1\text{ km} \\ \varpi_3 = \sqrt{\mu / r_{SSO}^3} \\ j_3 = 99.4845\text{ deg} \\ \xi_3 = 0 \end{cases} \tag{3.109}$$

3.1.3.2. Results and Discussion – Signatures of Non-Keplerian Orbit Families

A summary of the key characteristics of the signature of the three NKO families is given in the following sub-sections, one for each orbital element used. A detailed description of the evolution of each osculating element for each case study is not given here for the sake of conciseness.

Note that, in the following sub-sections, all the sinusoidal curves are described as $\cos(\varpi t + \varphi)$ in which φ is a phase angle which is a function of inclination j, RAAN ξ, and osculating element taken into account. Furthermore, $\tilde{\tau}$ represents the semi-amplitude of the cosine wave related to the element τ.

1. Non-Keplerian orbit to osculating Keplerian orbital elements map

Semi-major axis and **eccentricity** do not show any special signature, being both constant in time. The only characteristic that has been noted is that, in both cases, the in-plane displaced orbits have the largest difference respect to the Keplerian orbit.

$$a(t) = a_0 \tag{3.110}$$

$$e(t) = e_0 \tag{3.111}$$

The first key characteristic is seen in the mapping of the **inclination**. Two trends can be seen:

$$\begin{cases} i(t) = i_0 & \text{if } z = 0 \vee j = 0 \\ i(t) \approx \tilde{i}\cos(\varpi t + \varphi) & \text{otherwise} \end{cases} \tag{3.112}$$

in which

$$\begin{cases} \left|\tilde{i} - j\right| \le 0.002 \text{ deg} & \text{(GPS case)} \\ \left|\tilde{i} - j\right| \le 0.008 \text{ deg} & \text{(SSO case)} \end{cases} \tag{3.113}$$

The **right ascension of the ascending node** is characterized by three separate trends, as follows.

$$\begin{cases} \Omega(t) = \xi & \text{if } z = 0 \\ \Omega(t) = \Omega_0 + \varpi t & \text{if } j = 0 \\ \Omega(t) \approx \tilde{\Omega}\cos(\varpi t + \varphi) & \text{otherwise} \end{cases} \tag{3.114}$$

in which

$$\Omega_0 = \begin{cases} \dfrac{\pi}{2} & \text{if } z < 0 \\ \dfrac{3}{2}\pi & \text{if } z > 0 \end{cases} \tag{3.115}$$

and

$$\begin{cases} \left|\tilde{\Omega} - \xi\right| \le 0.003 \text{ deg} & \text{(GPS case)} \\ \left|\tilde{\Omega} - \xi\right| \le 0.008 \text{ deg} & \text{(SSO case)} \end{cases} \tag{3.116}$$

The **argument of perigee** is characterized by two separate trends, as follows.

$$\begin{cases} \omega(t) = \omega_0 & \text{if Keplerian orbit} \vee \left(j = 0 \wedge z \ne 0\right) \\ \omega(t) = \omega_1 + \varpi t & \text{otherwise} \end{cases} \tag{3.117}$$

in which

$$\omega_0 = \begin{cases} 0 & \text{Keplerian orbit} \\ \dfrac{\pi}{2} & \text{Type 1 } (z < 0) \wedge \text{Type 2 } (z > 0), \\ \dfrac{3}{2}\pi & \text{Type 1 } (z > 0) \wedge \text{Type 2 } (z < 0) \end{cases} \quad \omega_1 = \begin{cases} 0 & \text{Type 2} \wedge \text{Type 3 } (\rho > r) \\ \pi & \text{Type 1} \wedge \text{Type 3 } (\rho < r) \end{cases} \tag{3.118}$$

Lastly, two trends can be seen for the **true anomaly**, as follows.

$$\vartheta(t)=\begin{cases}\varpi t & \text{Keplerian orbit}\\ \vartheta_0 & \text{NKO}\end{cases} \tag{3.119}$$

in which

$$\vartheta_0=\begin{cases}0 & \text{Type 2}\wedge\text{Type 3}\ (\rho>r)\\ \pi & \text{Type 1}\wedge\text{Type 3}\ (\rho<r)\end{cases} \tag{3.120}$$

It is important to note that Eq. (3.120) shows that a spacecraft in a non-Keplerian orbit can only be either at the perigee or the apogee of its osculating Keplerian orbit, as it was already discussed in the simplified case.

2. Non-Keplerian orbit to osculating modified equinoctial elements map

Semi-latus rectum does not show any special signature, being constant in time. The only characteristic that has been noted is that, as for semi-major axis and eccentricity, the in-plane displaced orbits have the largest difference respect to the Keplerian orbit.

$$p(t)=p_0 \tag{3.121}$$

The first key characteristic is seen in the mapping of the **in-plane element *f***. Two trends can be seen:

$$\begin{cases}f(t)=0 & \text{Keplerian orbit}\\ f(t)\approx\tilde{f}\cos(\varpi t+\varphi) & \text{NKO}\end{cases} \tag{3.122}$$

However, the magnitude of oscillation for the out-of-plane displaced cases is very small, as shown in the following.

$$\begin{cases}\tilde{f}\le 10^{-6} & \text{if } z\neq 0\\ \tilde{f}\le 10^{-3} & \text{if } z=0\end{cases} \tag{3.123}$$

The **in-plane element *g*** is characterized by two separate trends, as the previous element.

$$\begin{cases}g(t)=0 & \text{Keplerian orbit}\\ g(t)\approx\tilde{g}\cos(\varpi t+\varphi) & \text{NKO}\end{cases} \tag{3.124}$$

However, the magnitude of oscillation for the out-of-plane displaced cases is very small, with values comparable with those of the other in-plane element f.

The **out-of-plane element *h*** is characterized by two separate trends, as follows.

$$\begin{cases}h(t)=h_{Kep} & \text{if } z=0\\ h(t)\approx\tilde{h}\cos(\varpi t+\varphi) & \text{if } z\neq 0\end{cases} \tag{3.125}$$

The magnitudes of oscillations respect to the Keplerian value are

$$\begin{cases} \left|\tilde{h}-h_{Kep}\right| \le 10^{-4} & \text{(GEO case)} \\ \left|\tilde{h}-h_{Kep}\right| \le 10^{-5} & \text{(GPS case)} \\ \left|\tilde{h}-h_{Kep}\right| \le 2\times 10^{-4} & \text{(SSO case)} \end{cases} \tag{3.126}$$

The **out-of-plane element *k*** is characterized by two separate trends, as the previous element.

$$\begin{cases} k(t) = k_{Kep} & \text{if } z = 0 \\ k(t) \approx \tilde{k}\cos(\varpi t + \varphi) & \text{if } z \neq 0 \end{cases} \tag{3.127}$$

The magnitudes of oscillations respect to the Keplerian value are

$$\begin{cases} \left|\tilde{k}-k_{Kep}\right| \le 10^{-4} & \text{(GEO case)} \\ \left|\tilde{k}-k_{Kep}\right| \le 10^{-5} & \text{(GPS case)} \\ \left|\tilde{k}-k_{Kep}\right| \le 2\times 10^{-4} & \text{(SSO case)} \end{cases} \tag{3.128}$$

Lastly, one trend can be seen for the **true longitude**, as follows.

$$L(t) \approx L(t_0) + \varpi t \tag{3.129}$$

The absolute differences respect to the Keplerian value are

$$\begin{cases} \left|L(t)-L_{Kep}\right| \approx 0 & \text{(GEO case)} \\ \left|L(t)-L_{Kep}\right| \le 0.001 \text{ deg} & \text{(GPS case)} \\ \left|L(t)-L_{Kep}\right| \le 0.01 \text{ deg} & \text{(SSO case)} \end{cases} \tag{3.130}$$

3.1.4. Non-Keplerian orbit to Osculating Orbital Elements Map: Summary of the Signatures

The key characteristics that can provide a clear and reliable indication that a spacecraft is being forced along a non-Keplerian orbit are listed here.

The signatures of NKOs on the osculating Keplerian orbital elements are the following.

$$\text{KEP}: \begin{cases} i(t) \approx \tilde{i}\cos(\varpi t + \varphi) & \text{if } z \neq 0 \wedge j \neq 0 \\ \Omega(t) = \Omega_0 + \varpi t & \text{if } z \neq 0 \wedge j = 0 \\ \Omega(t) \approx \tilde{\Omega}\cos(\varpi t + \varphi) & \text{if } z \neq 0 \wedge j \neq 0 \\ \omega(t) = \omega_0 + \varpi t & \text{if } z = 0 \vee j \neq 0 \\ \vartheta(t) = \vartheta_0 \end{cases} \tag{3.131}$$

The signatures of NKOs on the osculating modified equinoctial elements are the following.

$$\text{MEE}: \begin{cases} f(t) \approx \tilde{f}\cos(\varpi t + \varphi) \\ g(t) \approx \tilde{g}\cos(\varpi t + \varphi) \\ h(t) \approx \tilde{h}\cos(\varpi t + \varphi) & \text{if } z \neq 0 \\ k(t) \approx \tilde{k}\cos(\varpi t + \varphi) & \text{if } z \neq 0 \end{cases} \tag{3.132}$$

3.2. Inverse Map: Osculating Orbital Elements to Non-Keplerian Orbit

A generalized formulation of the inverse mappings has not being found. Nevertheless, the formulation of the inverse mappings shown in Section 2.2 for the simplified model has been expanded. Starting from the Cartesian position and velocity vectors (Eqs. (3.2) – (3.3)), families of NKOs are derived as a function of the known NKO elements given by the simplified inverse mappings.

All the families of solutions for $t_0 = 0$ are found by solving the following system of equations for the unknown NKO elements $\left[z, \rho, \varpi, j, \xi, t\right]$

$$\begin{cases} \boldsymbol{r}\left(z, \rho, \varpi, j, \xi, t\right) = \begin{bmatrix} \rho_0 \\ 0 \\ z_0 \end{bmatrix} \\ \boldsymbol{v}\left(z, \rho, \varpi, j, \xi, t\right) = \begin{bmatrix} 0 \\ \varpi_0 \rho_0 \\ 0 \end{bmatrix} \end{cases} \tag{3.133}$$

in which $\left[z_0, \rho_0, \varpi_0\right]^T$ is the set of NKO elements in the simplified case. Eq. (3.133) has been solved via Mathematica function *Reduce* with the following hypotheses.

$$\begin{cases} \left\{\rho, \rho_0, \varpi, \varpi_0\right\} > 0 \\ \left\{z, z_0, t\right\} \in \mathbb{R} \\ j \in \left[0, \pi\right) \\ \xi \in \left[0, 2\pi\right) \end{cases} \tag{3.134}$$

Two main groups of solutions have been found. These are shown in Eqs. (3.135) – (3.136).

$$A:\begin{cases} z = z_0 \\ \rho = \rho_0 \\ \varpi = \varpi_0 \\ j = 0 \\ \xi \in [0, 2\pi) \\ t = -\xi/\varpi \end{cases} \tag{3.135}$$

$$B: k_0^2 \neq 0 \wedge (C \vee D)$$

$$C: \varpi = -\frac{\varpi_0 \rho_0}{k_0} \wedge k_0 \neq \rho_0 \wedge \rho_0 \left(z^2 - z_0^2\right) + \rho_0^2 k_0 + z_0 (z_0 - z) k_0 \neq \rho_0^3 \wedge (C_1 \vee C_2) \qquad D: \varpi = \frac{\varpi_0 \rho_0}{k_0} \wedge k_0 \neq -\rho_0 \wedge \left(\rho_0^2 + z_0^2\right)(\rho_0 + k_0) \neq z\left(\rho_0 z + z_0 k_0\right) \wedge (D_1 \vee D_2)$$

$$C_1: \xi = \frac{\pi}{2} \wedge j = 2\tan^{-1}\left(\frac{\rho_0 + k_0}{z + z_0}\right) \wedge (C_{11} \vee C_{12}) \quad C_2: \xi = -\frac{\pi}{2} \wedge j = -2\tan^{-1}\left(\frac{\rho_0 + k_0}{z + z_0}\right) \wedge (C_{21} \vee C_{22}) \quad D_1: \xi = \frac{\pi}{2} \wedge j = 2\tan^{-1}\left(\frac{z - z_0}{\rho_0 + k_0}\right) \wedge (D_{11} \vee D_{12}) \quad D_2: \xi = -\frac{\pi}{2} \wedge j = 2\tan^{-1}\left(\frac{-z + z_0}{\rho_0 + k_0}\right) \wedge (D_{21} \vee D_{22})$$

$$C_{11}: \rho = k_0 \wedge 2\varpi_0 \rho_0 t + \pi k_0 (1 + 4K_1) = 0 \qquad C_{21}: \rho = k_0 \wedge 2\varpi_0 \rho_0 t + \pi k_0 (-1 + 4K_1) = 0 \qquad D_{11}: \rho = k_0 \wedge 2\varpi_0 \rho_0 t - \pi k_0 (-1 + 4K_1) = 0 \qquad D_{21}: \rho = k_0 \wedge 2\varpi_0 \rho_0 t - \pi k_0 (1 + 4K_1) = 0$$

$$C_{12}: \rho = -k_0 \wedge 2\varpi_0 \rho_0 t + \pi k_0 (-1 + 4K_1) = 0 \qquad C_{22}: \rho = -k_0 \wedge 2\varpi_0 \rho_0 t + \pi k_0 (1 + 4K_1) = 0 \qquad D_{12}: \rho = -k_0 \wedge 2\varpi_0 \rho_0 t - \pi k_0 (1 + 4K_1) = 0 \qquad D_{22}: \rho = -k_0 \wedge 2\varpi_0 \rho_0 t - \pi k_0 (-1 + 4K_1) = 0 \tag{3.136}$$

in which

$$\begin{cases} k_0 = \sqrt{\rho_0^2 + z_0^2 - z^2} \\ K_1 \in \mathbb{Z} \end{cases} \tag{3.137}$$

Note that the terms $C_{12}, C_{22}, D_{12}, D_{22}$ in Eq. (3.136) are never verified because both ρ and k_0 are always positive. Therefore, four separate families of solutions exist for the second group of solutions. For the same reason, the constraint $k_0 \neq -\rho_0$ shown within the solutions of the family D does not add anything and can be safely removed.

The families of solutions of the second group (Eq. (3.136)) are analyzed separately in the following sub-sections.

3.2.1. Family 1

The first family of solutions of the second group can be summarized by the following:

$$\begin{cases} \rho = k_0 \\ \varpi = -\varpi_0 \rho_0 / k_0 \\ j = 2\tan^{-1}\left(\left(\rho_0 + k_0 \right) / \left(z + z_0 \right) \right) \\ \xi = \pi / 2 \\ 2\varpi_0 \rho_0 t + \pi k_0 \left(1 + 4K_1 \right) = 0 \end{cases} \tag{3.138}$$

Note that all the elements depend on the value of the out-of-plane displacement z, which can be considered as a free parameter of the family. However, such element must satisfy the following constraints:

$$\begin{cases} |z| \neq r_0 \\ |z| \neq |z_0| \\ \rho_0 \left(z^2 - z_0^2 \right) + \rho_0^2 k_0 + z_0 \left(z_0 - z \right) k_0 - \rho_0^3 \neq 0 \end{cases} \tag{3.139}$$

Note that the third constraint listed in Eq. (3.139) does not add anything to the previous two constraints and, therefore, it can be removed without any loss of generality.

The solution related to the time t, shown at the end of Eq. (3.138), can be rewritten as

$$t = -\frac{\pi\rho}{2\varpi_0 \rho_0}\left(1 + 4K_1\right) = \frac{\pi}{2\varpi}\left(1 + 4K_1\right) = \frac{1}{\varpi}\left(\frac{\pi}{2} + 2K_1\pi \right) \tag{3.140}$$

Using the true anomaly $\vartheta = \varpi t$ instead of the time t, it is easily shown that the parameter K_1 can be omitted without any loss of generality. Therefore, the first family of solutions of the second group can be rewritten, as a function of the out-of-plane displacement z, as

$$\begin{cases} \rho = k_0 \\ \varpi = -\varpi_0 \rho_0 / k_0 \\ j = 2\tan^{-1}\left(\left(\rho_0 + k_0 \right) / \left(z + z_0 \right) \right) \\ \xi = \pi / 2 \\ \vartheta = \pi / 2 \end{cases} \tag{3.141}$$

3.2.2. Family 2

The second family of solutions of the second group can be summarized by the following:

$$\begin{cases} \rho = k_0 \\ \varpi = -\varpi_0 \rho_0 / k_0 \\ j = -2\tan^{-1}\left(\left(\rho_0 + k_0 \right) / \left(z + z_0 \right) \right) \\ \xi = -\pi / 2 \\ 2\varpi_0 \rho_0 t + \pi k_0 \left(-1 + 4K_1 \right) = 0 \end{cases} \tag{3.142}$$

Note that, also in this case, all the elements depend on the value of the out-of-plane displacement z, which can be considered as a free parameter of the family. However, this element must satisfy the following constraints (in which only the first two constraints are shown, as discussed for the first family).

$$\begin{cases} |z| \neq r_0 \\ |z| \neq |z_0| \end{cases} \tag{3.143}$$

As discussed for the first family, the second family of solutions of the second group can be rewritten, as a function of the out-of-plane displacement z, as

$$\begin{cases} \rho = k_0 \\ \varpi = -\varpi_0 \rho_0 / k_0 \\ j = -2\tan^{-1}\left((\rho_0 + k_0)/(z + z_0) \right) \\ \xi = -\pi/2 \\ \vartheta = -\pi/2 \end{cases} \tag{3.144}$$

Note that the solutions of the second family are characterized by

$$\begin{cases} \rho_2 = \rho_1 \\ \varpi_2 = \varpi_1 \\ j_2 = -j_1 \\ \xi_2 = -\xi_1 \\ \vartheta_2 = -\vartheta_1 \end{cases} \tag{3.145}$$

That is, the solutions of first and second families describe the same osculating Keplerian orbits, as it can be verified by substituting Eqs. (3.141), (3.144) into Eqs. (3.2) – (3.3). Considering the inclination $j \in [-\pi, \pi)$, the second family of solutions can be omitted without any loss of generality.

3.2.3. Family 3

The third family of solutions of the second group can be summarized by the following.

$$\begin{cases} \rho = k_0 \\ \varpi = \varpi_0 \rho_0 / k_0 \\ j = 2\tan^{-1}\left((z - z_0)/(\rho_0 + k_0) \right) \\ \xi = \pi/2 \\ 2\varpi_0 \rho_0 t - \pi k_0 \left(-1 + 4K_1 \right) = 0 \end{cases} \tag{3.146}$$

Note that, also in this case, all the elements depend on the value of the out-of-plane displacement z, which can be considered as a free parameter of the family. This, however, must satisfy the following constraints.

$$\begin{cases} |z| \neq r_0 \\ \left(\rho_0^2 + z_0^2 \right)\left(\rho_0 + k_0 \right) - z\left(\rho_0 z + z_0 k_0 \right) \neq 0 \end{cases} \tag{3.147}$$

Note that the second constraint of Eq. (3.147) does not have any solution in $\mathbb{R}$ and, therefore, it can be safely removed without any loss of generality.

As discussed for the first family, the third family of solutions of the second group can be rewritten, as a function of the out-of-plane displacement z, as

$$\begin{cases} \rho = k_0 \\ \varpi = \varpi_0 \rho_0 / k_0 \\ j = 2\tan^{-1}\left((z - z_0)/(\rho_0 + k_0) \right) \\ \xi = \pi/2 \\ \vartheta = -\pi/2 \end{cases} \tag{3.148}$$

3.2.4. Family 4

The fourth family of solutions of the second group can be summarized by the following.

$$\begin{cases} \rho = k_0 \\ \varpi = \varpi_0 \rho_0 / k_0 \\ j = 2\tan^{-1}\left(\left(-z + z_0\right)/\left(\rho_0 + k_0\right)\right) \\ \xi = -\pi/2 \\ 2\varpi_0 \rho_0 t - \pi k_0 \left(1 + 4K_1\right) = 0 \end{cases} \tag{3.149}$$

Note that, also in this case, all the elements depend on the value of the out-of-plane displacement z, which can be considered as a free parameter of the family. This, however, must satisfy the following constraints (where only the first constraint is shown, as discussed for the third family).

$$|z| \neq r_0 \tag{3.150}$$

As discussed for the first family, the fourth family of solutions of the second group can be rewritten, as a function of the out-of-plane displacement z, as

$$\begin{cases} \rho = k_0 \\ \varpi = \varpi_0 \rho_0 / k_0 \\ j = 2\tan^{-1}\left(\left(-z + z_0\right)/\left(\rho_0 + k_0\right)\right) \\ \xi = -\pi/2 \\ \vartheta = \pi/2 \end{cases} \tag{3.151}$$

Note that the solutions of the fourth family are characterized by

$$\begin{cases} \rho_4 = \rho_3 \\ \varpi_4 = \varpi_3 \\ j_4 = -j_3 \\ \xi_4 = -\xi_3 \\ \vartheta_4 = -\vartheta_3 \end{cases} \tag{3.152}$$

That is, the solutions of third and fourth families describe the same osculating Keplerian orbits, as it can be verified by substituting Eqs. (3.148), (3.151) into Eqs. (3.2) – (3.3). Considering the inclination $j \in [-\pi, \pi)$, the fourth family of solutions can be omitted without any loss of generality.

3.2.5. Discussion

Summarizing, only two families of solutions of the second group exist and they are described, as a function of the out-of-plane displacement z, as

Family 1

$$\begin{cases} \rho = k_0 \\ \varpi = -\varpi_0 \rho_0 / k_0 \\ j = 2\tan^{-1}\left(\left(\rho_0 + k_0\right)/\left(z + z_0\right)\right), \\ \xi = \pi/2 \\ \vartheta = \pi/2 \end{cases}$$

Family 3

$$\begin{cases} \rho = k_0 \\ \varpi = \varpi_0 \rho_0 / k_0 \\ j = 2\tan^{-1}\left(\left(z - z_0\right)/\left(\rho_0 + k_0\right)\right) \\ \xi = \pi/2 \\ \vartheta = -\pi/2 \end{cases} \tag{3.153}$$

in which $j \in [-\pi, \pi)$.

However, it can also be demonstrated that the two remaining families of solutions describe, in fact, the same family. From Eq. (3.153), it can be noted that both orbital radius and RAAN are the same for the two families. Moreover, both orbital angular velocity and true anomaly of the third family are the opposite with respect to those of the first family. In order to have the same non-Keplerian orbits from both family 1 and 3, it must be

$$\begin{bmatrix} \boldsymbol{r}_1(z_1, j_1, t) \\ \boldsymbol{v}_1(z_1, j_1, t) \end{bmatrix} = \begin{bmatrix} \boldsymbol{r}_3(z_3, j_3, t) \\ \boldsymbol{v}_3(z_3, j_3, t) \end{bmatrix} \tag{3.154}$$

for any time t. The result of Eq. (3.154) is

$$\begin{cases} z_3 = -z_1 \\ j_3(z_3) = \mathrm{mod}\left(j_1(z_1) + \pi, 2\pi\right) \end{cases} \tag{3.155}$$

Because the out-of-plane displacement z is a free parameter, the first condition of Eq. (3.155) can be always true. If the second condition of Eq. (3.155) can be demonstrated to be true, the equivalence of the two families of solution shown in Eq. (3.153) is demonstrated as well.

We wish to demonstrate that

$$\left| \frac{j_1(z)}{2} - \frac{j_3(-z)}{2} \right| = \frac{\pi}{2} \tag{3.156}$$

From Eq. (3.153), it can be shown that

$$\begin{cases} \tilde{\alpha} := \dfrac{j_1(z)}{2} = \tan^{-1}\left(\dfrac{\rho_0 + k_0}{z + z_0}\right) = \tan^{-1}\left(\dfrac{X_3}{X_1 + X_2}\right) \\ \tilde{\beta} := \dfrac{j_3(-z)}{2} = \tan^{-1}\left(\dfrac{-z - z_0}{\rho_0 + k_0}\right) = \tan^{-1}\left(-\dfrac{X_1 + X_2}{X_3}\right) \end{cases} \tag{3.157}$$

From the definition given in Eq. (3.157), it can again be shown that

$$\begin{cases} \tan\tilde{\alpha} = \dfrac{X_3}{X_1 + X_2} \\ \tan\tilde{\beta} = -\dfrac{X_1 + X_2}{X_3} \end{cases} \Rightarrow \tan^{-1}\left(\frac{X_3}{X_1 + X_2}\right) - \tan^{-1}\left(-\frac{X_1 + X_2}{X_3}\right) = \tilde{\alpha} - \tilde{\beta} \Rightarrow \tag{3.158}$$

$$\Rightarrow \tan\left(\tilde{\alpha} - \tilde{\beta}\right) = \frac{\tan\tilde{\alpha} - \tan\tilde{\beta}}{1 + \tan\tilde{\alpha}\tan\tilde{\beta}} = \frac{\dfrac{X_3}{X_1 + X_2} + \dfrac{X_1 + X_2}{X_3}}{1 - \dfrac{X_3}{X_1 + X_2} \cdot \dfrac{X_1 + X_2}{X_3}} = \frac{\dfrac{{X_3}^2 + (X_1 + X_2)^2}{X_3(X_1 + X_2)}}{0} = \infty \Rightarrow \tag{3.159}$$

$$\Rightarrow \tilde{\alpha} - \tilde{\beta} = \frac{\pi}{2} \quad \square \tag{3.160}$$

Eq. (3.160) also demonstrates that the second condition of Eq. (3.155) is true and, therefore, the two families of solutions shown in Eq. (3.153) are, in fact, the same family.

Because a positive orbital angular velocity is more intuitive than a negative one, the third family has been chosen to fully describe the solutions of the second group.

The two groups of solutions, for $t_0 = 0$, are described as follows.

$$A:\begin{cases} z = z_0 \\ \rho = \rho_0 \\ \varpi = \varpi_0 \\ j = 0 \\ \xi \in [0, 2\pi) \\ \vartheta = -\xi \end{cases} \qquad B:\begin{cases} z = \text{free s.t. } |z| \neq r_0 \\ \rho = k_0 \\ \varpi = \varpi_0 \rho_0 / k_0 \\ j = 2\tan^{-1}\left((z - z_0)/(\rho_0 + k_0)\right) \\ \xi = \pi/2 \\ \vartheta = -\pi/2 \end{cases} \tag{3.161}$$

Note that solution A shown in Eq. (3.161) is, in fact, a particular case of the more general solution B. In particular, zero-inclination NKOs are characterized by $\xi \in [0, 2\pi)$ and $\vartheta = -\xi$. Therefore, the general formulation of the family of non-Keplerian orbits at $t_0 = 0$ is given by

$$\begin{cases} z = \text{free s.t. } |z| \neq r_0 \\ \rho = k_0 \\ \varpi = \varpi_0 \rho_0 / k_0 \\ j = 2\tan^{-1}\left((z - z_0)/(\rho_0 + k_0)\right) \\ \xi = \pi/2 \\ \vartheta = -\pi/2 \end{cases} \tag{3.162}$$

3.2.6. Generalization for any time

Equation (3.162) shows the family of solutions found for $t_0 = 0$. However, a general expression for the family of NKOs is needed for any t_0. Because the NKOs taken into account are circular, it can be chosen to use the RAAN as a free element instead of time and leave the time as $t_0 = 0$. The relation that links the time to the RAAN is

$$\xi_0 = \varpi_0 t_0 \tag{3.163}$$

It has been noted that the RAAN is the only element that is directly related to the value of the RAAN of the known NKO. Therefore, the description of the family of NKOs for any time t_0 is given by

$$\begin{cases} z = \text{free s.t. } |z| \neq r_0 \\ \rho = k_0 \\ \varpi = \varpi_0 \rho_0 / k_0 \\ j = 2\tan^{-1}\left((z - z_0)/(\rho_0 + k_0)\right) \\ \xi = \xi_0 + \pi/2 \\ \vartheta = -\pi/2 \end{cases} \tag{3.164}$$

3.2.7. Summary

Given the elements of an NKO characterized by the orbital plane parallel to the equator, the family of all possible circular NKOs that share the same instantaneous Cartesian state with the known NKO is given as follows.

$$\begin{cases} z = \text{free s.t. } |z| \neq r_0 \\ \rho = k_0 \\ \varpi = \varpi_0 \rho_0 / k_0 \\ j = 2\tan^{-1}\left((z - z_0)/(\rho_0 + k_0) \right) \\ \xi = \xi_0 + \pi/2 \\ \vartheta = -\pi/2 \end{cases} \tag{3.165}$$

in which $k_0 = \sqrt{\rho_0^2 + z_0^2 - z^2}$. In particular, zero-inclination NKOs are characterized by $\xi \in [0, 2\pi)$ and $\vartheta = \xi_0 - \xi$.

3.2.8. Numerical test cases

In order to test the solution found and shown in Eq. (3.165), a numerical test case is considered. The known zero-inclination NKO is a Type 1 NKO described by

$$\begin{cases} z_0 = r_{GEO} \sin(20\,\text{deg}) \\ \rho_0 = r_{GEO} \cos(20\,\text{deg}) \\ \varpi_0 = \sqrt{\mu / r_{GEO}^3} \\ j_0 = 0 \\ \xi_0 = 0 \end{cases} \tag{3.166}$$

Starting from the particular NKO shown in Eq. (3.166), the entire family of NKOs has been numerically investigated considering $z \in [-2z_0, 2z_0]$ for two initial times t_0. For all the test cases shown, the Cartesian state is computed, by means of Eqs. (3.2) – (3.3), from the NKO elements found through Eq. (3.166). In all the test cases shown, the error in each element of the Cartesian position and velocity vectors is always less than 10^{-12} km and 10^{-16} km/s, respectively.

The characteristics of the first test case are shown in Eq. (3.167), whereas Figures 27 to 30 show the whole family of NKOs.

$$\begin{cases} \xi_0 = 0 \\ t_0 = 0 \end{cases} \tag{3.167}$$

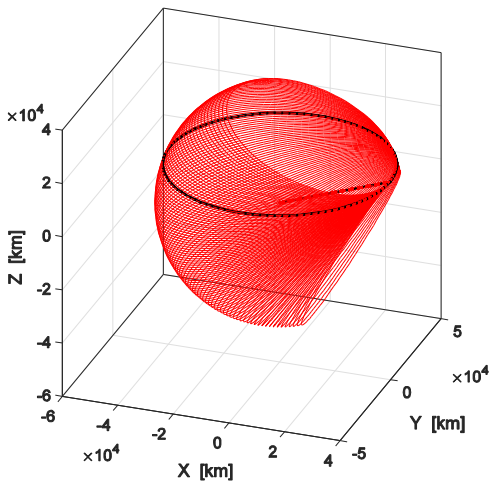

Figure 27. Test case 1. Known NKO (black) and other NKOs, which are part of the family (red), are shown.

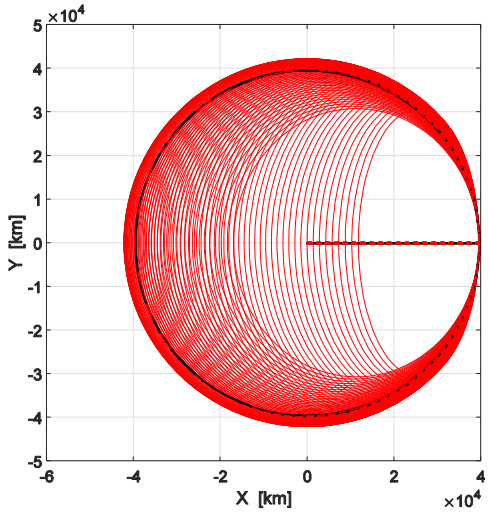

Figure 28. Test case 1. Known NKO (black) and other NKOs, which are part of the family (red), are shown. X-Y view.

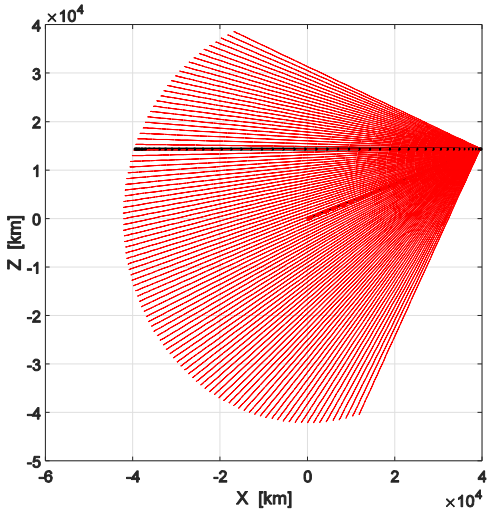

Figure 29. Test case 1. Known NKO (black) and other NKOs, which are part of the family (red), are shown. X-Z view.

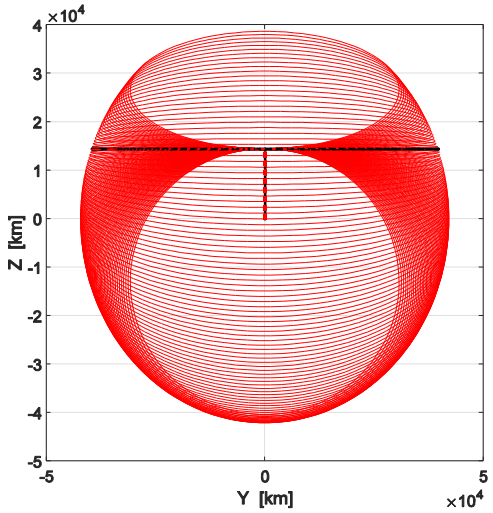

Figure 30. Test case 1. Known NKO (black) and other NKOs, which are part of the family (red), are shown. Y-Z view.

The characteristics of the second test case are shown in Eq. (3.168), whereas Figures 31 – 32 show the whole family of NKOs.

$$\begin{cases} \xi_0 = \pi/2 \\ t_0 = 0 \end{cases} \Rightarrow \begin{cases} \xi_0 = 0 \\ t_0 \approx 6 \text{ hours} \end{cases} \tag{3.168}$$

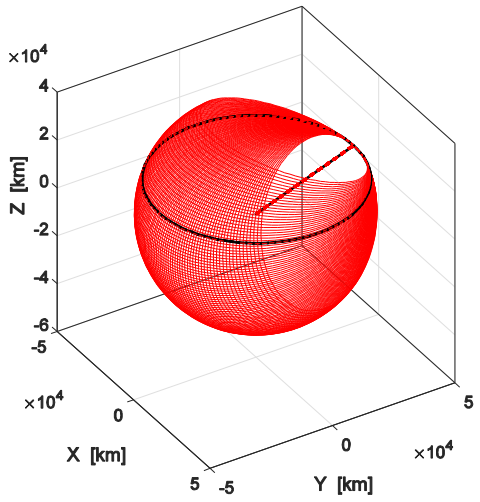

Figure 31. Test case 2. Known NKO (black) and other NKOs, which are part of the family (red), are shown.

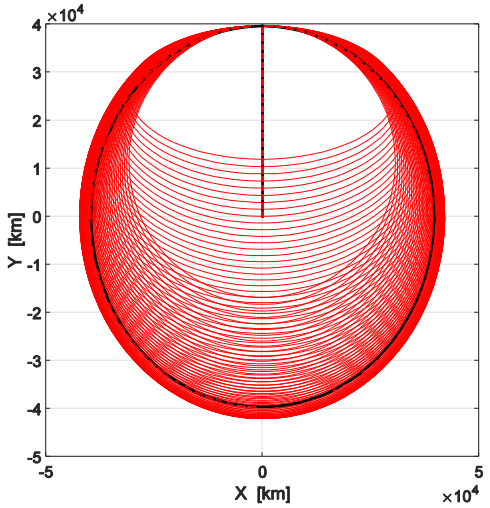

Figure 32. Test case 2. Known NKO (black) and other NKOs, which are part of the family (red), are shown. X-Y view.

3.3. Impact of Noise

The impact of noise on the NKO elements is now considered. This allows a determination if the NKO signatures are still clear. The same scenarios used to study the signatures have been considered. However, only the Type 1 NKOs with a positive displacement are used for this part of the study.

Three values for the noise have been considered in this study, consisting of upper/lower boundaries and a value inside this range. For the upper boundary, the maximum range error $|\Delta r| = 24$ m and range rate error $|\Delta \dot{r}| = 0.16$ m/s, due to the instrumental errors, are considered.[28] A second set of values for the noise is considered by dividing the upper boundary by a factor of 10. It will be seen that these values lie within the range defined by upper and lower boundaries. A lower boundary on the noise can be set by considering the errors in the orbit determination of the test cases. Because these errors are the result of filtering processes (i.e. a Keplerian orbit is assumed in the first place), these values are considered here as the lower boundary, as follows.[29-33]

$$\text{GEO}: \begin{cases} \|\Delta \boldsymbol{r}\| \approx 0.1 \text{ m} \\ |\Delta i| \approx 10^{-3} \text{ deg} \\ |\Delta \Omega| \approx 2 \times 10^{-3} \text{ deg} \end{cases}, \quad \text{GPS/SSO}: \begin{cases} \|\Delta \boldsymbol{r}\| \approx 1 \text{ m} \\ \|\Delta \boldsymbol{v}\| \approx 2 \text{ mm/s} \end{cases} \tag{3.169}$$

A Monte Carlo analysis has been carried out to obtain the maximum values of the errors on the Keplerian inclination $|\Delta i|$ and RAAN $|\Delta \Omega|$ from the aforementioned errors. 500 samples of Cartesian position and velocity vectors in a normal distribution have been considered with mean values corresponding to the nominal Cartesian states. The standard deviation considered for each component of the position vector is $\|\Delta \boldsymbol{r}\|$, assuming the range error being equal to $\|\Delta \boldsymbol{r}\|$. The standard deviation considered for each component of the velocity vector is $\|\Delta \boldsymbol{v}\|$, assuming the range rate error being equal to $\|\Delta \boldsymbol{v}\|$. Considering the conversion from Cartesian state to KEP, the errors given by the aforementioned values provide an estimate of $|\Delta i|$ and $|\Delta \Omega|$. The three sets of errors considered here are, therefore, the following.

$$\text{Case 1 (upper bound)}: \begin{cases} \|\Delta \boldsymbol{r}\| = 24 \text{ m} \\ |\Delta i| = 0.01 \text{ deg} \\ |\Delta \Omega| = \begin{cases} 180 \text{ deg} & \text{if GEO} \\ 0.01 \text{ deg} & \text{otherwise} \end{cases} \end{cases}$$

$$\text{Case 2}: \begin{cases} \|\Delta \boldsymbol{r}\| = 2.4 \text{ m} \\ |\Delta i| = 0.001 \text{ deg} \\ |\Delta \Omega| = \begin{cases} 180 \text{ deg} & \text{if GEO} \\ 0.001 \text{ deg} & \text{otherwise} \end{cases} \end{cases}$$

$$\text{Case 3 (lower bound)}: \begin{cases} \text{GEO}: \begin{cases} \|\Delta \boldsymbol{r}\| = 0.1 \text{ m} \\ |\Delta i| = 10^{-3} \text{ deg} \\ |\Delta \Omega| = 2 \times 10^{-3} \text{ deg} \end{cases} \\ \text{GPS/SSO}: \begin{cases} \|\Delta \boldsymbol{r}\| = 1 \text{ m} \\ |\Delta i| = 10^{-4} \text{ deg} \\ |\Delta \Omega| = 10^{-4} \text{ deg} \end{cases} \end{cases} \tag{3.170}$$

It is important to note that $|\Delta\Omega| = 180$ deg in the cases 1-2 related to GEO. This is due to the planar nature of GEO and, therefore, the fact that RAAN is arbitrarily set to zero. Even a small error can introduce a small inclination and, therefore, a value of $\Omega \in [0, 2\pi)$. On the other hand, the value of the error on RAAN for case 3 is significantly lower because of the filtering.

The errors $\{\|\Delta\boldsymbol{r}\|, |\Delta i|, |\Delta\Omega|\}$ are used to estimate the noise to be considered for the NKO elements. A Monte Carlo analysis has been carried out with 500 samples of NKO elements in a normal distribution. The mean values considered are the nominal values of NKO elements $\{z_0, \rho_0, j_0, \xi_0\}$, whereas the standard deviations are $\left\{\|\Delta\boldsymbol{r}\|\sin(z_0/\rho_0), \sqrt{3}\|\Delta\boldsymbol{r}\|, |\Delta i|, |\Delta\Omega|\right\}$, respectively. The value of the angular velocity is simply given by $\varpi = \sqrt{\mu/\rho^3}$, in which ρ is the NKO orbit radius with noise.

Figures 33 and 34 show both GEO and Type 1 NKO in the presence of noise as from Eq. (3.170) for Cases 1 and 2, respectively. Both figures have been generated using the Cartesian position vectors resulted from the osculating KEP obtained through the forward map from NKO elements with noise. The figures show that, by looking at their orbits, the Keplerian GEO and the NKO are clearly distinguishable for the value of noise related to Case 2. On the contrary, the same is not true for the three-dimensional orbits of both the GPS and SSO cases. That is, in the GPS and SSO cases, one cannot understand if the orbit they are looking at is a Keplerian or a non-Keplerian one.

Figure 35 shows a comparison between all the scenarios and noise levels taken into account in this study. The evolution of the out-of-plane MEE k has been chosen for the comparison. From the plots, it can be seen that the first level of noise is too large to be able to distinguish Keplerian from non-Keplerian orbits. On the other hand, with the third level of noise, which has been considered as the lower bound, all the test cases show a clear division between the two types of orbits. If the second level of noise is considered, the signatures of a spacecraft being forced along a NKO are still clear in the GPS and SSO cases. In fact, the constant trend of k that is peculiar of a Keplerian orbit is clearly opposed to the sinusoidal trend of k, which is characteristic of a NKO. On the contrary, the GEO case is still too noisy to be able to separate the two trends. This is due to the very large error on RAAN considered (Eq. (3.170)).

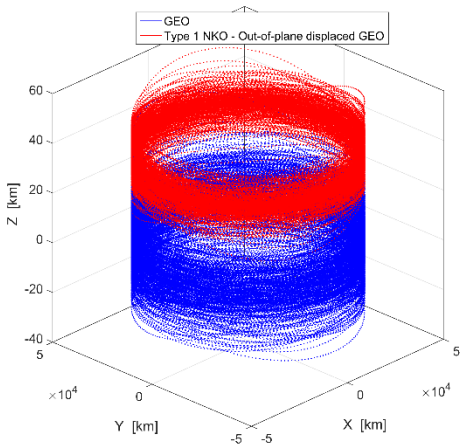

Figure 33. Case 1. GEO and NKO with noise.

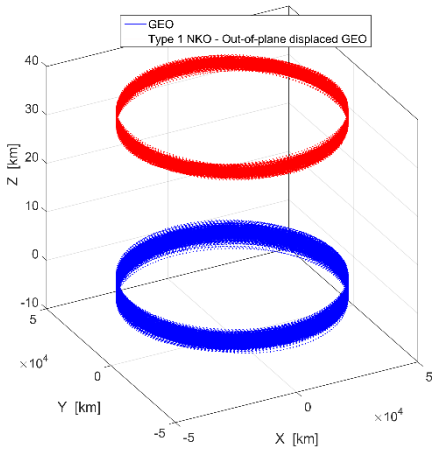

Figure 34. Case 2. GEO and NKO with noise.

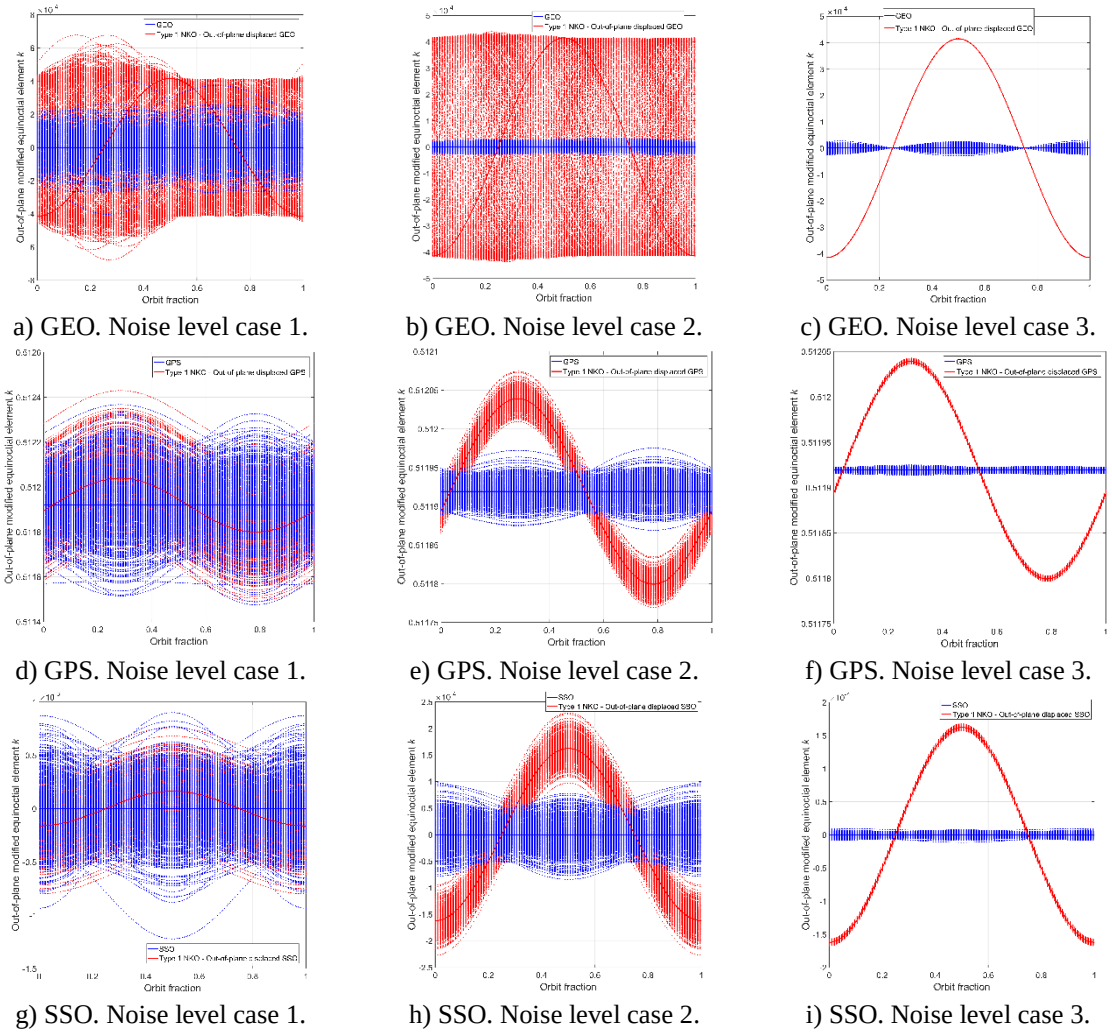

a) GEO. Noise level case 1. b) GEO. Noise level case 2. c) GEO. Noise level case 3.

d) GPS. Noise level case 1. e) GPS. Noise level case 2. f) GPS. Noise level case 3.

g) SSO. Noise level case 1. h) SSO. Noise level case 2. i) SSO. Noise level case 3.

Figure 35. Evolution of *k* over one orbit. All mission scenarios and noise levels are shown.

Lastly, it is interesting to study the thrust-induced acceleration needed to follow the osculating elements in the presence of noise. However, the formulation of the acceleration as a function of the osculating elements shown in Eqs. (2.152) – (2.157) has been derived for a reference frame so that *viewed from an inertial frame of reference, such solutions correspond to circular orbits displaced above the central body.*[2] That is, the reference frame should be rotated following inclination and RAAN of the nominal Keplerian orbit before computing the magnitude of acceleration. Assuming a knowledge of the nominal Keplerian orbit, the reference frame can be rotated by the RAAN and inclination following the rotations $\mathbf{R}_3(\Omega) \rightarrow \mathbf{R}_1(i)$. This is a good assumption since the data are noisy around the nominal value. Therefore, the values of RAAN and inclination can be considered as the mean values of the data available. This way, the rotated Cartesian state describes a noisy orbit with approximately zero inclination. Therefore, the analytical formulation of the acceleration given either osculating KEP or MEE shown in Eqs. (2.152) and (2.155) can be used to have a first-guess approximation of the magnitude of the acceleration needed to follow the observed NKO. Moreover, the value of the magnitude of acceleration can be a further indication of the use of a NKO. Figures 36 and 37 show the magnitudes of acceleration computed considering the second level of noise for the GEO and GPS cases, respectively.

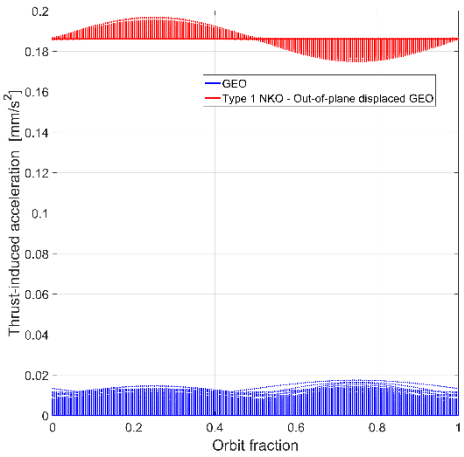

Figure 36. Magnitude of acceleration over one orbit. GEO. Noise level case 2.

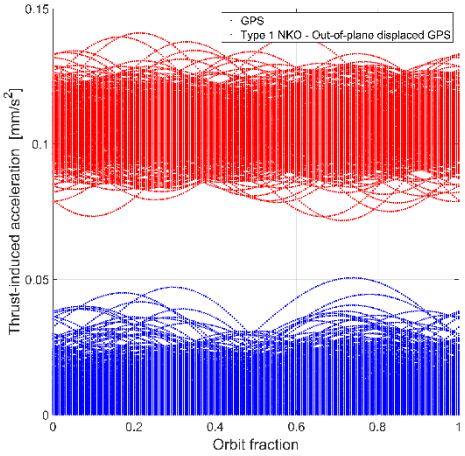

Figure 37. Magnitude of acceleration over one orbit. GPS. Noise level case 2.

In Table 10, the impact of noise on the mappings is summarized. Those signatures that, despite the noise, can provide a clear and reliable indication that a spacecraft is being forced along a non-Keplerian orbit are highlighted for each case study under consideration.

Table 10. Summary of impact of noise on the NKO signatures.

	Signatures	**Issues**
GEO	GEO and NKO are clearly defined from the following (Cases 2-3 only): • 3D orbits • Osculating inclination • $\|\boldsymbol{a}\|$ (simplified analytical approach)	• Case 1 is too noisy • From $\{\Omega, \omega, \vartheta\}$ and all MEE, GEO and NKO are not clearly defined
GPS SSO	GPS/SSO and NKO are clearly defined from the following (Cases 2-3 only): • Elements $\{i, \Omega, h, k\}$ • $\|\boldsymbol{a}\|$ (simplified analytical approach)	• Case 1 is too noisy • From $\{\omega, \vartheta\}$, GPS/SSO and NKO are not clearly defined • The magnitude of the in-plane MEE is too small • GPS/SSO and NKO are not clearly defined from the 3D orbits • $\|\boldsymbol{a}\|$ can be used only if i and Ω are known.

4. Conclusions

This work has presented a mapping between highly non-Keplerian orbit (NKO) geometry and classical orbital elements for both the direct and inverse problem. Three sets of elements have been discussed and mappings have been derived in closed, analytical form. Two models have been considered for the NKOs: a simplified model, in which the NKO orbital plane is parallel to the equatorial one, and a generalized model, in which no assumptions are made.

For the simplified model, it has been shown that the main drawback of using the classical Keplerian elements (KEP) is due to the piecewise formulation required for a forward mapping. A simpler formulation characterizes, instead, a forward mapping that uses the augmented integrals of motion. However, the main drawback of using this set of elements is the extreme sensitivity to uncertainties in eccentricity and true longitude that characterizes the inverse mapping. Lastly, the modified equinoctial elements (MEE) provide both a simple formulation and have low sensitivity to uncertainties in both forward and inverse mappings.

For the generalized model, the forward map has been derived in closed, analytical form. It has been shown that both KEP and MEE are characterized by piecewise formulations. Three test cases have been chosen that show a broad range of applicability of the maps. Key characteristics of the signature have been highlighted which can provide a simple and reliable indication that a spacecraft is being forced along a non-Keplerian orbit. Moreover, starting from the Cartesian state of NKOs, with their orbital plane parallel to the equatorial plane, all the families of NKOs which have no assumption on their orbital plane have been derived in a closed, analytical form as a function of the out-of-plane displacement.

Using the same test cases introduced for the study of the generalized forward maps, noise has been added to the initial NKO elements to assess the impact on estimates of the classical orbital elements. It has been demonstrated that, despite the noise, signatures exist that can provide a clear and reliable indication that a spacecraft is being forced along an NKO. Lastly, it has been shown that a first-guess approximation of the magnitude of the acceleration needed to follow the observed NKO can be obtained. Both KEP and MEE have equal advantages and drawbacks in the case of the generalized forward map. Therefore, in order to clearly distinguish a Keplerian orbit from a NKO using their orbital elements, it is important to look at: a) three-dimensional orbit; b) osculating i and Ω; c) osculating out-of-plane MEE h and k; and d) magnitude of the thrust-induced acceleration. This can provide an initial understanding for future, detailed analysis of optimal estimation using statistical filtering.

5. References

[1] McKay, R., Macdonald, M., Biggs, J. and McInnes, C., "Survey of Highly Non-Keplerian Orbits with Low-Thrust Propulsion", *Journal of Guidance, Control, and Dynamics*, Vol. 34, No. 3, 2011, pp. 645-666. doi: 10.2514/1.52133
[2] McInnes, C. R., "The Existence and Stability of Families of Displacement Two-Body Orbits", *Celestial Mechanics and Dynamical Astronomy*, Vol. 67, No. 2, 1997, pp. 167-180. doi: 10.1023/a:1008280609889
[3] McInnes, C. R., "Dynamics, Stability, and Control of Displaced Non-Keplerian Orbits", *Journal of Guidance, Control, and Dynamics*, Vol. 21, No. 5, 1998, pp. 799-805. doi: 10.2514/2.4309
[4] Heiligers, J., McInnes, C. R., Biggs, J. D. and Ceriotti, M., "Displaced geostationary orbits using hybrid low-thrust propulsion", *Acta Astronautica*, Vol. 71, 2012, pp. 51-67. doi: 10.1016/j.actaastro.2011.08.012
[5] Xu, M. and Xu, S., "Nonlinear dynamical analysis for displaced orbits above a planet", *Celestial Mechanics and Dynamical Astronomy*, Vol. 102, No. 4, 2008, pp. 327-353. doi: 10.1007/s10569-008-9171-4
[6] McInnes, C. R., "Displaced non-Keplerian orbits using impulsive thrust", *Celestial Mechanics and Dynamical Astronomy*, Vol. 110, No. 3, 2011, pp. 199-215. doi: 10.1007/s10569-011-9351-5
[7] Macdonald, M., McKay, R. J., Vasile, M., Bosquillon De Frescheville, F., Biggs, J. and McInnes, C., "Low-Thrust-Enabled Highly-Non-Keplerian Orbits in Support of Future Mars Exploration", *Journal of Guidance, Control, and Dynamics*, Vol. 34, No. 5, 2011, pp. 1396-1411. doi: 10.2514/1.52602
[8] McKay, R., Macdonald, M., Bosquillon de Frescheville, F., Vasile, M., McInnes, C. R. and Biggs, J. D., "Non-Keplerian Orbits Using Low Thrust, High ISP Propulsion Systems", *60th International Astronautical Congress*, Daejeon, South Korea, 2009.
[9] Driver, J. M., "Analysis of an Arctic Polesitter", *Journal of Spacecraft and Rockets*, Vol. 17, No. 3, 1980, pp. 263-269. doi: 10.2514/3.57736
[10] Forward, R. L., "Light-levitated geostationary cylindrical orbits using perforated light sails", *Journal of the Astronautical Sciences*, Vol. 32, No. 2, 1984, pp. 221-226.
[11] Baig, S. and McInnes, C. R., "Light-Levitated Geostationary Cylindrical Orbits Are Feasible", *Journal of Guidance, Control, and Dynamics*, Vol. 33, No. 3, 2010, pp. 782-793. doi: 10.2514/1.46681
[12] Heiligers, J., Ceriotti, M., McInnes, C. R. and Biggs, J. D., "Displaced geostationary orbit design using hybrid sail propulsion", *Journal of Guidance, Control, and Dynamics*, Vol. 34, No. 6, 2011, pp. 1852-1866. doi: 10.2514/1.53807
[13] Ceriotti, M. and McInnes, C. R., "Generation of Optimal Trajectories for Earth Hybrid Pole Sitters", *Journal of Guidance, Control, and Dynamics*, Vol. 34, No. 3, 2011, pp. 847-859. doi: 10.2514/1.50935
[14] Baoyin, H. and McInnes, C. R., "Solar Sail Equilibria in the Elliptical Restricted Three-Body Problem", *Journal of Guidance, Control, and Dynamics*, Vol. 29, No. 3, 2006, pp. 538-543. doi: 10.2514/1.15596
[15] Ceccaroni, M. and Biggs, J. D., "Extension of Low-Thrust Propulsion to the Autonomous Coplanar Circular Restricted Four Body Problem with Application to Future Trojan Asteroid Missions", *61st International Astronautical Congress - IAC 2010*, IAC-10-C1.1.3, International Astronautical Federation, Prague, Czech Republic, 2010.
[16] Ceriotti, M., Diedrich, B. L. and McInnes, C. R., "Novel mission concepts for polar coverage: An overview of recent developments and possible future applications", *Acta Astronautica*, Vol. 80, No. 0, 2012, pp. 89-104. doi: 10.1016/j.actaastro.2012.04.043
[17] Spilker, T. R., "Saturn Ring Observer", *Acta Astronautica*, Vol. 52, No. 2–6, 2003, pp. 259-265. doi: 10.1016/S0094-5765(02)00165-0
[18] McInnes, C. R., "Space-based geoengineering: Challenges and requirements", *Proceedings of the Institution of Mechanical Engineers, Part C: Journal of Mechanical Engineering Science*, Vol. 224, No. 3, 2010, pp. 571-580. doi: 10.1243/09544062jmes1439
[19] Wang, W., Mengali, G., Quarta, A. A. and Yuan, J., "Analysis of relative motion in non-Keplerian orbits via modified equinoctial elements", *Aerospace Science and Technology*, Vol. 58, 2016, pp. 389-400. doi: 10.1016/j.ast.2016.09.001
[20] Wang, W., Yuan, J., Mengali, G. and Quarta, A. A., "Invariant Manifold and Bounds of Relative Motion Between Heliocentric Displaced Orbits", *Journal of Guidance, Control, and Dynamics*, 2016, pp. 1-13. doi: 10.2514/1.G001751
[21] Walker, M. J. H., Ireland, B. and Owens, J., "A set modified equinoctial orbit elements", *Celestial mechanics*, Vol. 36, No. 4, 1985, pp. 409-419. doi: 10.1007/bf01227493
[22] Curtis, H., *Orbital Mechanics for Engineering Students*, Second Edition, Elsevier Science, 2009, pp. 209 - 212.
[23] Broucke, R. A. and Cefola, P. J., "On the Equinoctial Orbit Elements", *Celestial Mechanics*, Vol. 5, No. 3, 1972, pp. 303-310. doi: 10.1007/BF01228432
[24] Betts, J. T., *Practical Methods for Optimal Control and Estimation Using Nonlinear Programming*, Society for Industrial and Applied Mathematics, Philadelphia, PA, 2010, pp. 265-267.

[25] De Pascale, P. and Vasile, M., "Preliminary Design of Low-Thrust Multiple Gravity-Assist Trajectories", *Journal of Spacecraft and Rockets*, Vol. 43, No. 5, 2006, pp. 1065-1076. doi: 10.2514/1.19646
[26] Gates, M., Stich, S., McDonald, M., Muirhead, B., Mazanek, D., Abell, P. and Lopez, P., "The Asteroid Redirect Mission and sustainable human exploration", *Acta Astronautica*, Vol. 111, 2015, pp. 29-36. doi: 10.1016/j.actaastro.2015.01.025
[27] Howard, R. T., Bryan, T. C., Brewster, L. L. and Lee, J. E., "Proximity operations and docking sensor development", *2009 IEEE Aerospace conference*, edited by I. A. a. E. S. Society, 1287, IEEE Aerospace and Electronic System Society, Big Sky, MT, USA, 2009, pp. 1-10.
[28] Kronmiller, G. C. and Baghdady, E. J., "The Goddard Range and Range Rate Tracking System: Concept, Design and Performance", *Space Science Reviews*, Vol. 5, No. 2, 1966, pp. 265-307. doi: 10.1007/bf00241057
[29] Knogl, J. S., Henkel, P. and Gunther, C., "Precise positioning of a geostationary data relay using LEO satellites", *53rd International Symposium ELMAR-2011*, edited by IEEE, 12306201, Zadar, Croatia, 2011, pp. 325-328.
[30] Wang, F., Zhang, X. and Huang, J., "Error analysis and accuracy assessment of GPS absolute velocity determination without SA", *Geo-spatial Information Science*, Vol. 11, No. 2, 2008, pp. 133-138. doi: 10.1007/s11806-008-0038-3
[31] Serrano, L., Kim, D., Langley, R. B., Itani, K. and Ueno, M., "A GPS Velocity Sensor: How Accurate Can It Be? - A First Look", *ION National Technical Meeting*, Institute of Navigation, San Diego, CA, 2004, pp. 875-885.
[32] Švehla, D. and Rothacher, M., "Kinematic positioning of LEO and GPS satellites and IGS stations on the ground", *Advances in Space Research*, Vol. 36, No. 3, 2005, pp. 376-381. doi: 10.1016/j.asr.2005.04.066
[33] "IGS Products", URL: https://igscb.jpl.nasa.gov/components/prods.html [retrieved 08 November 2016].